RESIDUAL STRESS DUE TO FINISH FACING COMPARING TRADITIONAL AND MODULATED TOOL PATH MACHINING PROCESSES

by

Travis Anderson

A thesis submitted to the faculty of
The University of North Carolina at Charlotte
in partial fulfillment of the requirements
for the degree of Master of Science in
Applied Energy and Electromechanical Systems

Charlotte

2015

Approved by:

_____
Dr. Rod Handy

_____
Dr. Peter Schmidt

_____
Dr. Wesley Williams

_____
Dr. Jonathan Morrell

ABSTRACT

TRAVIS ANDERSON. Residual stress due to finish facing comparing traditional and modulated tool path machining processes. (Under the direction of DR. ROD HANDY.)

Traditional machining processes, where material is removed by a cutting tool from a workpiece, can introduce changes in the state of stress of a component at the machined surface. Knowledge of these changes is important for determining if the component is suitable for service. Changes to the machining process, such as feed rates, surface speeds, and tooling geometry can be used to mitigate these effects. This study examined the effects of a modulated tooling path, used to control chip geometry, on the surface stress of selected materials. Residual stress in machined samples was determined using X-Ray Diffraction (XRD), by comparing the modulated path method with a more traditional material removal (i.e., constant surface speed and constant contact) methodology.

Utilizing a small computer numerically controlled (CNC) tool lathe, the cutting insert was programmed to run different tool paths to determine how much the machining process contributes to the stress in the machined material. Related researches included analyses of different tool paths to study tool wear and tool cutting forces. This research looked more specifically at the material's response to different machining processes. Residual stress was measured by the use of a PANalytical® X'Pert Pro MRD™—referred to as an X-Ray Diffraction (XRD) machine in this report—and PANalytical's proprietary "Stress™" software.

Results from stress analyses were listed in table form and plotted for comparison purposes. Analysis of preliminary studies suggested that there is a standard range of

stress levels based on turning process relevant to material type. Moreover, the aspect of preventing chips from becoming entangled around the cutting tool could be a desired benefit in the areas of safety and economics.

A series of discontinuous cuts was programmed as a modulated tool path referred to as a modulated tool path process. Using the programmed modulated tool path process reduced chip length for all materials used in this experiment. Maximum chip length for the modulated tool path process was less than two inches. Furthermore, the x-ray diffraction process provided a method to non-destructively analyze the residual stress left by the different processes. Stress measurements analyzed indicated that different alloys of metals may respond uniquely to the turning process used. Aluminum 6061-T6 and tantalum 97Ta3W showed more of a trend in residual stress as the result of the different turning processes than the Inconel® 718 alloy.

Therefore, the comparison of traditional turning and modulated tool path processes could yield varied results for different metal alloys. This project had trends in d-spacing analysis for the aluminum 6061-T6 and tantalum 97Ta3W; however, the Inconel® 718 did not yield a noticeable trend. Options for further development of this research would be to increase the sample population for better statistical analysis. Also, for alloys like Inconel® 718, altering the modulated tool path process could yield more consistent results. Some of the control variables that could be altered would include depth of cut in the X- or Z-axis, cutting speed, or insert used. Data that was gathered for this project revealed that better statistical analysis could have been achieved if there were more experiments for each sample. With more data, the relation of the previous stress

might have been used to determine how the previous stress affected the residual stress resulting from each turning process type.

TABLE OF CONTENTS

INTRODUCTION

Traditional turning uses a tool path with a continuous cutting path where the cutting insert stays in contact with the material being cut from start to finish of the cutting profile. Alternatively, modulated tool paths change the depth of cut or intermittingly remove the cutting tool from the material during the cutting operation. Oscillating, vibrating, and modulated tool path cutting are all modified machining processes that have end goals of reducing tool stress, work-piece stress, difficulty of machining, and/or energy consumption as desired by the given application. A benefit of using a modulated tool path is chip management [1]. As an evident fact of removing the cutting tool from the material, any chips will be limited in length by the duration of the engagement with the material. From previous studies, intermittent engagement between the cutting tool and the workpiece reduces the peak cutting forces [2] and the cutting tool temperature [3]. A basic image of the motions of the cutting tool and workpiece is shown in Figure 1.

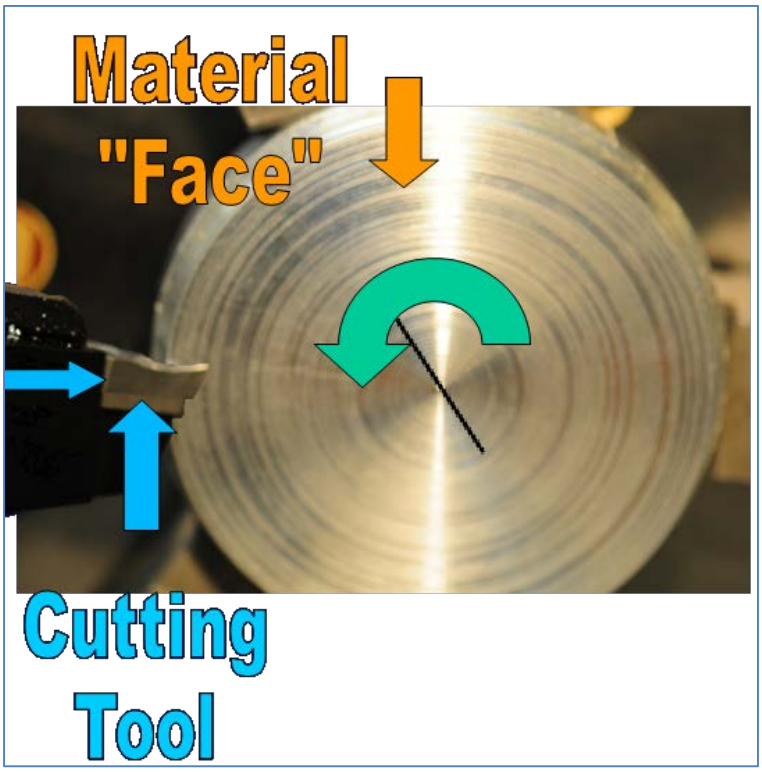

Figure 1: Illustration of direction of cutting tool and rotating workpiece during traditional turning process.

Ultrasonic vibrations or oscillating tools can help to reduce the cutting force required by moving the cutting edge of the tool to and from the area of highest pressure concentration [2] & [4]. This work focused on material residual stresses attributable to different machining methodologies for the turning process. Specifically, this project compared a specific modulated tool path to traditional finish face turning.

One of the specific applications that this project was to explore involved the possible reduction stress in the machining of depleted uranium. Uranium is more susceptible to degradation from stress than many other materials. Creep, embrittlement, and shape deformation due to material stresses are concerns specifically in the use of uranium for fuel rods [5]. Materials such as uranium fuel rods are subjected to high temperatures which reduces material yield strength. Moreover, materials that must

remain in use for 20 or more years should include design tolerances to compensate for material creep. Internal and residual stresses during forming or shaping will contribute to creep, and residual stresses introduced during fabrication can reduce the lifespan or maximum working stress of a material. Based on personal conversation with the sponsor of this project, corrosion of materials can be accelerated by hydrogen corroding areas of high stress. Therefore, the residual surface stress left by a particular machining process could provide further understanding of corrosion over the lifetime of a given material sample.

Materials will tend to "relax" and stresses can cause the material to deform microscopically. Materials that need to be in place over long periods of time (i.e., 20 years or more) must maintain their original form and strength. Materials with extensive storage life expectations can be costly to maintain. Degraded materials removed from long term storage may cause catastrophic failures if the level of degradation that occurred was greater than expected. One immediate objective of the modulated tool path process studied in this work was to process workpieces while producing scrap chips with lengths less than 50 mm, and therefore, reducing the tendency of these chips to become entangled during component processing. An alternate goal of investigating this process was to determine if the modulated tool path process reduces induced stresses in workpieces. This research compared the residual stress levels in selected materials after being processed using the modulated tool path methodology and a more traditional turning approach.

Vibration in milling processes has been used in previous research to provide smoother finishes; additionally, that research revealed that material cracks were not as

prevalent when compared to traditional milling processes [6]. Liu's referenced work examined how tool nose radius size altered the depth and magnitude of stresses. Liu's analysis determined that increased depth of plastic deformation dictated how much of the induced stress was distributed through the material surface and sub-surface. Other research projects theorized or implied that flatter surface finishes through machining and grinding processes more evenly distributed residual stresses ([7] and [6]).

Measurements of residual surface stress were collected from the use of an x-ray diffraction (XRD) machine (PANalytical® X'Pert Pro MRD) and associated software packages (PANalytical® X'Pert Data Collect and PANalytical® Stress). The most common use for XRD instruments is to identify chemical elements. Some of those applications are for quality control to verify proper mixtures or certain levels of purity. Other uses of x-ray diffraction include process inspection for welds and proper shot peening process verification in order to achieve uniform compressive stresses ([8]).

XRD technology can also be used to analyze the stress in machined surfaces. At the Pennsylvania branch of the Naval Foundry and Propeller Center, XRD has successfully been used to prove proprietary machining processes that revealed residual stress as a result of those machining processes was alloy specific (Jones, K., personal communication, April 16, 2014). This project was proposed with the goal to examine the residual surface stress difference between traditional turning and a modulated tool path (MTP) processes. Traditional turning operations make cuts on material in one pass along a given path. The MTP process was implemented to reduce chip length by removing the cutting insert from the path and then resuming the cut. The modulated tool path operation was a programmed modulated tool path that repeated sequential loops.

Modulated tool path programmed moved the cutting tool into and out of the material during cuts. Removal of the cutting tool and resuming of the cutting process in several short successive cycles was built in as a loop feature for process repetition.

The purpose of this research was to develop a MTP process to determine a possible improvement to existing material turning methods. If changing the traditional turning process could yield longer lifetime of machined components, many industries could benefit from a process change such as adding a modulated tool path process. Applications that could benefit from the research of residual stress could vary by industry. By pre-determining stress levels in components, material surfaces could essentially be pre-loaded like a spring to reduce surface stresses during use. Benefits would include longer lifespan of components and reduction of replacement or repair services. Thus, increasing the production time to add a modulated tool process to achieve specified stress levels could be economical for a company. Furthermore, residual surface stress level values and constraints could be developed into a standard specification on blueprints similar to Rockwell® hardness specifications.

This project intended to experimentally determine a plausible process improvement in the overall material turning regimen which could yield the benefit of pre-determining residual stress. The following sections provide the experimental methodology developed and tested for this research as well as the data/results obtained during various trials with different materials, with conclusions and recommendations for future studies elucidated.

THEORY AND LITERATURE REVIEW

Background

Machining a part by removing material is an extremely versatile and widely used process. As an alternative to grinding, turning offers advantages of "…flexibility, low-cost, [and] environmentally friendly production in comparison with the grinding process…" [7]. The automotive and aerospace sectors of manufacturing are two sectors that rely on the precision and high speed metal forming process of material removal [9]. With software able to provide more complete and immediate finite element model (FEM) analysis, model predictions of cutting behaviors have been created and used [9]. Typically, the sound attributable to the vibration of a cutting tool during machining is an indicator to most machinists that the tool is vibrating in contact with the workpiece and is producing a less than desirable surface finish. Therefore, vibration during machining is typically perceived as "…detrimental [to] the process…" [2]. (Note: Need a sentence describing the fact that cutting forces contribute to residual stress in machined components, along with a reference, here). However, controlled vibrations can reduce the cutting forces required [10].

Furthermore, controlled vibrations or oscillations can be utilized to reduce chip length when a specific or required cut would otherwise result in long and entangling waste material. Production machining processes require the removal and the disposal of waste materials, commonly known as the "chip(s)". To reduce chip handling difficulties during machining and waste disposal, the chip length should be reduced. Shorter chips leave more space vacant and are more easily compacted than long, continuous chips. Long or "stringy" chips can entangle around the part being machined, the cutting tool, or

other chips. Longer lengths of chips tend to create larger obstacles of wound chips referred to as “bird nesting.” Bird nesting results when a chip or multiple chips are long enough to become entangled and cause a hazardous or obstructive shape (e.g., spherical or egg-like). Entangled chips tend to act like a spring and resist being compressed for more compact disposal. Also, the entangled mass of chips tends to get caught on any protruding object such as the tool, bolt heads, or hand/control knobs if brought past non-smooth surfaces. Figure 2 shows how a small amount of chips can start to become entangled around the cutting area. The benefit of reduced chip length from the proposed modulated tool path process was shown in Figure 3.

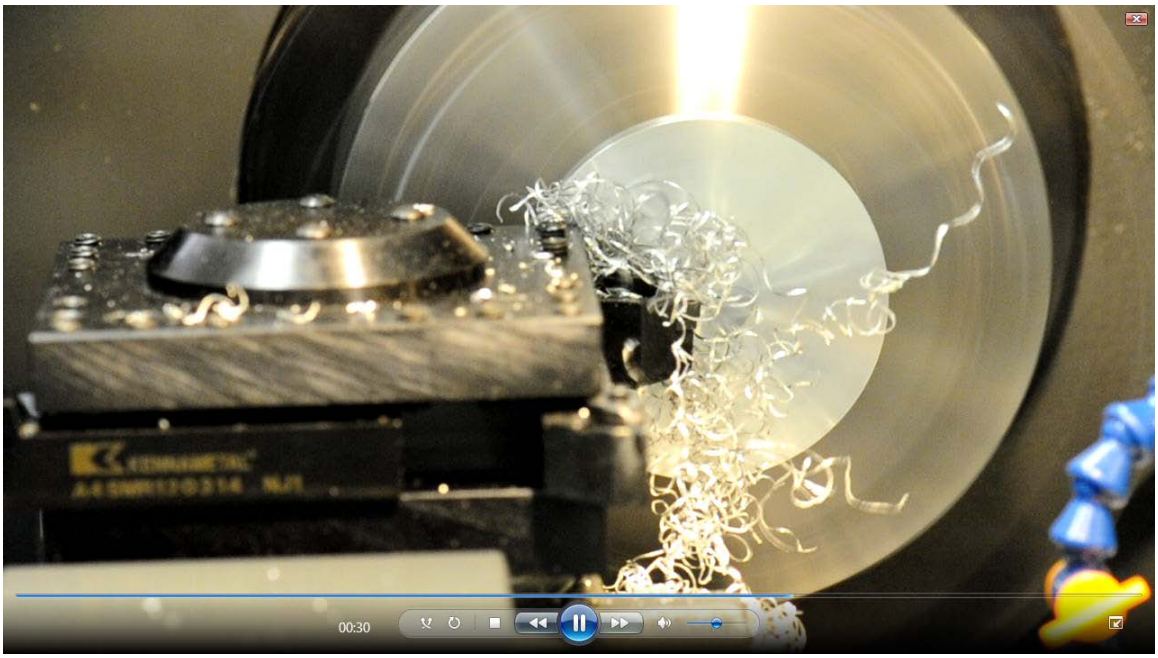

Figure 2: Chips during traditional style cutting on the face of aluminum sample entangled around cutting tool near the cutting area.

Figure 3: Image of early modulated tool path process that reduced chip length and tendency to entangle with previous chips.

This project sought to determine benefits of a modulated tool path (MTP). Chip length and material stresses were the key areas of focus in determining if there was a benefit of the modulated tool path process over the traditional process. Basic computer numerical code (CNC) was generated and run on a HAAS Tool Room Lathe (TL-1). An assortment of six materials were pre-selected and narrowed to three based on availability and feasibility for the equipment available. A PANalytical brand x-ray diffraction machine and associated software were used in the residual stress analysis. Experimental procedures and data/results of this project are included in the following Methodology and Results sections to explain the experimental research in further detail.

Bragg's law was a key scientific understanding that allowed for the use of x-ray diffraction to identify and analyze the material samples. Even though the diffractograms that were created from the phase identification XRD scans could have been used to

identify material composition, a handheld Thermo Scientific Niton® X-Ray Fluorescence (XRF) analyzer was used to identify material composition. The XRF was quicker in identifying material than the analysis of the XRD phase identification would have been. The XRF gave results in as little as 30 seconds. Data from the XRF were recorded and are provided in the Results section of this paper. However, the XRD was required to analyze the material stress by focusing on the lattice structure and through the use of Bragg's law. A brief explanation of Bragg's law is given using the following variables, equation, and diagram courtesy of VEQTER Ltd. [11]. Figure 4 provides a diagram illustrating Bragg's law.

2θ=diffraction angle
d=lattice spacing
ψ=tilt angle of sample surface
n=integer to indicate different layer or level

Equation II.1. $n\lambda = 2d\sin\theta$

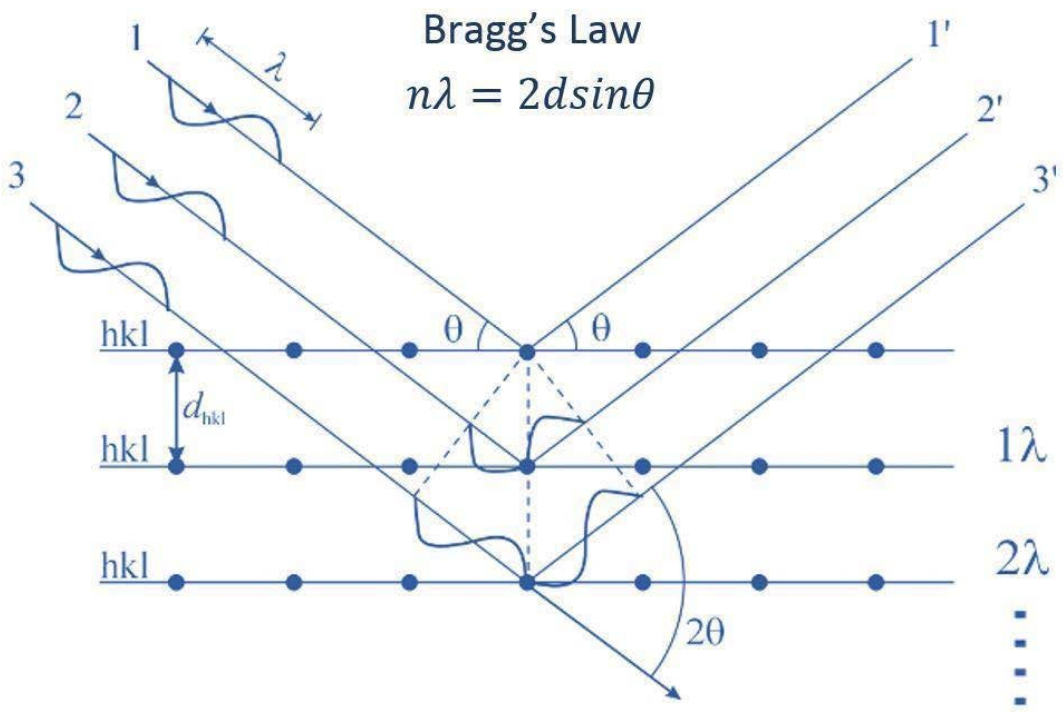

Figure 4: Diagram illustrating basic idea of Bragg's law [12].

The crystalline structure of uranium varies with temperature. There are at least three phases of the uranium crystalline structure [5]. These structures are identified as orthorhombic, tetragonal, and body-centered cubic at temperature ranges indicated in Table 1. Crystalline structures of possible surrogate materials are also listed in Table 1 along with modulus of elasticity (Young's modulus) and Poisson's ratio values that were used for the stress evaluation. Lattice structure referred to as the d-spacing was used as part of the stress analysis. Increases in d-spacing indicated tensile stresses and decreases in d-spacing indicated compressive stresses when analyzed using the $\sin^2\Psi$ method.

Table 1: Material properties used for stress evaluation.

Material	Cell Structure	Young's Modulus, E (GPA)	Poisson's Ratio, ν	Reference(s)
Aluminum 6061-T6	Face-Centered Cubic	68.90	0.33	[13] & [14]
Inconel® 718	Cubic	205.00	0.30	[15]
Tool Steel (M-42)	Cubic	211.60	0.29	[16]
Stainless Steel Nitronic 33	Face-Centered Cubic	199.00	0.31	[17] & [18]
Tantalum 97Ta3W	Cubic	186.00	0.35	[19]
Zircaloy-4	Hexagonal	99.30	0.37	[20] & [21]
α-Uranium, stable up to 662°C	Orthorhombic	208.00	0.23	[3] & [22]
β-Uranium, stable from 662 to 769°C	Tetragonal	-	-	[3]
γ-Uranium, stable from 769 to 1130°C	Body-Centered Cubic	-	-	[3]

Combining Bragg's Law and material properties with software for stress analysis for the $\sin^2\Psi$ method of analyzing d-spacing provides useful information on stress state and magnitude. Slope of the d-spacing versus $\sin^2\Psi$ plot indicates tensile (positive) or compressive (negative) normal stress. Evaluation of x-ray diffraction scans was completed in this project by accompanying software by PANalytical®. Part of PANalytical® Stress™ software evaluates the data gathered through use of several equations. Equations used by the software include evaluating intensity, determining equipment constants for a particular setup, and calculating stress by correlating d-spacing. Evaluation of d-spacing using the $\sin^2\Psi$ method to determine stress was of

significant interest to this project. Change in the d-spacing along the scanned angles was mathematically evaluated as part of a ratio shown by the following variables and equations [23].

d=lattice spacing
$d_{\varphi,\Psi}$=strained d-spacing with tilt angle Ψ and rotation φ
d_0=strain-free d-spacing
m=slope of plot
σ_1,σ_2=normal stress of the diffracting lattice plane
s_1, $1/2s_2$=X-ray elastic constants (XEC's)
φ=rotation angle (perpendicular axis to face in center of circular sample)
Ψ=tilt angle of sample surface

Equation II.2. $$\sigma_\varphi = \sigma_1 \cos^2\varphi + \sigma_2 \sin^2\varphi$$

Equation II.3. $$\frac{m}{d_0} = \frac{1}{2} s_2 \sigma_\varphi = \frac{1}{d_0} \frac{\Delta d_{\varphi,\Psi}}{d \sin^2\Psi}$$

Analysis of residual stress by software usually extrapolates the strain-free d-spacing with the assumption that stress is zero in the free surface [24]. The immediate outer surface layer is assumed to be strain-free and variations in deeper layers would then be compared to the assumed strain-free layer (Blanton, T., personal communication, June 9, 2015). That assumption was useful because forming processes can alter the d-spacing. Possible changes in d-spacing based on processing type was part of this project's analysis. With an understanding of induced stresses, corrosion at high stress areas could be better understood.

Proof of the repeatability of the identification of peaks from XRD phase identification scans was done with visual overlays of assorted ranges with key emphasis on the peaks. Peaks with the highest intensity (i.e., at low angles of 2Theta) were mainly useful in identifying major element composition. Scans at higher angles of 2Theta (past

90° 2Theta) were used for the stress analysis. Preferred angles for stress measurement was desired to be above 125° 2Theta; however, the copper tube in the XRD did not provide useable distinguished peaks for the aluminum and tantalum samples above 125° 2Theta. Also, fluorescence with the copper tube and other iron alloys prevented the analysis of stress for the tool steel and nitronic stainless steel alloys. A cobalt tube was purchased for future XRD analysis of iron alloys.

Oscillating Tool

Oscillating the tool in different directions produces different effects. Controlling the magnitude of "…the vibration amplitude, frequency, and direction" provides a way to determine what conditions can benefit in reduced cutting force [2]. Controlled vibration in an oscillating fashion reduces the cutting force required. Discontinuity of cuts is of importance when determining chip length and oxide layer for frictional estimates. Horizontal cutting force is reduced most significantly where chip breaking occurs. Oscillations that do not allow chips to break do not benefit from the oscillation since the constant contact with the material does not allow any reduced cutting force [2]. Tools that oscillate require controls for activating the movement of the tool. This method with programmable logic controllers (PLC's) could be coupled with modulated tool paths for specific motions not achievable by the machine. Other types of tooling movement could also be added to modulated tool paths.

Vibration Assisted Machining (VAM)

Vibration assisted machining (VAM) is different from traditional machining because of the type of material deformation that occurs during machining. Traditional machining involves an initial contact penetration that leads to plastic deformation of the

material. During each cycle of the VAM process, the material is subjected to elastic deformation before and after each plastic deformation [25].

Ultrasonic vibration is a branch of vibration assisted machining that is significantly analyzed for benefits in micro- and nano-machining. Typically, some form of transducer or magnetostrictive device with a tool holder is attached [4]. As technologies developed, more refined VAM systems have become available that produces and monitors the vibrations [10].

Tool wear is another concern that VAM studies analyze. For this experiment, polycrystalline diamond (PCD) inserts were not selected because of the tendency to shatter or fracture under certain impact conditions in accordance to Kennametal's senior application engineer Mike Schulte. Sintered PCD inserts perform better in terms of tool longevity and surface finish with larger depths of cut than most finishing skim cuts [26]. Different diamond type tooling for scratching or engraving is more suitable for VAM in removing small amounts of material from surfaces and the tool wear can be reduced [27]. In determining how ultrasonic vibration affects workpiece, it was theorized that the ultrasonic impacts caused the material to lose some of its strength—this idea was disproved and it has been "…concluded that no significant reduction of the mechanical strength of the workpiece...[due to] …the ultrasonic vibration used" [4].

Residual Stress & Surface Finish

Surface finish can be used to analyze the machining process by "reading the lines" like reading the growth lines of a tree to tell what was accomplished in the past. Measuring surface finish can be conducted with the use of a portable profilometer to give a quantitative value for comparison [4]. Roughness of the surface can be affected by the

tool nose radius. The tool nose radius will mainly determine how high the peaks are in between cuts. A larger tool nose radius will decrease the peaks between cuts, especially when cuts are closer together. Therefore, a correlation between tool nose radius and surface finish can be made to help predict residual stresses at the machined surface [7]. Depending on the material, the surface finish can be improved [6] and possibly reduce the residual surface stress.

Summary of Previous Works

With new and different technologies, there are always factors that determine which process is the most applicable for any given situation. Cost of development, availability of materials, and even the available technology limit the efficiency that can be achieved. As with most research studies conducted, limited resources can be a potential constraint. An example for this project was that the available turning machine was a small lathe, which limited the maximum diameter for the piece. Another example of an experimental constraint was that the XRD used for this project had a weight limit of 0.5 kilograms (kg).

Previous studies helped to define the value of parameters and determine which process was the most ideal for the given circumstance. Modifying traditional machining with non-conventional methods (e.g., modified tool paths and vibration assistance) has been studied for increased machinability of hard materials [28]. A significant goal of this work was to gather an assortment of data related to the comparison of just two machining processes in hope of further studies that can advance upon gathered data. Also, this project had another goal of tying the referenced material and similar topics together in

order for a standard process to be developed. This process could then be used to develop tool paths as an equation that considers tooling and material conditions.

Project Distinctiveness

Unique to this project was more than just the comparison of two turning processes. From the literature review, the other available published works in this area did not analyze the residual stress of two or more different turning processes. However, there were several projects that evaluated stress from other processes. It should also be noted that none of the previous works—referenced or otherwise reviewed prior to this project—analyzed the stress in the material as result of a process similar to modulated tool paths. Referenced works of Skelton were the most similar in adding oscillations and vibrations to the cutting tool; however, Skelton only published force on inserts and did not analyze stress in the workpiece. Many previous works cited Skelton's research for cutting tool analysis.

With confidence in the research of cutting tools done many times by independent researchers and cutting tool manufacturers, this area was not an issue addressed in this report. Instead, focus was given to the analysis of exploring the relation of residual stress to turning process used. Utilizing a modulated tool path process in turning appears to have become somewhat obsolete since Skelton's research circa 1968 to 1970. Improvements in tool path control for new cutting machines using higher resolution encoders with quicker processing and executing of CNC coding has become a standard in machine shops, providing an opportunity to evaluate the usefulness for a broad array of people with access to CNC lathes.

In development of the modulated tool path, different methods were used to create and execute the modulated tool path cycle. Development and changes of the modulated tool path process are included in the Methodology section of this thesis. Procedures for making stress measurements and evaluating residual stress are also included in the Methodology section.

The use of an x-ray diffraction scan and associated stress software has been less frequently published, possibly due to the added expense of obtaining such software. Fortunately, this project had the opportunity to use software that analyzed stress measurements from the XRD to calculate material stress. Those calculations were relevant to material properties listed in the first section of Theory and Literature Review (i.e., Background). Stress analysis of results included comparison of d-spacing (the lattice structure) and software calculated stresses. Analysis of multiple materials was another distinctive aspect that very few projects of this nature had included in its scope at the time of this report's proposal.

RESEARCH METHODOLOGY

Utilizing the available resources at the University of North Carolina at Charlotte (UNCC) and supplies and instruments provided by the project sponsor, the comparison of modulated tool path and traditional machining was conducted experimentally on a computer numerical control (CNC) Haas TL-1 (lathe). This research was conducted over the span of approximately two years, beginning during the Summer/Fall of 2013, and was funded by B&W/Y-12 of Oak Ridge, TN. The first eight months of the project duration were set aside for determining and understanding what was to be analyzed, how similar research had been conducted previously, and what process would best suit this project. Sample preparation was given a two month span for selecting materials, determining sample sizes, and creating a sample tracking process. The remaining time was split with overlapping segments of the process, with data collection and analysis completed during the first half of 2015.

Machining with CNC code provides a more repeatable process than does manual machining. Determining the correct parameters and selecting the most appropriate method can be analyzed by using flow charts [9]. Feasibility analysis was used to determine the exact modulated tool path process. Codes for tool paths were written using a combination of programs due to the accessibility of the programs. The final versions of the programs were edited at the turning center to meet all machine constraints. Use of the CNC lathe provided one of first levels of quality assurance as the code could be used repeatedly to achieve the same process as opposed to the less consistent manual operation of the lathe.

Cutting inserts for this project were selected after review Kennametal® printed and online resources. More importantly, Kennametal® technical representatives were able to identify the most appropriate inserts based on the machining parameters listed below in the "General Procedures" section 3.f. Inserts that were selected were grouped by cutting radius (1/32 inch and 1/64 inch), by coating type (uncoated or coated), and by appropriate material use (aluminum 6061-T6, Inconel® 718, and tantalum 97Ta3W). Insert shape was based on the insert holder used in Jameson K. Nelson's 2012 publication of "Acoustic Emission Detection and Alloys During Machining Operations."

The mentioned inserts are 35° (included angle) "V" style inserts (*Innovations*, 2013). Uncoated cutting inserts were Kennametal® brand made of typical ISO carbide grade materials (K68 and K313). Cemented carbide inserts that were also planned for use were Kennametal® brand with their proprietary physical-vapor-deposition (PVD) coatings (KC730, KCP25, KCU10, and KCU25) which are variations of TiCN-Al and AlTiN coatings. Even though multiple inserts were selected, only the uncoated inserts were used for this report. Changes in the modulated tool path process, equipment malfunction and repair, and cost of time to use the x-ray diffraction equipment hindered the evaluation of multiple insert comparisons. Instead, the K313 uncoated, 1/32" nose radius insert was used. A new cutting edge was used for each of the final turning processes included in the investigation. Inserts added another level of quality assurance because of the manufacturing tolerances used in the formation of the carbide inserts is more repeatable than any manually-ground cutting tool can achieve. Tolerances for such inserts often are more repeatable than 0.00001 inch.

Before materials could be machined, a repeatable method to hold those materials had to be established. For holding round disks in a lathe, soft jaws were cut to size. Soft jaws were low carbon steel fixtures for the 3-jaw, self-centering clamping chuck on the lathe headstock. The untreated (i.e., non-heat treated) soft jaws provided an inexpensive way to machine fixtures to hold a specific size diameter at a fixed depth. Two sets of soft jaws were cut for four-inch diameter parts. Sets were marked with letters to indicate set group and numbers to indicate jaw placement relevant to chuck "0" (zero) marking. The first set was stamped A1, A2, and A3; leaving the second set to be stamped B1, B2, and B3. The depths of the jaw sets were cut differently. A deeper holding depth was to allow for more stability for thicker samples when developing and testing the modulated tool path process. Hence, the shallower holding depth was used to cut the thinner samples for the formal analysis after learning the maximum thickness for the XRD stage was 11 millimeters (mm) [0.4331 inches (in.)] from the equipment manager. However, from use of the X'Pert Pro software used to operate the XRD, it was apparent that anything past 10 mm (0.3937 in.) was not practical and less than 8 mm (0.3150 in.) was preferential. The use of dial indicator provided an immediate way to verify repeatability of the jaws within a tolerance of 0.0005 inch.

During the project, machined samples were marked with alignment marks and sample designation. The sample designation marks were formatted in a way that indicated material type and sample number. Using those marks (and ink markings for detail), each sample was uniquely identifiable. An example of a milled notch (left) for orientation during X-Ray Diffraction (XRD) scans is shown below in Figure 5. Also, sample identification designation was scratched into the "back" surface as soon as sample

disk was cut as shown in Figure 7. Orientation marking was important for later analysis at different phi orientations, where the sample is rotated about the center of the circular face.

Figure 5: Sample orientation marking.

Sample designation was designated by material type and sample number. The format for determining each workpiece's unique sample identification number is provided in Appendix F: General Procedure section 3.d. This was shortened to show the format used in Figure 6 and an example of the first tool steel M-42 shown in Figure 7.

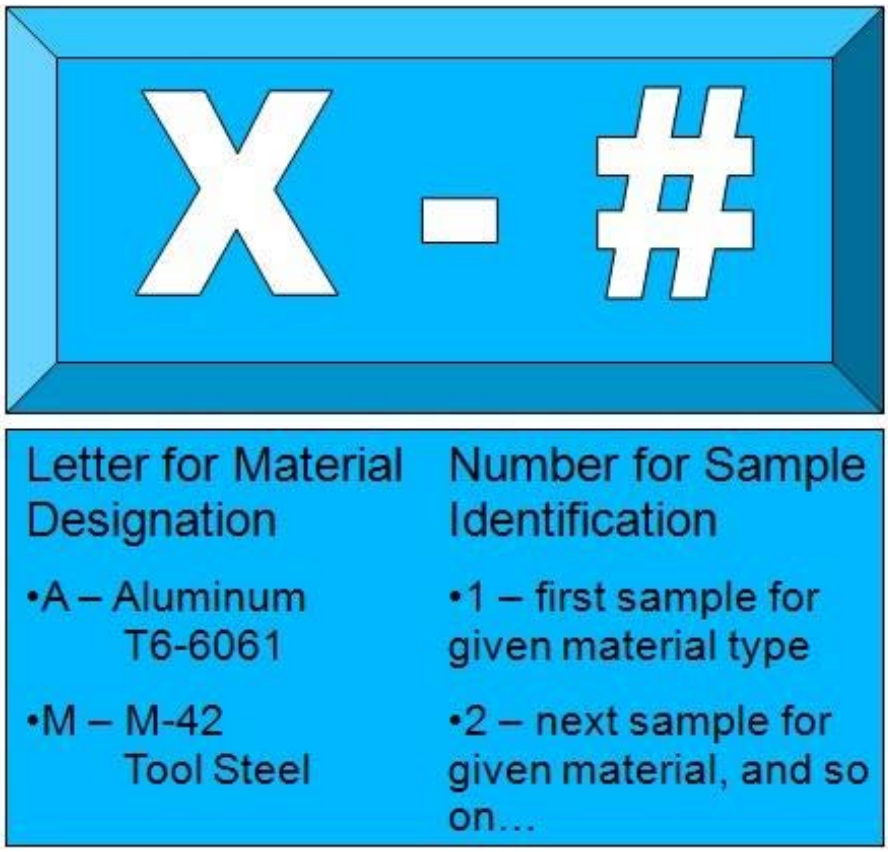

Figure 6: Sample identification format.

Figure 7: Enhanced markings to illustrate sample identification markings.

Test materials were analyzed by the utilization of PANalytical® X'Pert Pro MRD™ (referred to as an X-Ray Diffraction (XRD) machine in this report) located on

the campus of the University of North Carolina at Charlotte. Since the X-Ray Diffraction (XRD) machine in did not have a fixture capable of holding larger and heavier samples, an upside down “T” shaped fixture was designed to hold the large disc samples. As part of the XRD's analysis process, the mounting plate tilts up 90 degrees from horizontal. This vertical position requires more holding force and the “T-jaw” fixture was a proposed simple design that could accommodate multiple sizes within the XRD's limitations.

Figures in Appendix A illustrate the design concept for the mounting plate. In addition, fixtures were made for holding the sample materials on the mounting plate. Samples were placed flat on the mount in a horizontal position and then rotated 90° to a vertical position. The mounting stage was analyzed to determine the simplest fixture type. Geometry of the circular mounting stage was sketched. There were three inverted “T” slots extending from the center to the circumference. Fixtures were made to fit those slots. Those fixtures included #4-40 pitch threaded holes for holding the fixtures in place. Each fixture also had a step that extended outward from the face of the mounting stage with a threaded hole and a set screw to hold the sample in place during the scans.

To prevent damage and marring of the aluminum stage, the set screws to hold the fixtures in place were designed with nylon tips. For cost effectiveness, the fixtures were machined out of available keystock using a vertical knee mill. To verify the holding strength, a slightly oversized sample was mounted in the XRD and rotated 180° so that the fixture had to suspend the sample in an upside down position. Based on that limited test and visual inspection, it was determined that the fixtures were sufficiently designed and machined to hold the samples. Images of the mounting plate and designed fixture can be found in Appendix A. In the vertical position (i.e., 90° from horizontal mounting

position), the metallic samples were scanned using X'Pert Data Collector™. Initial setup training was provided by the equipment manager at UNCC.

Even though the XRD had the capability to provide element analysis, the quicker x-ray fluorescent (XRF) handheld unit by Thermo Electric® was used to provide composition data. The XRF pictured in Figure 8 shows how small the handheld XRF was compared to the notebook paper used to take notes on material composition. Material composition values have been provided in the Results section of this paper. Any future development upon this research would require the gathered material composition for comparisons of specific alloys. The gathered material composition was listed by alloy with the most prevalent elements listed by weight percentage and possible error of measurement as calculated by the XRF.

Figure 8: Handheld XRF Niton XL3t model made by Thermo Electric.

Scans that were utilized are listed below in the "General Procedure" section 3.e. Parameters of listed scans were developed through conversations with the XRD manager and various technical representatives. E-mail correspondence and phone conversations with technical representatives helped to determine that the initial 2-Axis scan was an inappropriate method to measure stress in solid metallic samples with textured surfaces. Instead, a specific scan for stress measurement had to be selected for use. Settings for the $\sin^2$ (Psi) were also initially set inappropriately for proper stress analysis according to multiple representatives from PANalytical®. The $\sin^2$ (Psi) setting of 0.4 was too low and needed to be adjusted to 0.8. Furthermore, an XRD manufacturer held a seminar in that helped to provide a better understanding of using XRD for research. Notes from the seminar were used to help develop the procedure in Appendix F. Data from scans were analyzed using PANalytical's Stress™ software.

For future studies, extraneous data could be gathered such as heat generation and particulate distribution. Hardness of materials was tested using a Wilson® Rockwell® 2000 Series hardness tester and data was placed in the Results. All relevant data reported was for future studies to reproduce and improve upon this study to understand corrosion of material over the sample's lifetime. After analyzing the stress induced into the material from machining processes, heat transfer could be examined to determine how heat generation is related to material stresses. In Shi Bin and Helmi Attia's 2010 article regarding modeling and simulating machining, a relationship between carbon content, heat transfer, and deformation for steels was mentioned [9]. This project identified some steels as possible surrogate materials but did not focus on any particular steel grades.

Measurements of force on the tool have been performed by using "...four strain gauges arranged in diametrically opposite pairs…" [4] and with more modern "…strain-gauge type dynamometer" [7]. Since this project did not focus on machining stresses, use of a dynamometer was not a priority; moreover, attachment of a dynamometer was limited with the current available tool-post. This would be an area of interest to be analyzed once a tool-post capable of holding the dynamometer is available.

Studies done previously have typically been completed with "standard" tooling of that time period. In R.C. Skelton's 1969 publication on "Effect of Ultrasonic Vibration on the Turning Process," he used "[a] standard toolholder for triangular carbide tips." While triangular carbide tips are still in use today, those are typically used on manual machines where the production quantity is low. Today, "carbide" and cubic boron nitride (CBN) indexable inserts are the standard for high production and high repeatability machining. Newer indexable inserts allow same shape inserts to be used in nearly the exact placement with the ability to switch inserts to try different chip breaking geometries and different tool nose radii. Liu Meng *et. al.* (2004) published an article on tool nose radius relating to residual stress and surface finish—which used CBN inserts. There have been several studies on residual stress [7] and tool nose radius effect on machined material. Previous studies cover some form of alternative machining practice or tool nose size. Vibration assisted machining typically requires additional equipment. This research analyzed different tool nose radii and CNC programmable tool paths that oscillate. The outlined process in list format is located in Appendix F.

The original idea involving the comparison of traditional turning versus a modulated tool path process had several variables that could be altered. Many variables

would have added to the complexity of the project and required more time to properly analyze. Future studies could analyze other scenarios changing equipment, processes, or materials with more configurations to determine the best process for each application. A major aspect of this project was to develop an understanding of the needs and application for the project sponsor.

Typical machining processes are generally classified as either roughing or finishing. Roughing is the process of removing large volumes of material as opposed to finishing which removes a small amount of material. Of the three depths outlined by the project procedure (noted in Appendix F, section 3.f.iv.1.), the depth of focus was (3.f.iv.1.a.) 0.010 in. as suggested by the sponsor. Suggestion to focus on the 0.010 in. depth was based on the sponsor's conversation with machinists that were part of the main target group to help by the experimentation of this project.

Material selection was based upon surrogate materials obtained for Nelson's previous work (2012) and the sponsor's comments. Aluminum 6061-T6 was used because it was a relatively easy material to machine and efficiently test CNC codes. Moreover, the elastic property of aluminum produced a chip that tended not to break like that of depleted uranium. Tool steel M-42 and Inconel® 718 were selected as surrogates because they were considered difficult to machine like depleted uranium. Tantalum 97Ta3W had the highest density and was the closest in molecular weight to depleted uranium of the alloys used. The stainless steel nitronic 33 alloy was the preferred choice of surrogate material selected by the project sponsor to compare with other research conducted on the machining of depleted uranium. However, the copper tube created too much fluorescence to be useful with alloys rich in iron.

A brief explanation of the fluorescence caused with iron alloys from excited copper x-ray tubes was related to the energy of the electron valence shells as stated by various experts in the diffraction field. As mentioned by PANalytical's technical representatives, the cobalt tube would have been the correct tube for the XRD to scan tool steel M-42 and stainless steel nitronic 33. Due to the cost of the cobalt tube, the purchase procedure required quotes and proper paperwork to be fulfilled before approval of purchase. At the time of the arrival of the cobalt tube, the XRD had been out of service for repairs. A new copper tube was installed in the XRD by the Optics department's request. Following the installation was a lengthy time to get the new tube aligned and calibrated correctly. After verification of the tube alignment by the facility manager, there did not appear to be any opportunity to switch the cobalt tube in place of the copper tube due the estimated service charge of $1,000.00 (U.S.D.) for tube changes. The last equipment manager with the knowledge to change the tubes retired shortly after the new tube was aligned. Therefore, the minimum selection of materials aluminum 6061-T6, Inconel® 718, and tantalum 97Ta3W were used. Those three materials produced peaks around the desired 100° to 140° 2Theta range for stress measurements.

A major project goal was the determination of the most effective and efficient method for conducting the modulated tool path process. The choice of the most appropriate modulated tool path technique was most limited by the capabilities of the HAAS TL-1 lathe. The specific tool post on the TL-1 lathe would not easily accommodate an add-on apparatus to induce vibrations. Accuracy was also a factor to consider. Therefore, the modulated tool path process had to have a motion path that was achievable without causing position errors by moving too fast back and forth across

position encoders. A few modulated tool paths were developed (See sections 3.f.iv.3.b-d.).

The first draft of the modulated tool path was a series of linear progressing loops. To reduce tool path length, the loops were replaced by a simple sine wave style path. "Rough MTP" was a coarse process that had a single sine wave with amplitude of 0.010 inches (in.) in the Z-direction (into and out of material face) on the lathe. The aforementioned modulated tool paths yielded very textured surfaces. A multiple set of modulated tool path passes was then coded. "Multiple MTP" used four passes of sine wave style modulated tool path processes using three different amplitudes and four unique shifts. The different amplitudes were reduced, shifted in phase, and moved in the Z direction closer to the material to maintain the same end of depth of cut in the Z-axis. However, the multiple passes required what seemed like unnecessary time spent, with little material removed on the final pass. Consequently, a single pass path was developed with a fine X-axis feed (into the circumference)—referred to as "Fine MTP" process. This was the last iteration of the modulated tool path development for this project.

All of the cutting processes, both traditional and modulated tool path, used constant surface speed (CSS) coding. CSS allowed for the assumption to be made that the cuts made across the cutting range had comparable forces and material removal rates (MRR). MATLAB™ was used to create programs that could be manipulated to create CNC codes for each of the modulated tool path processes and were placed in Appendix E. Character format was edited using Programmer's Pad®. Resulting codes were also placed in Appendix E with corresponding MATLAB™ code. Portions of the chips generated from the different machining processes were collected and placed in glass

containers. Collected chips could be used as references for future development of this project.

Moreover, the XRD process was also improved as a consequence of conducting several trials. The first instructions provided for the operation of the XRD were relevant to sample identification for powder samples. An initial misunderstanding of the peak selection was based on the idea that the peak with the highest intensity would be best for stress analysis. Through conversations with PANalytical's technical service, a preferred range for selecting a peak was given to be above 125° or at least close to the range of 100° to 150° 2Theta. Previous instructions were still useful for the basic setup of the machine and samples. However, the sample holders were intended for small silica disks of very light weight. A custom designed fixture was made (See Appendix A) to hold the heavier samples that were close to the maximum weight limit. Sample sizes were between 1/4 inch and 3/8 inch thickness to avoid getting false data from the stage.

During the XRD information seminar in 2014, several items were addressed on properly staging samples. Thickness of material was one of those topics from the seminar. Thin films typically have to consider using a "zero background" material to prevent scans from penetrating through the film and into the stage. The solid samples had a thickness that did not have that issue. Selection of optics was also a topic at the XRD seminar. As indicated in the general procedure (located in Appendix F), two sets of incident optics were used. Those optics were selected by the XRD equipment manager at UNCC and affirmed appropriate for use by a PANalytical's technical representative.

At the XRD seminar, the reason for changing from a 1/32° slit to a 1/2° slit was explained as a way to control intensity. A wide divergence slit gives more intensity but

less peak separation. Therefore, the 1/32° provided a reduction of intensity during beam alignment and, the 1/2° allowed for more intensity that was required for the higher angles. Also, a Soller slit—meaning a singular unit of several thin sheets—was on the diffracted side to minimize the divergence in the perpendicular plane to that of the divergence slit. Equipment available (and industry standard) was to use a 0.04 Rad Soller slit. Since stress evaluation was the main purpose and not composition identification, a specific type of scan had to be used. This is known as a stress measurement scan.

Use of the stress measurement scan was completed using one sweep of readings in only the positive direction. However, from conversations with PANalytical's technical representatives, only one direction sweep of readings does not allow a complete data set for calculating shear stress. As a result, the stress measurement scan was modified to include a positive and pseudo negative sweep so that shear stress could be calculated with the same data used calculate the normal stress. A detailed list of the general procedure with modifications and limited notation is provided in Appendix F. Use and adherence to the general procedure helped to insure the quality of the project in several aspects, including the repetition of the machining and scanning processes.

Data gathered from the stress measurement scans was analyzed using the Stress™ software as mentioned previously. Furthermore, the data gathered is included in the following section as well as in relevant appendices. Plots from data were visually analyzed to look for possible patterns that were expected to result from the different processes of traditional turning and modulated tool path. The following section provides the results from the various trial runs on the different surrogates as well as a discussion of how to interpret this data.

RESULTS

The following paragraphs detail the results obtained from various comparisons of traditional machining techniques with those of the experimental modulated tool path (MTP) machining process. As was mentioned in the previous section, the modulated tool path process that was eventually chosen for the study was ultimately determined only after several trials and iterations were conducted on the test materials. The finalized protocol for this process, with the machining codes for developing the modulated tool path, is included in the Appendix E of this paper. In addition to this technique comparison/contrast, an attempt was made to characterize the residual stress components for all of the materials tested as well as to surmise a correlation between the stresses determined and the influence from the non-traditional, modulated tool path process.

At the project on-set, weight compositional data for the project materials was determined by the use of the handheld XRF and recorded in Table 2. Composition was recorded in descending order of elements by weight percentage. Accuracy of composition was calculated by the XRF and also recorded as part of Table 2. Specific alloy composition could be a factor that affects the development of residual stresses and would be relevant for future comparisons.

Table 2: XRF results of material compositions.

Aluminum 6061-T6			**Inconel 718**			**Tool Steel M-42**		
Element	**%**	**±2σ**	**Element**	**%**	**±2σ**	**Element**	**%**	**±2σ**
Al	99.05	0.05	Ni	52.82	0.29	Fe	74.33	0.61
Cu	0.333	0.016	Cr	19.14	0.20	Mo	9.44	0.20
Fe	0.330	0.029	Fe	18.40	0.20	Co	7.81	0.44
Cr	0.113	0.016	Nb	5.04	0.06	Cr	4.16	0.25
			Mo	2.98	0.05	W	1.55	0.25
			Ti	1.07	0.12	V	1.06	0.21
Stainless Steel Nitronic 33			**Tantalum 97Ta3W**			**Zircaloy-4**		
Element	**%**	**±2σ**	**Element**	**%**	**±2σ**	**Element**	**%**	**±2σ**
Fe	65.33	0.22	Ta	95.4	0.58	Unable to obtain material.		
Cr	18.07	0.12	W	3.61	0.47			
Mn	12.26	0.16						
Ni	3.80	0.10						
V	0.135	0.031						
Mo	0.146	0.006						

Various sources were used to determine the typical standards for each material and those standards were shown in Table 3. While every element did not always fall into the tolerance for the standard values for each sample reading, the XRF was still able to identify the materials correctly to the presumed material composition given the possible error from use of the handheld XRF.

Table 3: Weight percent standards of material compositions.

Aluminum 6061-T6			**Inconel(R) 718**			**Tool Steel M-42**		
Element	**Wt. % Range**		**Element**	**Wt. % Range**		**Element**	**Wt. % Range**	
Al	95.8	98.6	Ni + Co	50.00	55.00	Fe	71.6	76.3
Cu	0.04	0.016	Cr	17.00	21.00	Mo	9.00	10.00
Fe	0.330	0.029	Fe	12.0	23.5	Co	7.75	8.75
Cr	0.113	0.016	Nb	4.75	0.06	Cr	3.50	4.25
Mg	0.8	1.2	Mo	2.80	3.30	W	1.15	1.85
Mn	0	0.15	Ti	0.65	1.15	V	0.95	1.35
Source:	[14]		Source:	[15]		Sources:	[31] & [32]	
Stainless Steel Nitronic 33			**Tantalum 97Ta3W**			**Zircaloy-4**		
Element	**Wt. % Range**		**Element**	**Wt. % Range**		**Element**	**Wt. % Range**	
Fe	65.33	0.22	Ta	97	97.5	Unable to obtain material.		
Cr	18.07	0.12	W	2.5	3	Zr	97.56	98.27
Mn	12.26	0.16				Fe	0.18	0.24
Ni	3.80	0.10				Cr	0.07	0.1
V	0.135	0.031				Sn	1.2	1.7
Mo								
Source:	[18]		Source:	[19]		Source:	[21]	

Further material properties that were gathered included hardness based on the Rockwell® hardness scales “B” and “C”. Materials were tested first on “C” scale to identify the appropriate scale as a safety measure to prevent damage to ball indenter for “B” scale. Data from hardness tests and typical standards were placed in Table 4. An interesting note is that the tool steel M-42 sample was not a hardened sample. Instead, the tool steel M-42 was machined in the annealed state (pre-hardening treatment).

Table 4: Hardness results and expected results.

Rockwell Hardness Test of Sample Material						
Test #	**Scale**	**Aluminum 6061-T6**	**Inconel® 718**	**Tool Steel M-42**	**Stainless Steel Nitronic 33**	**Tantalum 97Ta3W**
1	C	-19.6	9.1	13.8	23.1	-11.2
2	C	-	11.7	19.6	32.0	-
3	C	-	9.1	17.2	29.4	-
4	C	-	10.8	16.1	27.7	-
5	C	-	-	19.4	20.0	-
6	B	63.9	92.9	99.5	99.0	73.8
7	B	63.7	91.8	100.5	99.0	84.4
8	B	63.8	90.6	100.5	99.0	77.5
9	B	63.1	92.0	100.6	99.1	78.3
10	B	62.9	92.8	98.3	98.1	82.4
Average Hardnes	**C**	-19.6	10.2	**17.2**	**26.4**	-11.2
	B	**63.5**	**92.0**	**99.9**	**98.8**	**79.3**
Expected Hardness	C	-	31 to 45	20	-	-
	B	60	-	-	100 (max.)	50 to 93.5
Reference(s)		[14]	[15]	[33]	[18]	[19]

Sample logs included machine process information, such as insert and program used. Surface roughness was measured and recorded as a single value at the conclusion of each turning process. Records for each sample also included XRD data references. Data from the XRD were first plotted as data points of refraction intensities through the range of the scan. A secondary software program was then used to upload the intensity plots and to characterize material stress based on height and width of selected peaks. Subsequently, turning processes were then compared to determine if there was any change in material stress based upon the previous machining technique. The completed analysis included an array of data that related the experiments performed with the sample identification markings for text and artifact references. Figure 9 provides a simple model of the project components.

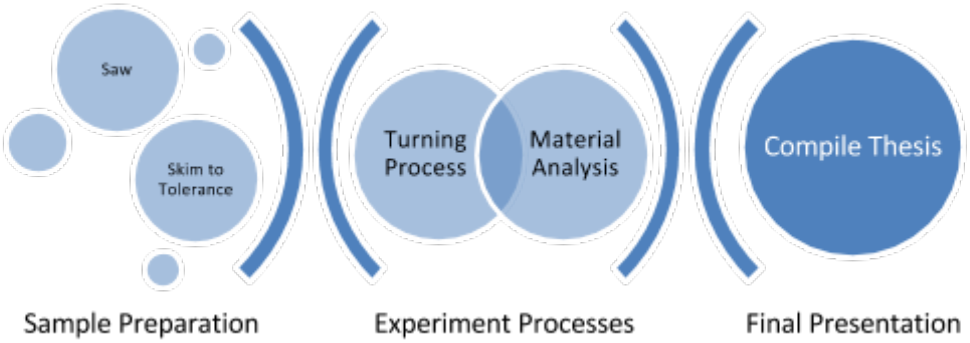

Figure 9: Project horizontal flow diagram.

One of the first goals of this project was to reduce the length of the chip and stop "bird nesting" as shown in Figure 10. Modulated tool path processes shortened the chips so that resulting chips were too short to become entangled. Figure 11 shows chips from a "Rough MTP" process that fell in a scattered and loose pattern that could easily be removed from the work area. Even shorter chips were created from the "Fine MTP" process. Chip length for the modulated tool path process proved to be related to each alloy's physical properties. Aluminum 6061-T6, typically considered a "gummy" material because of its elastic properties, had the longest chips for the fine modulated tool path (MTP) process. Inconel® 718 alloy chip length was intermediate, while Tantalum 97Ta3W had the shortest chips that ranged from 1/64 to ¼ inch, respectively.

Figure 10: Long coils of chips potentially lead to entangled "bird's nest" of contorted chips.

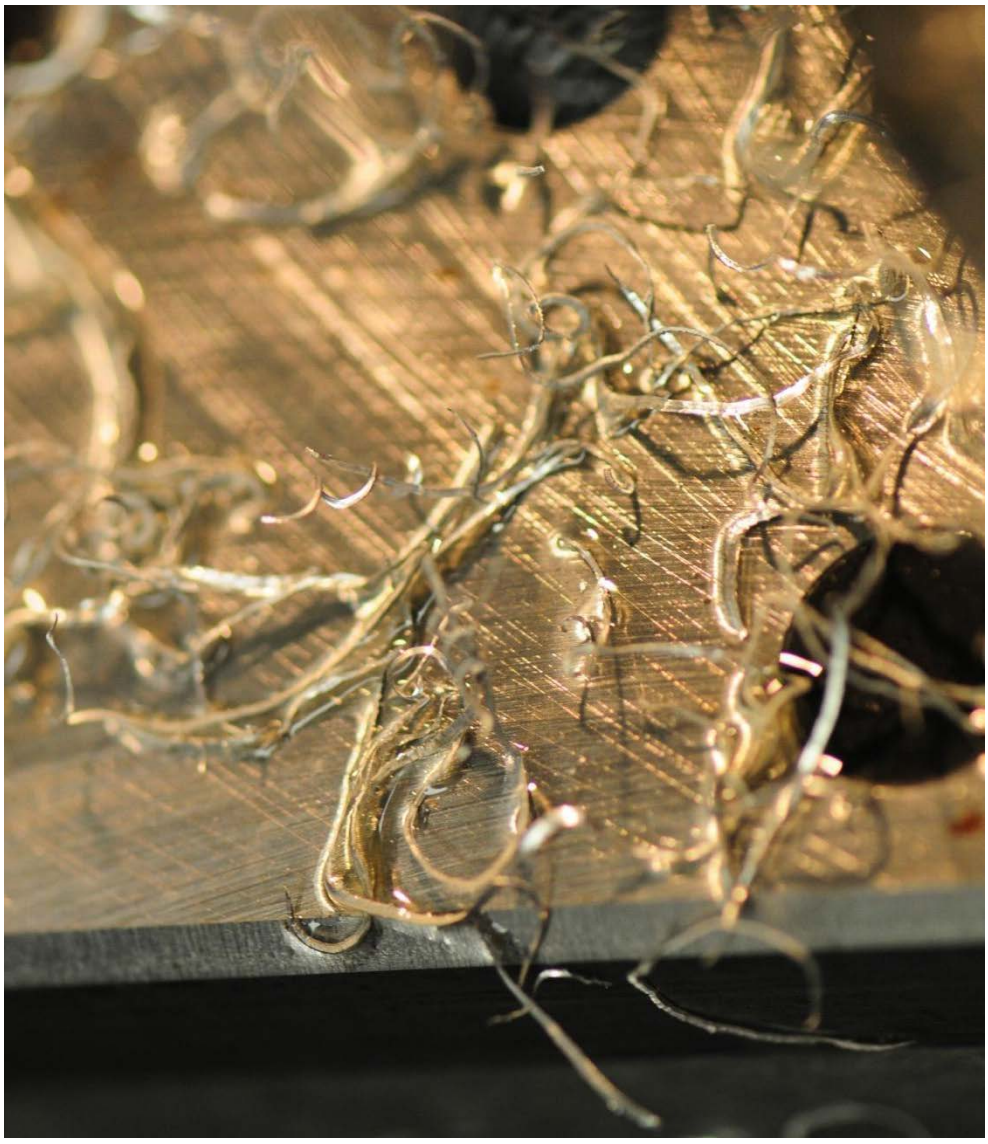

Figure 11: Chips from "Rough MTP" process are loose and can be removed easily.

Throughout the process, chips from trial runs and from the final processes were stored in glass containers shown in Figure 12. Material removed from turning processes were collected and samples of those collections are shown in following images to illustrate some of the differences between traditional turning and modulated tool path processes.

Figure 12: Assorted collection of chips from turning processes.

Using the following figures as examples of the comparison of the chips generated between modulated tool path and traditional turning processes, the goal of reducing chip length was clearly achieved. Resulting chips from the traditional turning process for aluminum 6061-T6, tool steel M-42, and Inconel® 718 all exhibited the tendency for chips to remain intact to create long coils. Collected samples of long coils displayed the tendency to remain entangled and intact after later opening the containers to photograph collected samples. The aluminum chips displayed in Figure 13 were from a traditional turning process.

Figure 13: Entangled coil-like chips as a result of traditional turning process used on aluminum sample.

Even though the tool steel was not useable for x-ray analysis with the copper tube because of fluorescence, the tool steel did exhibit the same problem of lengthy, continuous coil-like chips (Figure 14). Another material that had too much fluorescence with the copper tube during the x-ray diffraction process to be analyzed was the stainless steel nitronic 33 alloy. As a result of the traditional turning process, the stainless steel alloy nitronic 33 yielded long, coil-like and “stringy” chips (not pictured).

Figure 14: Tool steel M-42 coil-like chips resulting from traditional turning process.

Similar to the previous materials (aluminum 6061-T6, tool steel M-42, and stainless steel nitronic 33), the Inconel® 718 also tended to create long, coil-like chips. Collected chips from the traditional turning process were displayed in Figure 15.

Figure 15: Image showing continuous coil-like chips of Inconel® 718 wound into glass container for storage (from tradition turning).

Unlike the other materials shown previously, the tantalum 97Ta3W did not form lengthy strands of continuous, coil-like chips during traditional turning with a Z-axis depth of 0.010 inch. Instead, chips from the traditional turning process for tantalum 97Ta3W created short chips, rarely coiled more than one revolution before breaking (as shown in Figure 16). This trend was dissimilar to the machining of depleted uranium and was dissimilar to the machining of the previous surrogates mentioned previously. According to the project sponsor, a theory for the cause of tantalum's tendency to break chips into smaller segments might have been due to density of tantalum. However, the traditional turning of depleted uranium (a material of similar density to tantalum) tends to be more like the surrogate materials aluminum 6061-T6, Inconel® 718, tool steel M-42, and especially stainless steel nitronic 33.

Figure 16: Glass container and traditional turnings for tantalum 97Ta3W.

Use of the modulated tool path process for tantalum further reduced the chip length (Figure 17). A comparison of the relative difference in chip size was shown in Figure 18. For tantalum, there was not much benefit in using the modulated tool path process to reduce chip length.

Figure 17: Chips from fine MTP process yielded very fine chips (CNC code O30201.nc).

Figure 18: Tantalum chip samples from traditional turning (left) and "Fine MTP" process (right).

Of the surrogate materials analyzed, aluminum 6061-T6 and Inconel® 718 had machining characteristics similar to the depleted uranium based. The traditional turning yielded long, "stringy" or continuous, coil-like chips that could become entangled around previous sections of the chips or tools. As displayed by the images of chips from the modulated tool path, utilization of the modulated tool path process yielded shorter chips than traditional turning for all of the materials tested.

Chip length for the aluminum 6061-T6 was reduced to more manageable lengths of less than 50 mm (under 2 inches), with an average length around 25 mm (about 1 inch). Figure 19 was used to show that the new chip formations could be compacted more tightly into a container for disposal than the continuous, coil-like chips from traditional turning. Furthermore, when the chips are removed from the container, the

shorter chips did not remain entangled. The short length allowed for quicker separation of chips when needed.

Figure 19: Aluminum 6061-T6 chips from “Fine MTP” process.

Results from the modulated tool path process’ ability to reduce chip length for the desired goal of eliminating the machining hazard of entangling chips was also proven when used to make cuts into the Inconel® 718 alloy. As shown in Figure 20, the continuous, coil-like chips from the traditional turning continued to remain entangled after being removed from the glass container. Those samples were collected from long strands of chips from the traditional process that were not entangled prior to collection

and placement within the glass container. Therefore, an implication of this would be that longer chips have more points that may become entangled; thus, more points of entanglement would lead to the resistance of the chips to become untangled. A closer look at the chips from the "Fine MTP" process as shown in Figure 21 shows that the coil-like chips were reduce in diameter and in length.

Figure 20: Inconel® 718 chip samples from traditional turning (left) and "Fine MTP" process (right).

Reduction of diameter would aid in the ability to compact layers of waste materials (chips) more densely. Length reduction was the most desired benefit of change in chip formation. The reduced length allowed chips to be removed more easily because the shorter chips would not get entangled around objects nor become an entangled object too large to go through chip conveyors or auger systems for chip removal.

Figure 21: Closer examination of the Inconel® 718 chips comparing the continuous, coil-like chips from traditional turning (left) to the short segments of chips resulting from the use of the "Fine MTP" process (right).

Material stress was determined by the use of an XRD and Stress™ software. Each material had a peak that was identified from a 2Theta-Omega phase identification scan that ranged from about 20° 2Theta to about 150° 2Theta, which are detailed in Appendix B of this thesis. After cutting the material to the initial sample thickness with the band saw, XRD stress measurement scans were taken for each sample included in this study. Subsequent X-ray diffraction scans were completed for stress analysis after traditional turning and the fine modulated tool path processes for the materials listed previously.

X-ray diffraction scans using the 2Theta-Omega method provided a diffractogram that showed peaks that could be used to indicate material composition; however, this was mainly used to locate a high angle peak in the 100° to 140° 2Theta range for stress analysis. Aluminum had a high intensity peak at a low angle around 38° 2Theta as shown in Figure 22. Peaks at lower angles produce peaks that are more useful in identifying elemental composition rather than characterizing stress. To verify that the peaks were repeatable and related to material composition, several scans were taken across various ranges and overlaid to show that the peaks could be found at the same angles. This is also shown in Figure 22.

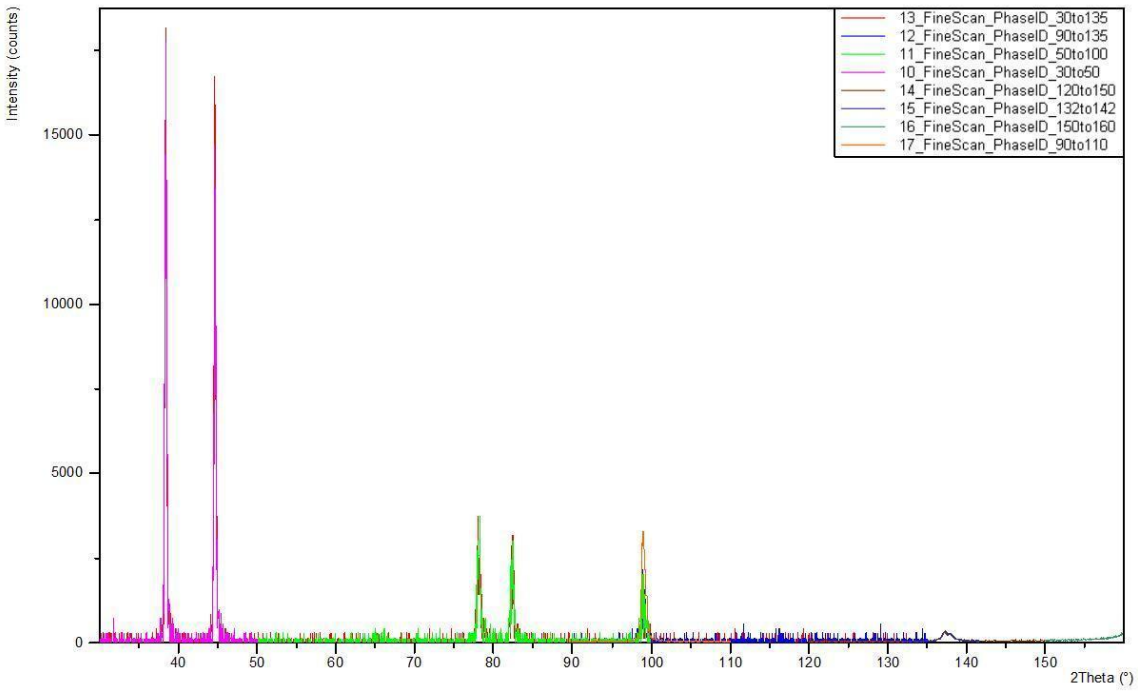

Figure 22: Supplemented phase ID scans from 20° to 150° 2Theta for aluminum 6061-T6.

For the aluminum 6061-T6 samples, the best peak for stress analysis was identified at 99° 2Theta, with the copper anode tube installed on the XRD. The isolated peak at 99° is shown in Figure 23. The high angle above 135° was difficult to scan at the

beginning of this project due to the old style attenuator that was originally on the XRD. The older style automatic attenuator protruded outward from the incident optics and limited the travel to a maximum of 130° 2Theta. Later in the project, the attenuator was removed and replaced with a newer version that could be mounted so that the attenuator did not limit the detector travel in the 2Theta range. The approximate peak at 99° seemed to be the optimal choice because the intensity in units of counts was significantly greater in magnitude as compared to the net heights of peaks from the other materials listed later in this section.

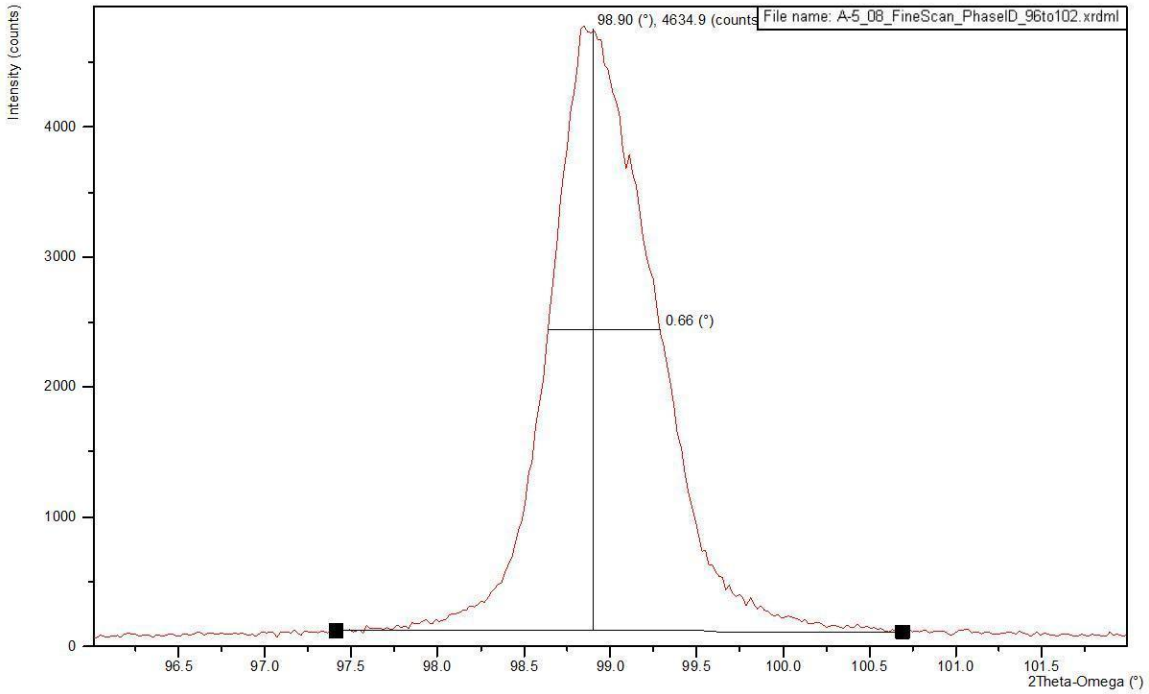

Figure 23: Peak at 98.90° identified for stress analysis of aluminum 6061-T6.

Also, after each turning process, a stress measurement scan was made using the XRD. Each stress scan had multiple absolute scans (See Figure 24) which were used to evaluate the stress.

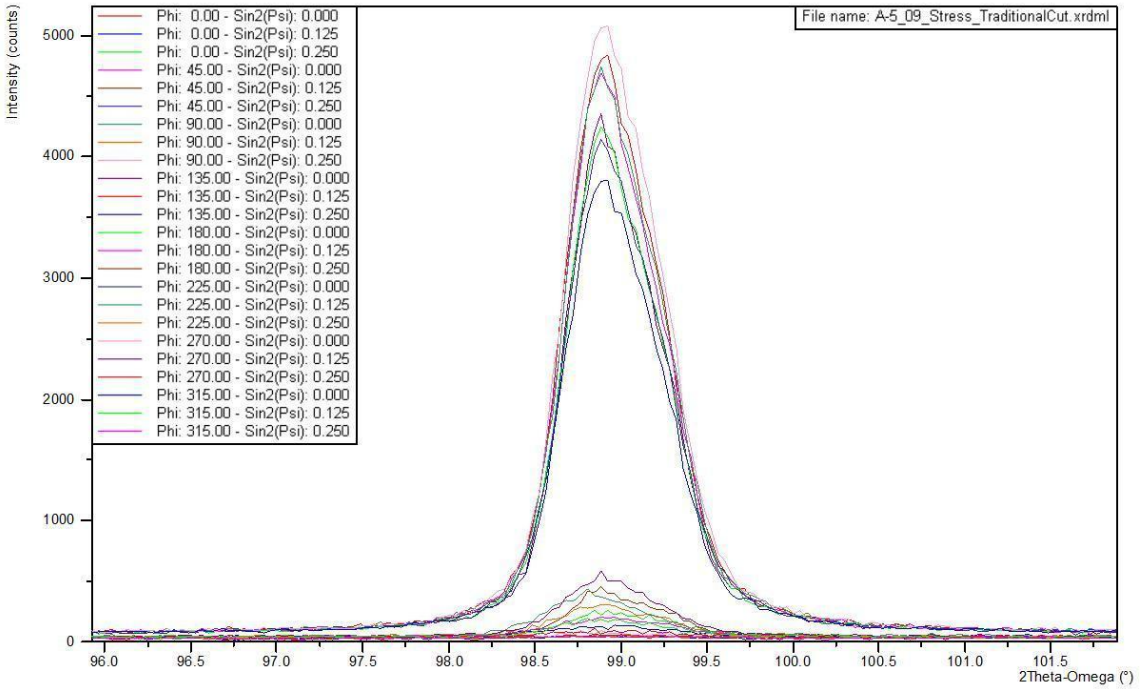

Figure 24: Stress measurements shifts and rotations displayed across 2Theta axis versus intensity for aluminum 6061-T6.

Following the same format, a scan from 20° to 155° 2Theta was performed for Inconel® 718. Utilizing the capabilities of the Stress™ software, all major peaks could be identified and marked along the 2Theta axis as shown in Figure 25. The identified peak around 137.5° 2Theta was too close to the peak at 145° 2Theta, and both had to be re-scanned (Figure 26). The associated Stress™ software isolated and analyzed the peak at 137.5° after each process, using the same stress measurement scan as the aluminum and tantalum sample. However, the Inconel® 718 required a slower step time to attain adequate peak net height for stress measurements, with the resulting scan displayed in Figure 27.

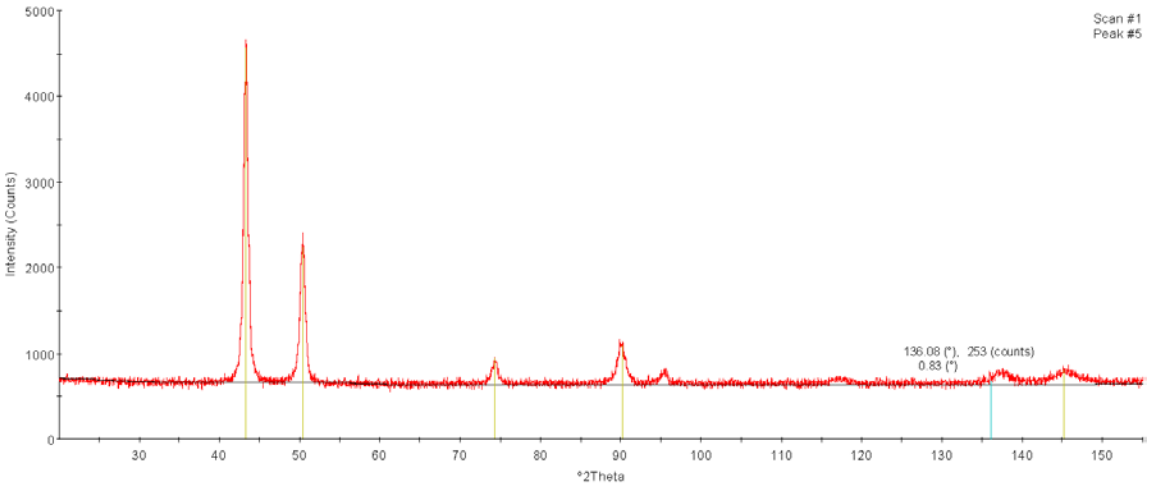

Figure 25: Phase identification scans from 20° to 155° 2Theta for Inconel® 718.

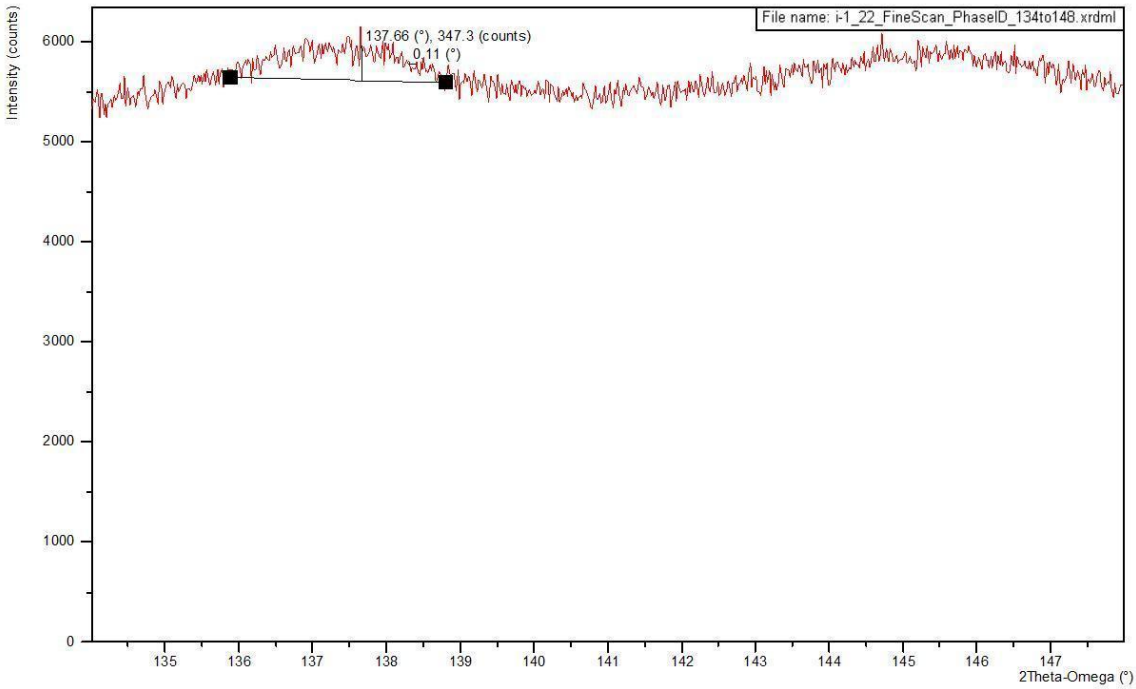

Figure 26: Peak at 137.66° 2Theta identified for stress analysis of Inconel® 718.

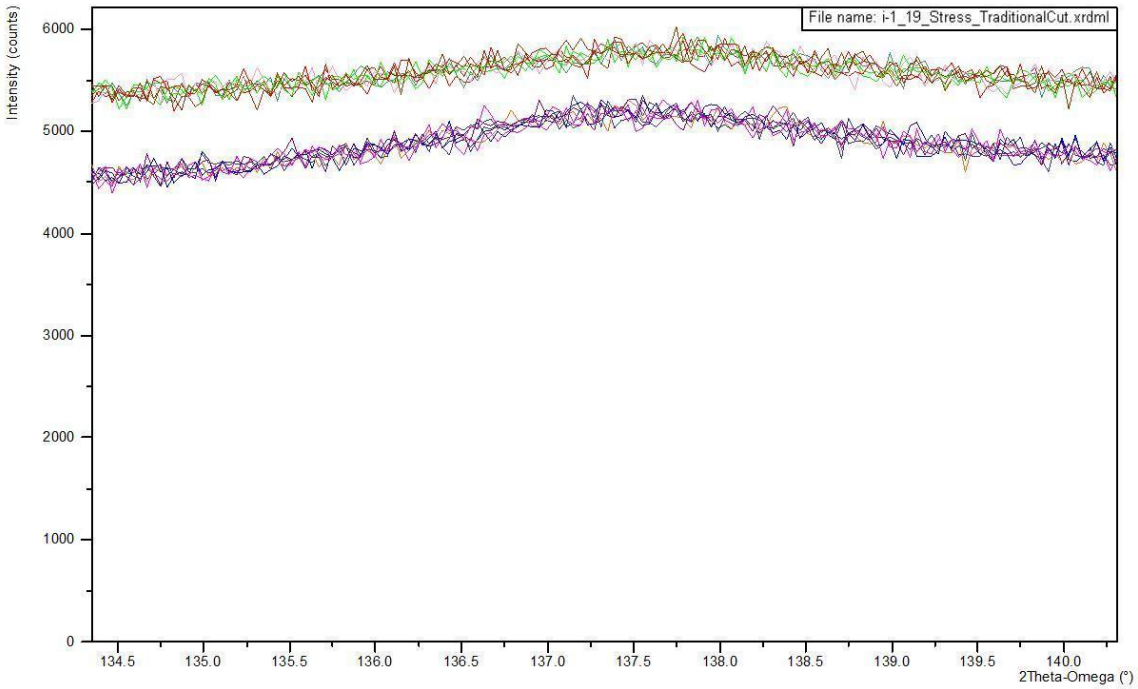

Figure 27: Stress scan for Inconel® 718 of identified peak.

Tantalum was also analyzed using the same methodology. A 2Theta-Omega "Phase ID" scan was performed (Figure 28) and the isolated peak (Figure 29) was scanned using the stress measurement scan (Figure 30).

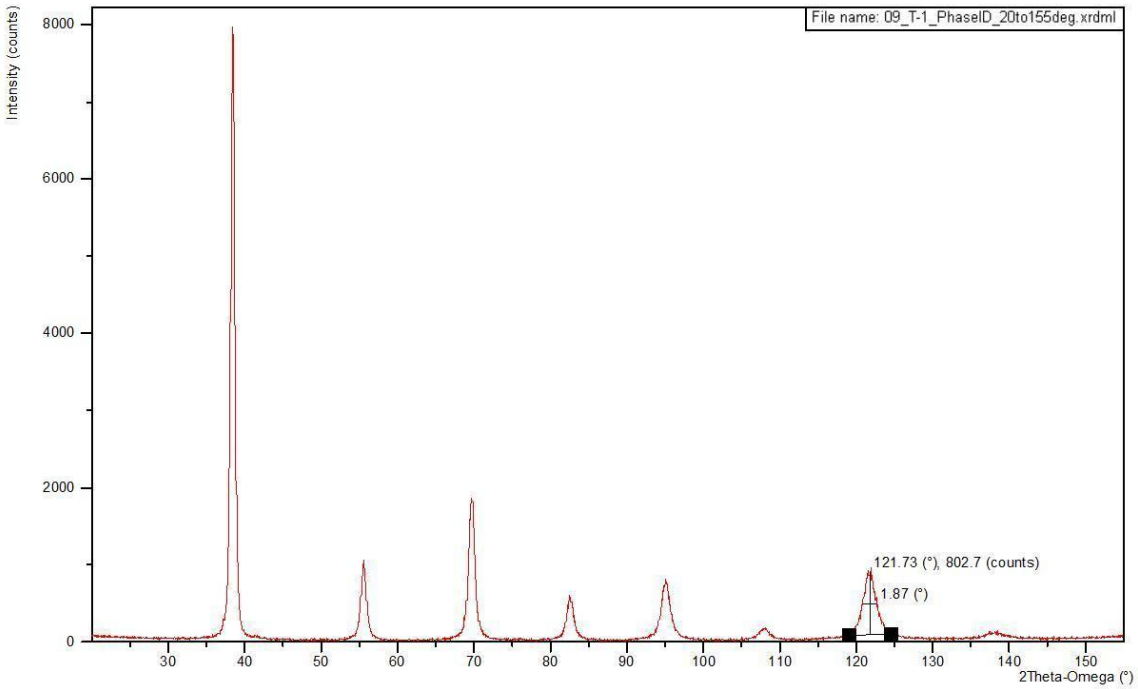

Figure 28: Phase identification scan (2Theta-Omega) from 20° to 155° 2Theta for tantalum 97Ta3W.

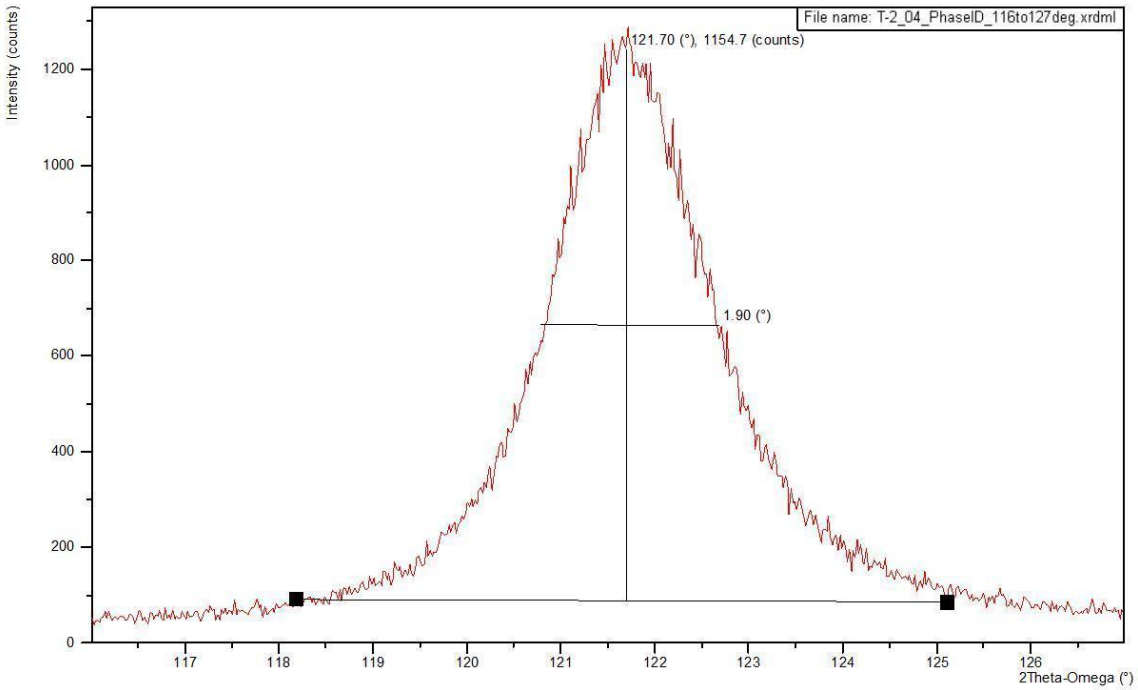

Figure 29: Peak identified at 121.70° 2Theta for tantalum 97Ta3W.

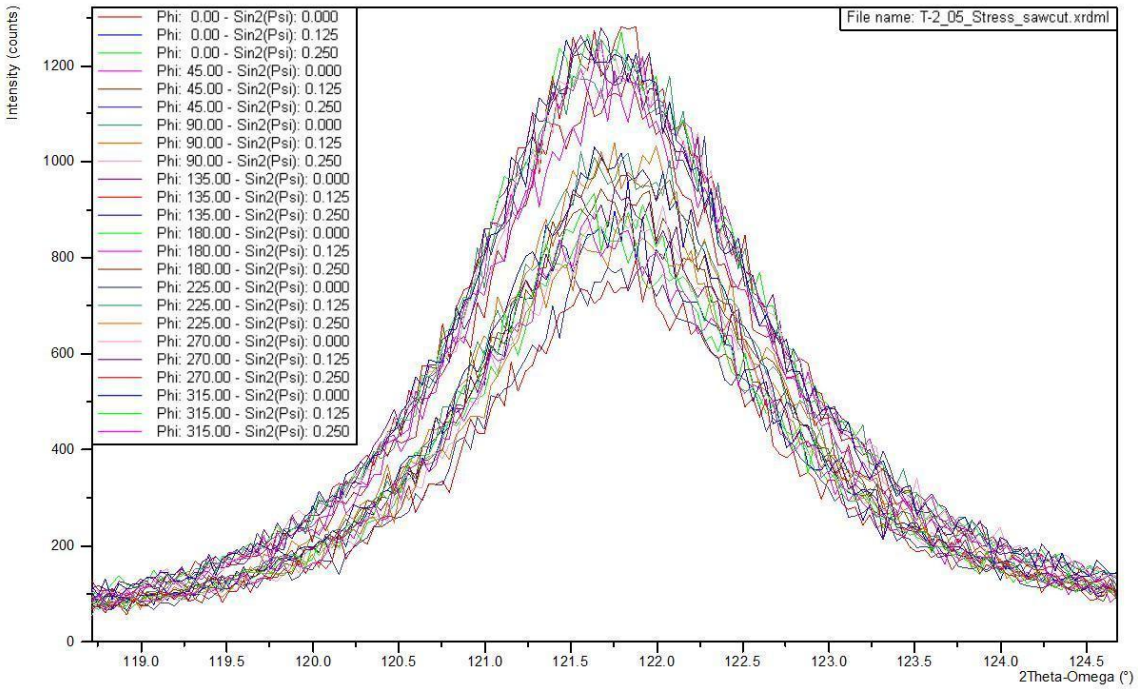

Figure 30: Stress scans used to evaluate peak at 121.70° 2Theta for tantalum 97Ta3W.

Scans after each process were analyzed by the use of Panalytical's Stress™ software. As shown previously, the data gathered from the stress scans included the level of intensity (measured in counts) along the 2Theta-Omega range (measured in degrees). Within the accompanying software, multiple automated sequences of data refinement occurred. Some of those refinements included background level identification, Lorentz-Polarization, K-alpha2-stripping, and other automated estimations. Background identification was important to determine the net height of identified peaks. As a method of cleaning up the plotted points, Lorentz-Polarization was used. K-alpha2-stripping was completed automatically by the accompanying software for further data refinement based on the anode type. As mentioned in the procedure located in Appendix F, a copper anode was used for this experiment.

Stress scans were a series of positive and pseudo negative sweeps across the 2Theta-Omega range as indicated in Appendix F. After each sweep, a shift in the Phi axis of 45° was made before the next scan. Of those scans, there were four steps in the Phi axis. For each of those scans, the peak was identified. Examples of the peak position search for the aluminum 6061-T6 are shown in Figure 31, and a peak search table is provided in Appendix C of this paper (Table 7).

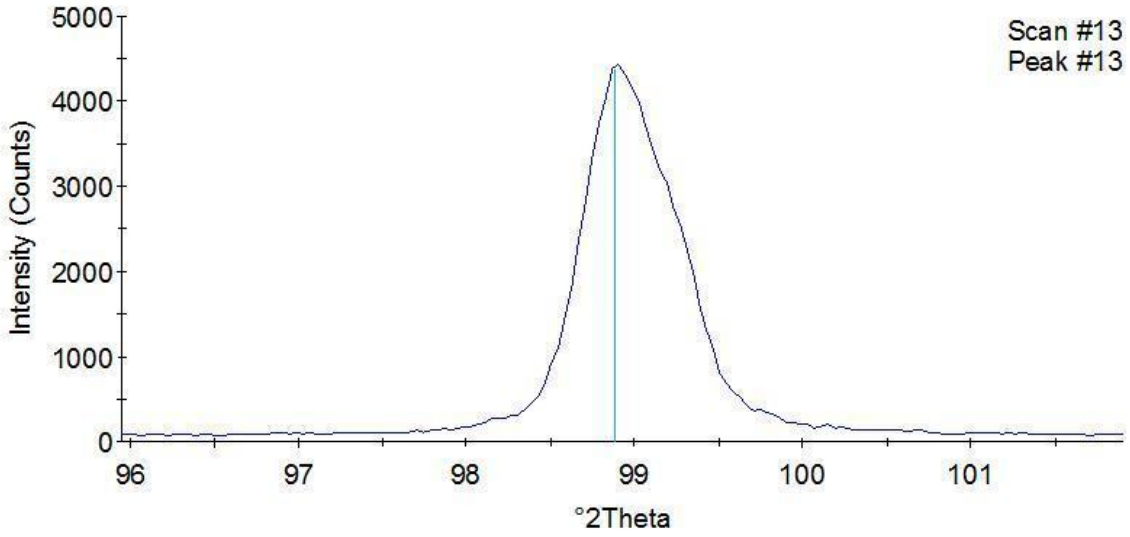

Figure 31: Scan number 13 of 24 in series of stress scan set for Aluminum sample A-5 with saw cut surface prior to traditional turning.

Data interpretation for the stress analysis in the accompanying software had included the specification of the material type and material properties to calculate the strain-free parameters as a basis for stress (see Figure 32). Data for the material database was input as indicated in the Theory and Literature Review of this thesis. That data included cell array structure, Young's modulus, *E*, and Poisson's ratio, *v*. Each material had its own data as determined by the referenced sources (Table 1).

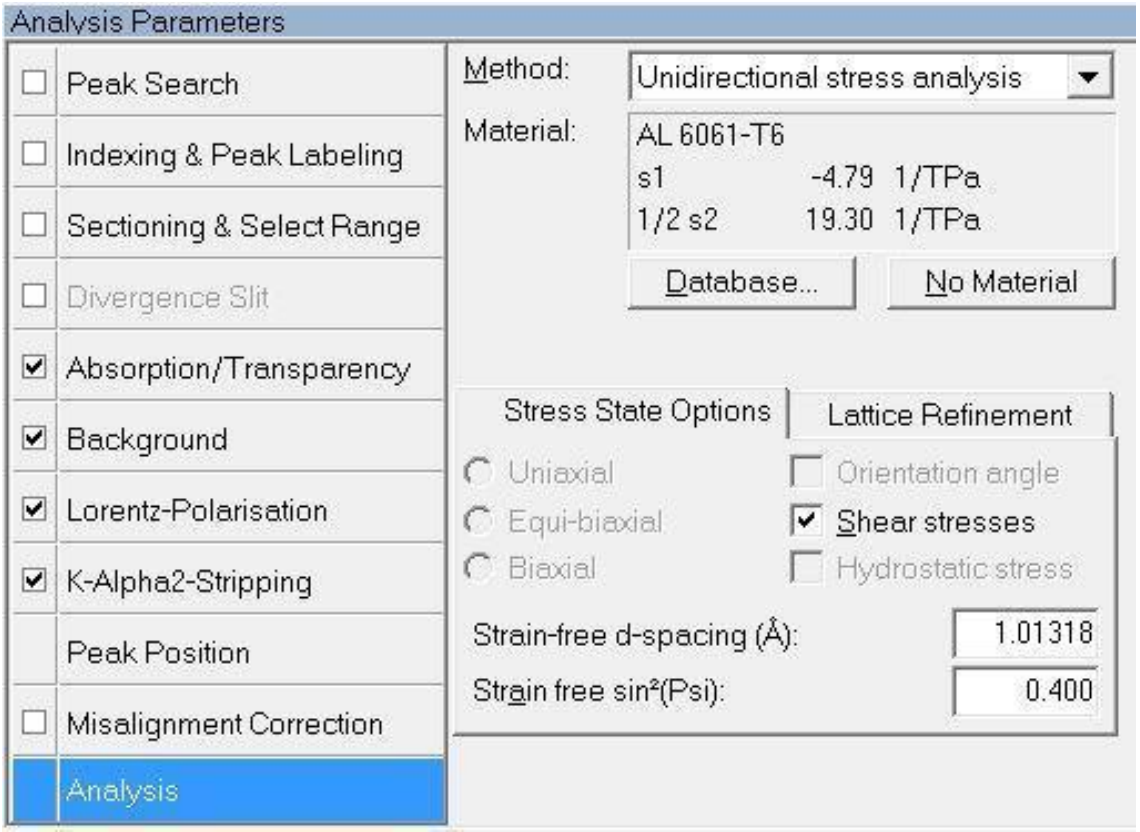

Figure 32: Image illustrating one of the interfaces for analysis of samples.

Specific stress data from those scans can be found in Appendix C. Plots from the stress data are illustrated in Appendix D. In general, the plots for stress did not prove the theory that a specific type of stress was induced based on the turning process as illustrated by the scatter plots in following figures. The scatter plots were grouped by the rotation of the phi axis (i.e., rotation about the center of the mounting stage). Those figures showed stress as calculated per rotation of phi to compare measured stress versus process type.

Each stress type was given a specific color and symbol to help identify possible patterns. Sigma (normal) stress data points were red colored triangles. Tau (shear) stress data points were green colored circles. The software program Stress™ calculated a

summation of the stresses in two perpendicular directions to determine Sig11+Sig22. Likewise, the Sig11+Sig22 used a blue colored square to mark data points on the scatter plots. Units of stress for the vertical axis were MegaPascals (MPa). Positive values above the horizontal line at zero indicated tensile stresses and negative values indicated compressive stresses for the Sigma (normal) stress. Sign convention for Tau (shear) stresses indicated direction of rotation as being positive or negative as shown in Figure 33.

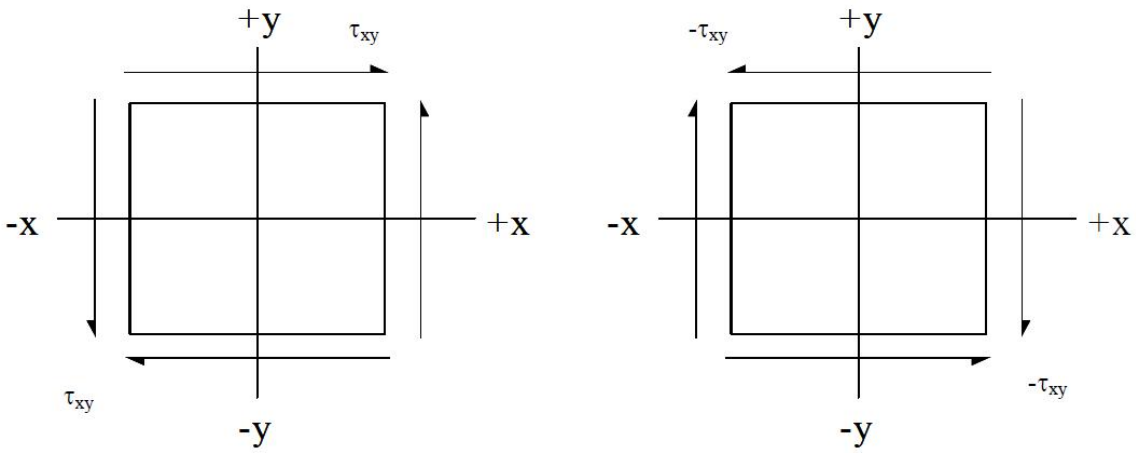

Figure 33: Shear stress sign convention shows positive shear on left and negative on right. (Image courtesy of National Physical Laboratory [34].)

After each cut of 0.010 inch off of the face of the sample, a different set of lattice layers was analyzed for each cutting process type. In theory, the different layer should allow stresses to have been analyzed significant only to each cutting process. With each material and each cutting process analyzed at phi orientations, the data illustrated that the Sig11+Sig22 was a good summation of the Sigma (normal) and Tau (shear) stresses. Each plot allowed for analysis of the different orientations of the sample. The expectation was to find a significant trend by these comparisons to better understand stresses developed based on turning process used.

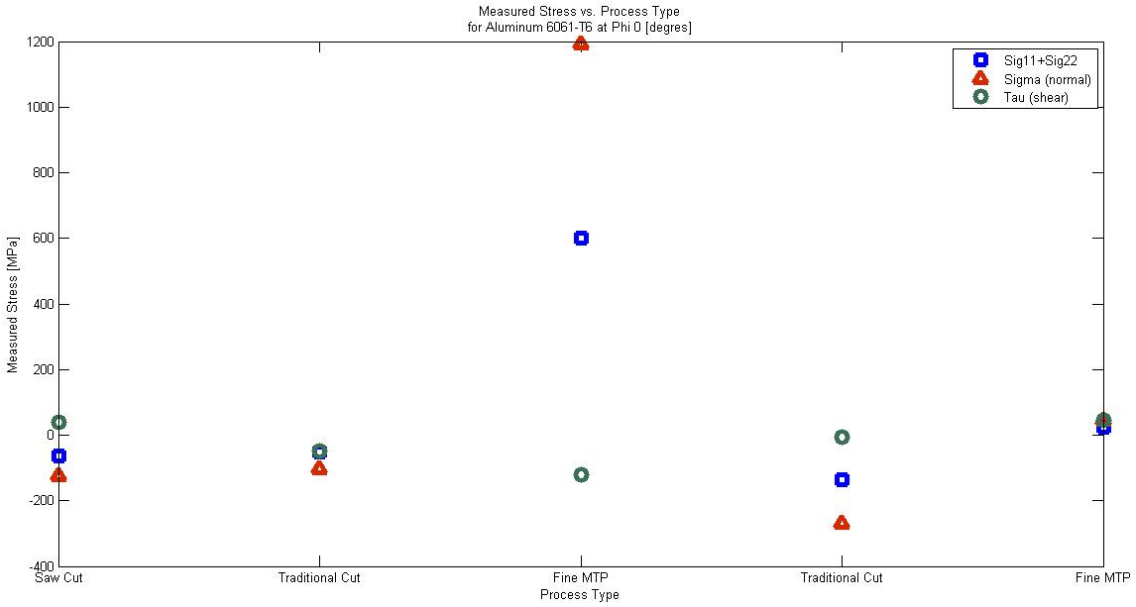

Figure 34: Scatter plot of stress data for aluminum 6061-T6 at phi rotation of 0 degrees.

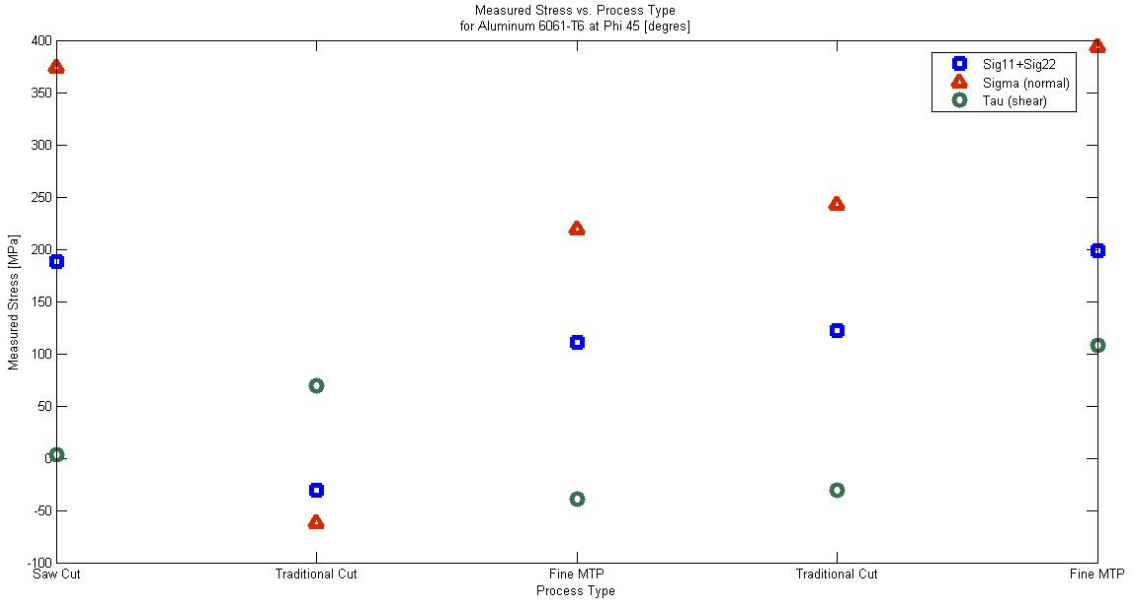

Figure 35: Scatter plot of stress data for aluminum 6061-T6 at phi rotation of 45 degrees.

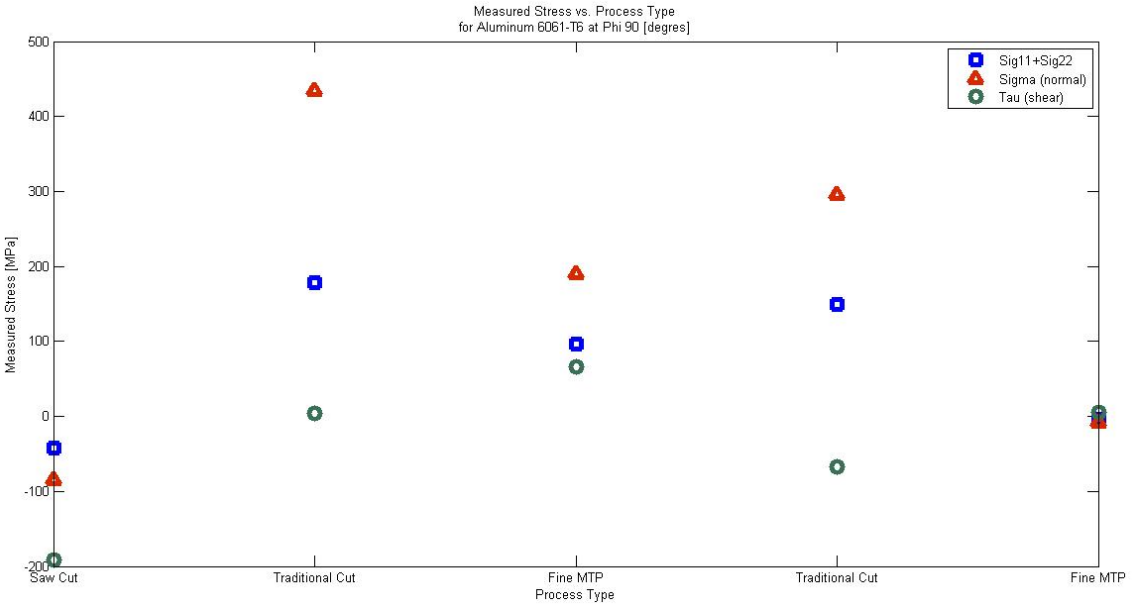

Figure 36: Scatter plot of stress data for aluminum 6061-T6 at phi rotation of 90 degrees.

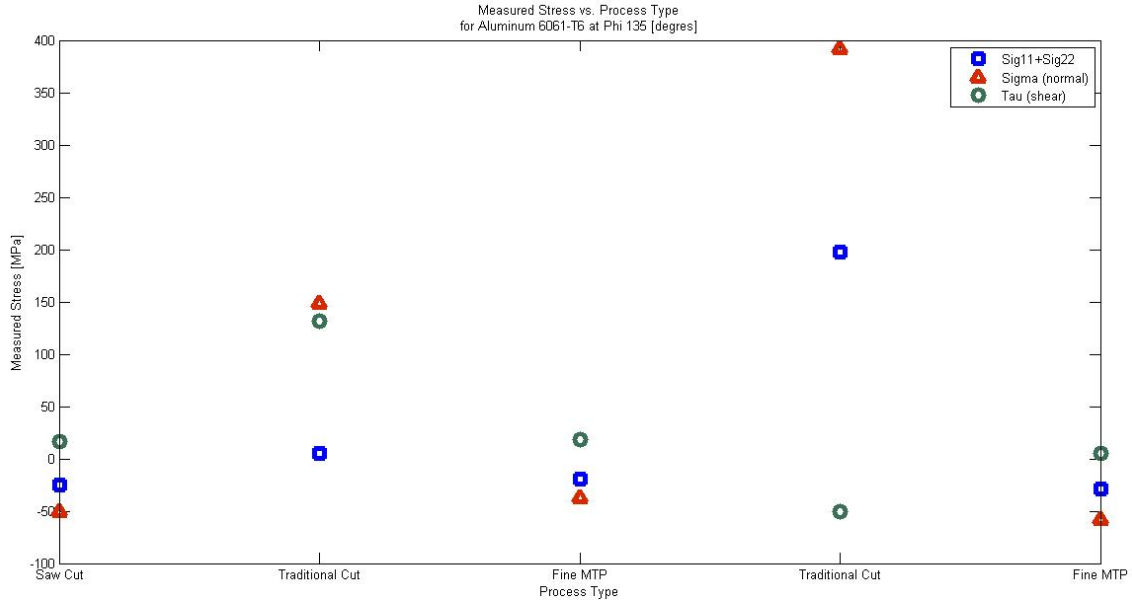

Figure 37: Scatter plot of stress data for aluminum 6061-T6 at phi rotation of 135 degrees.

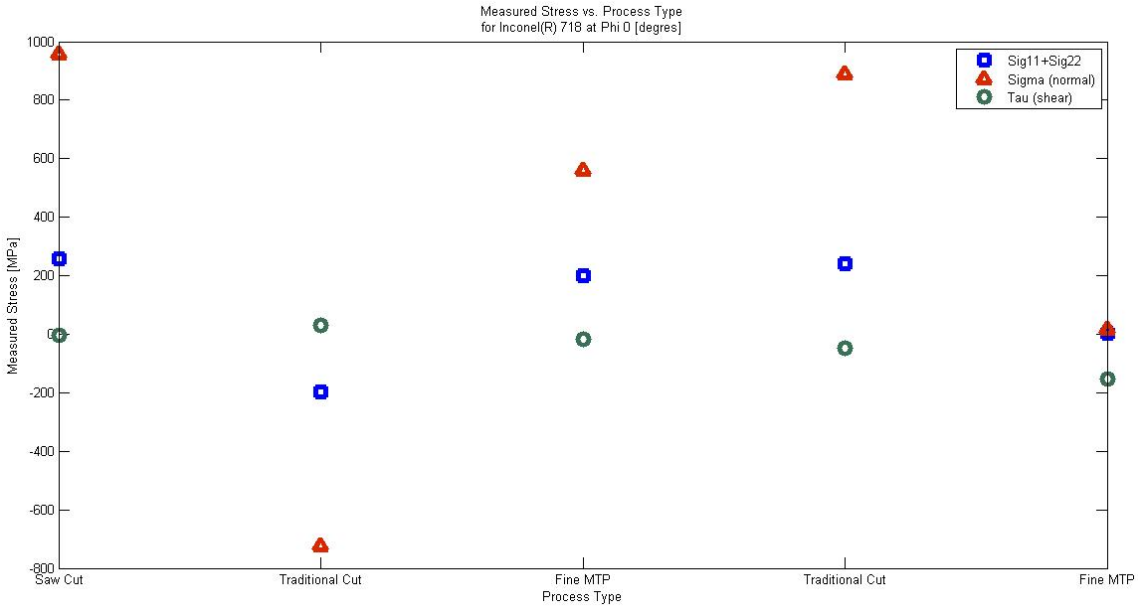

Figure 38: Scatter plot of stress data for Inconel® 718 at phi rotation of 0 degrees.

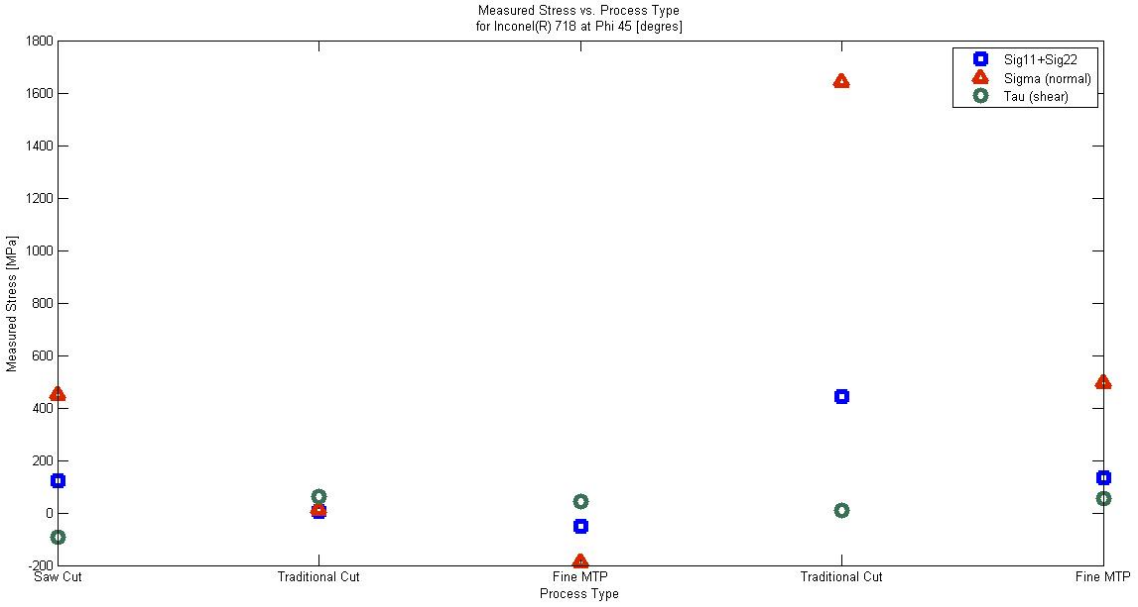

Figure 39: Scatter plot of stress data for Inconel® 718 at phi rotation of 45 degrees.

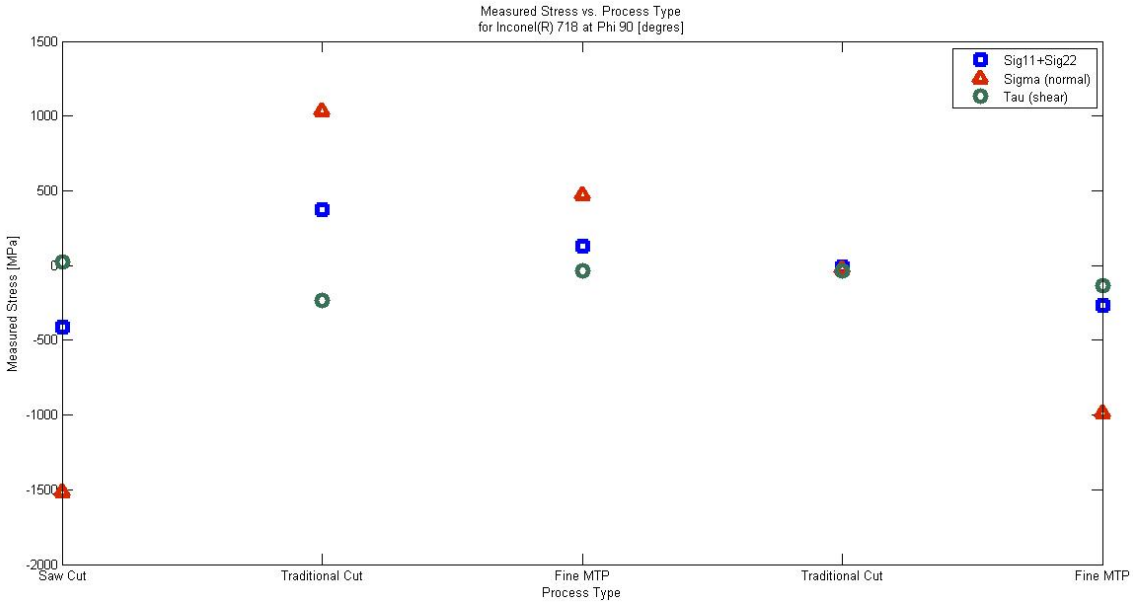

Figure 40: Scatter plot of stress data for Inconel® 718 at phi rotation of 90 degrees.

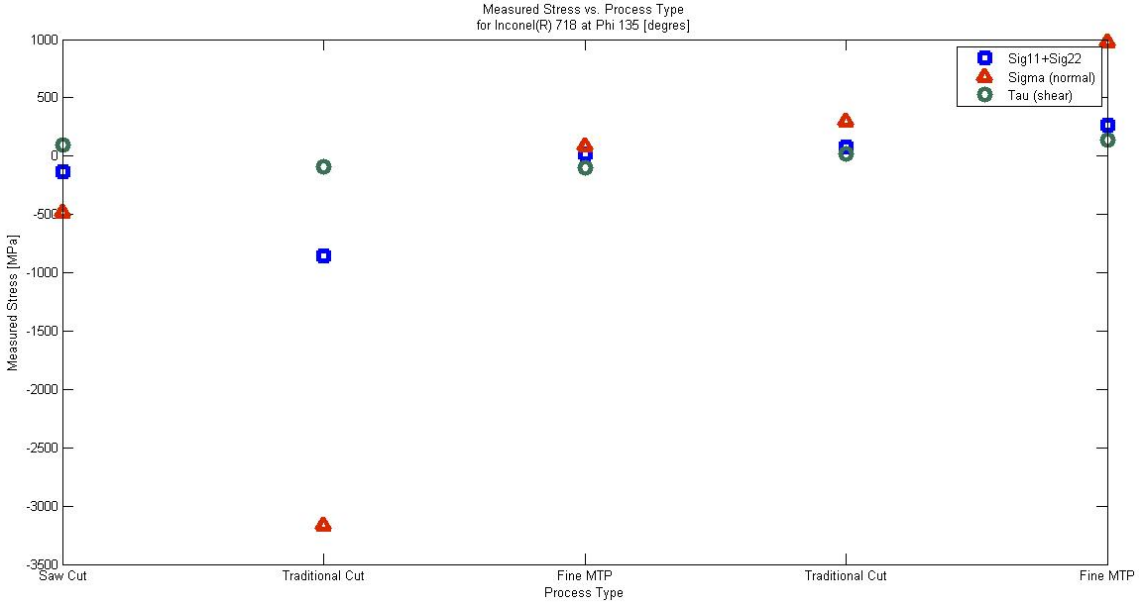

Figure 41: Scatter plot of stress data for Inconel® 718 at phi rotation of 135 degrees.

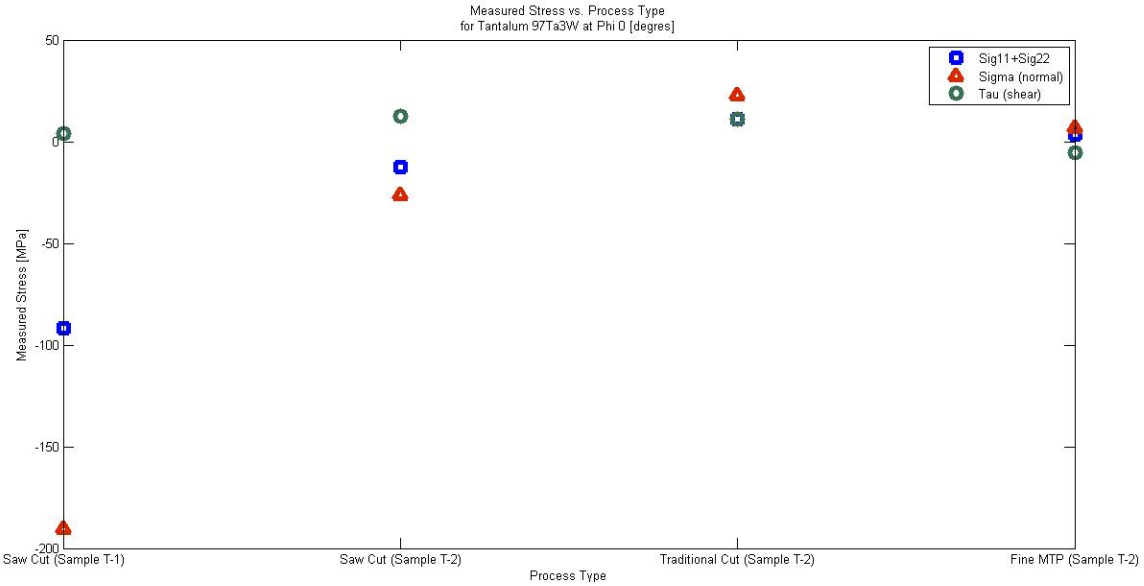

Figure 42: Scatter plot of stress data for tantalum 97Ta3W at phi rotation of 0 degrees.

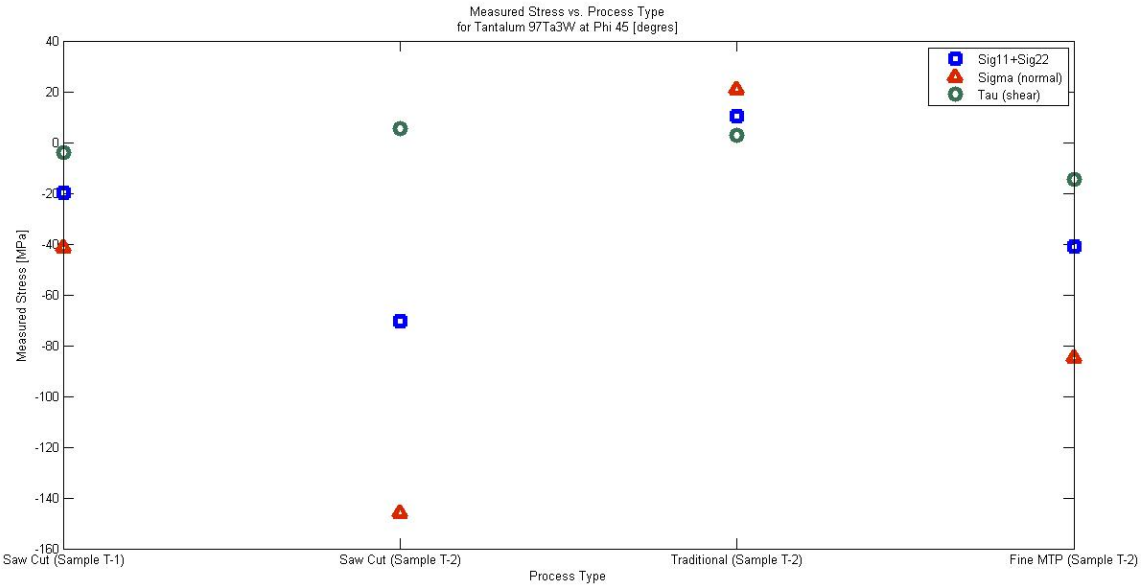

Figure 43: Scatter plot of stress data for tantalum 97Ta3W at phi rotation of 45 degrees.

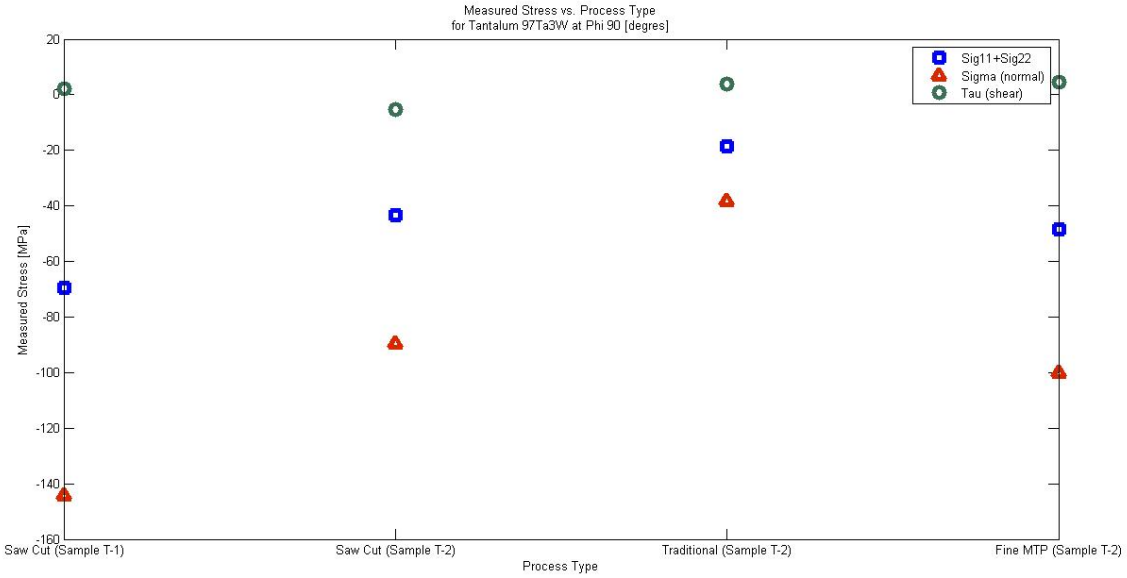

Figure 44: Scatter plot of stress data for tantalum 97Ta3W at phi rotation of 90 degrees.

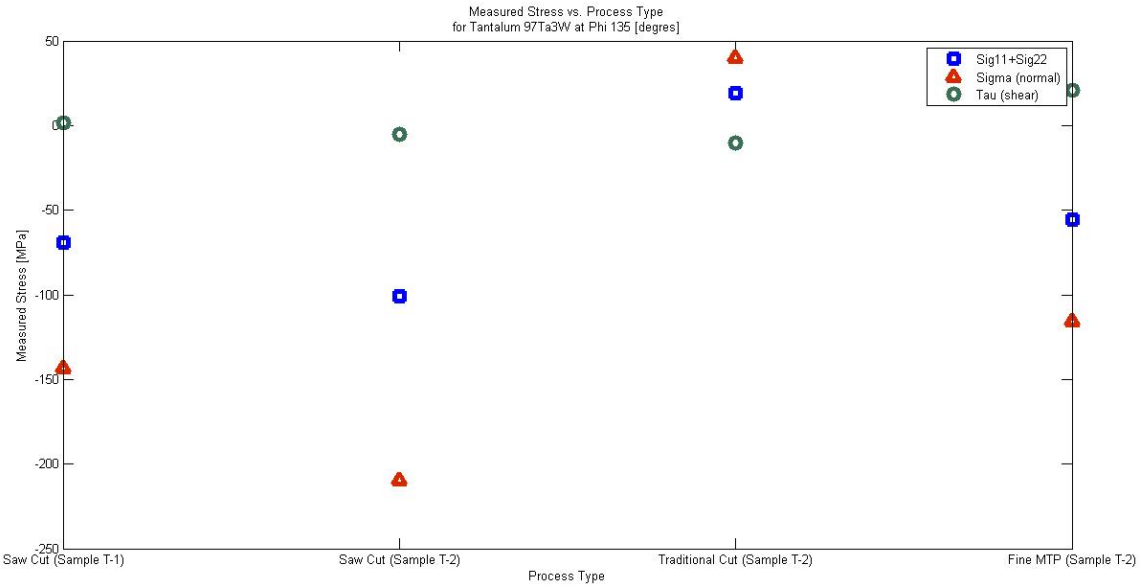

Figure 45: Scatter plot of stress data for tantalum 97Ta3W at phi rotation of 135 degrees.

Based upon the Stress™ software calculations for stress, no clear pattern was observed. Instead, a different and more basic form of data was evaluated as a means to characterize the residual stresses imparted by the modulated tool path process on the test

materials. Since stress was calculated using relations of cell structure and material properties, the d-spacing could be used as a basic comparison. Helpful results to determine a pattern relating the possible stresses to turning processes was sought using the analysis of the strain-free d-spacing. The strain-free d-spacing was determined by calculation in PANalytical's Stress™ software from the stress measurement scans and material data shown in Theory and Literature Review of this thesis. Plots for d-spacing were plotted using a line graph format. A blue line is plotted to show progression of the sample through the different cutting phases:

1. Saw Cut
2. Traditional Turning (First iteration)
3. Fine MTP (First iteration)
4. Traditional Turning (Second iteration)
5. Fine MTP (Second iteration)

To illuminate the relative similarity between first and second iterations, a connecting line illustrates the change per process type. A green, dashed line with triangles at each end indicates the traditional turning processes. Likewise, a red, dotted line with diamonds at each end indicates the fine MTP processes. These plots are shown for samples aluminum 6061-T6 in Figure 46 and Inconel® 718 in Figure 47.

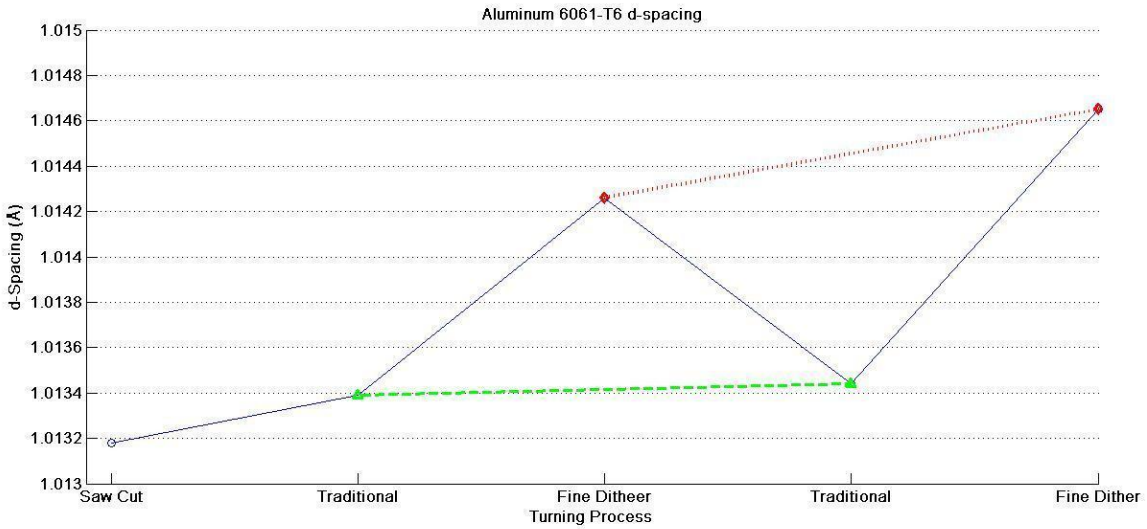

Figure 46: Strain-free d-spacing plotted linearly with progression of sample operations.

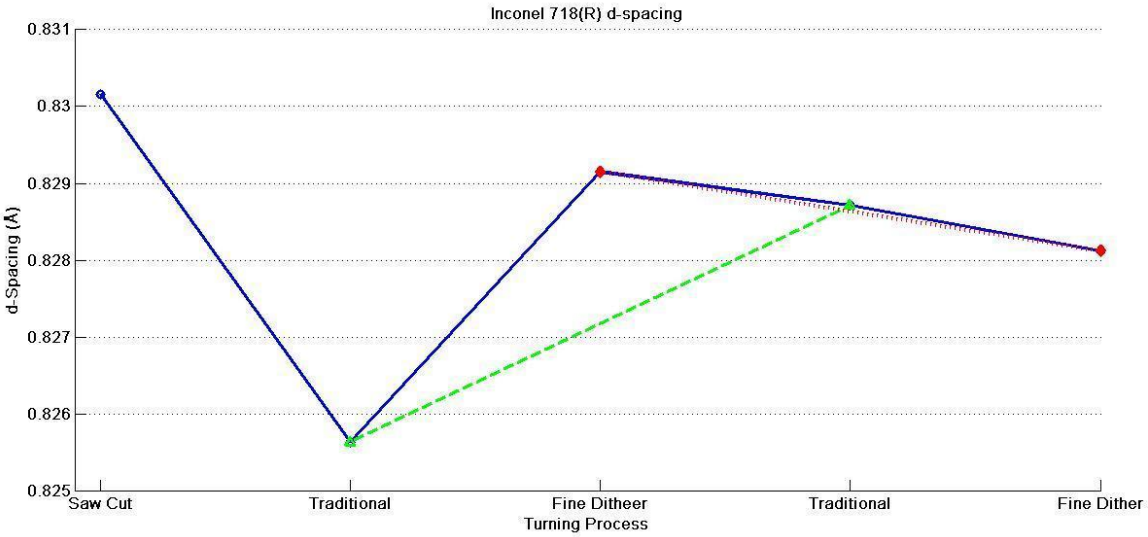

Figure 47: Strain-free d-spacing plotted linearly with progression of sample operations.

The process of progress was different for tantalum because sample T-1 had to be switched for T-2 due to material thickness. In this instance, the limiting factor was that sample T-1 was too thin to be turned with existing lathe clamping jaws; thus, the process progression for tantalum was as follows:

1. Saw Cut (sample T-1)
2. Saw Cut (sample T-2)
3. Traditional Turning (sample T-2)
4. Fine MTP (sample T-2)

One unique aspect of this change was that two samples were analyzed after the same process. The resulting d-spacing for both samples after saw cut operations were very similar as shown in Figure 48.

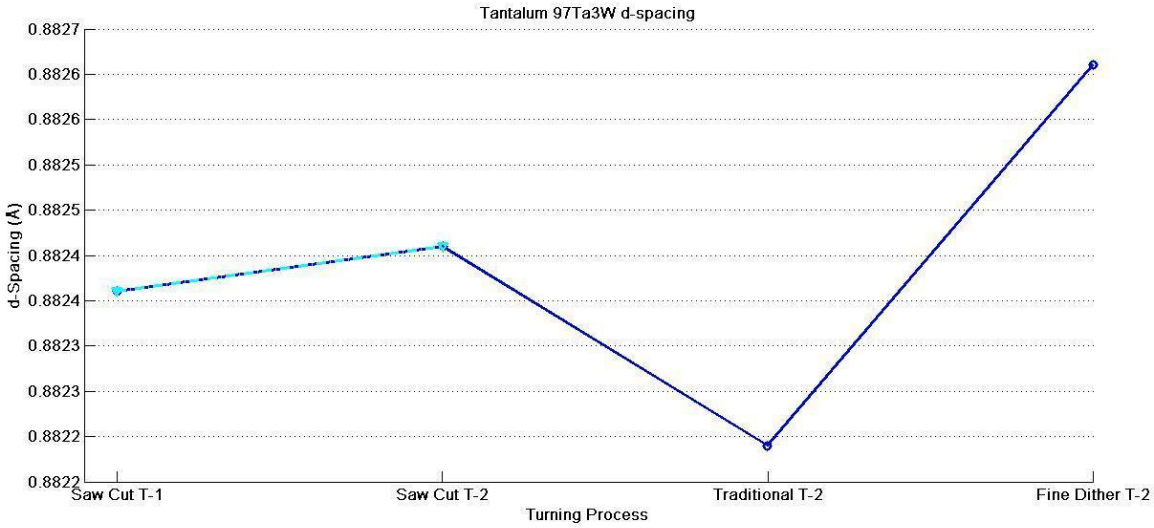

Figure 48: Strain-free d-spacing plotted linearly with progression of sample operations.

Using the $\sin^2\psi$ method, the plot of the d-spacing versus $\sin^2\psi$ provides an efficient method of determining the stress type exhibited [23]. The slope of the line in the d-spacing versus $\sin^2\psi$ plot was used to calculate the stress [23]. An upward slope (moving from left to right along $\sin^2\psi$ axis) indicates a tensile stress. Accordingly, a downward sloped indicates a compressive stress, numerically shown with a negative sign (-). When zero strain exists in measured axes, a linear behavior in the relation of the d-spacing versus $\sin^2\psi$ would exist [35]. This linear behavior was estimated by the

accompanying stress software. However, the components of the of the positive and pseudo negatives sweeps were non-zeros. Since the scanned samples were solids and not powders, the strain values were non-zeros. Therefore, the values of d-spacing measured along the positive and pseudo negative sweeps of the scan would be different causing a split in the behavior across the estimated linear relation known as "ψ-splitting" [35]. Psi-splitting was seen in all of the d-spacing versus $\sin^2\psi$ plots.

Analysis of the d-spacing versus $\sin^2\psi$ plots, referred to in this document as stress plots, provided additional information in understanding the stress in the sample materials. As a general method of interpretation, the relative magnitude of the shear stress compared to the magnitude of the normal stress can easily be determined by quickly analyzing the width of the "ψ-split" (i.e., the open end of parabola shaped curve). Tensile stresses were indicated by positive slopes of the d-spacing versus $\sin^2\psi$ plots which indicates increase in d-spacing. Conversely, compressive stresses were indicated by negative slopes of the d-spacing versus $\sin^2\psi$ plots which indicates decrease in d-spacing. The stress plots include each of the four phi orientations from 0° to 135° in 45° increments. The phi axis was the rotation about the axis perpendicular to the face of the scanned samples.

With the previous information in mind, Figure 49 was not clear in providing an initial trend or constant for the aluminum 6061-T6. Instead, compressive and tensile stresses were seen at possibly random groupings. Due to the fact that several crystalline structures were within the scanned rectangular area, it was possible that a different set of crystalline structures were scanned at each orientation. In the saw cut state, the stress scans did provide what appeared to be a fairly consistent range for the ratio of the shear stress to the normal stress for the different phi rotations.

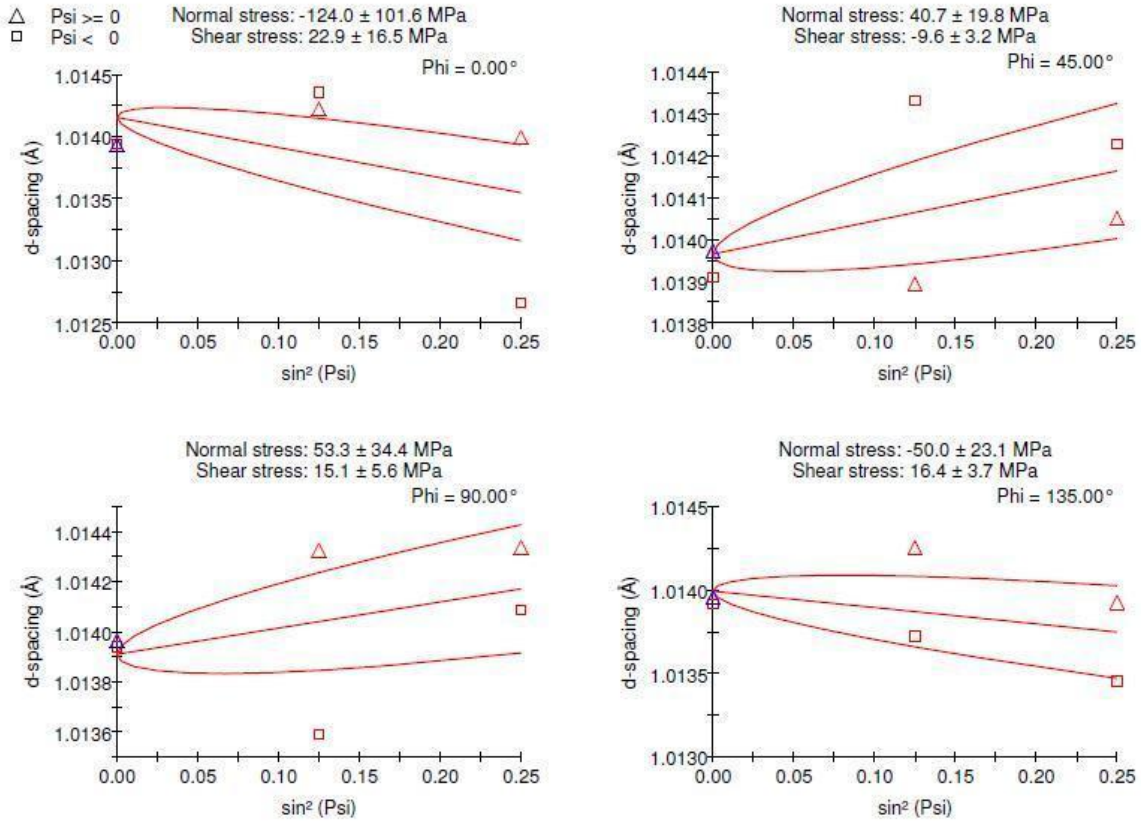

Figure 49: Stress plots of d-spacing versus $\sin^2\psi$ for aluminum 6061-T6 with saw cut surface.

The visual relative range of shear stress ratio to normal stress did not remain consistent for the phi orientations for the traditional turning or the fine MTP process. Figure 50 and Figure 52 did support the idea that a specific process would tend to have certain trends for stress. Even though the magnitudes changed, the relative shear stress was small for phi orientations of 0°, 45°, and 90°. At 135° rotation in the phi axis, the relative shear value for both tradition turning operations of the aluminum 6061-T6 were more pronounced than the previous three orientations of phi. The slopes of the two traditional turning operations did not provide a clear trend for interpretation.

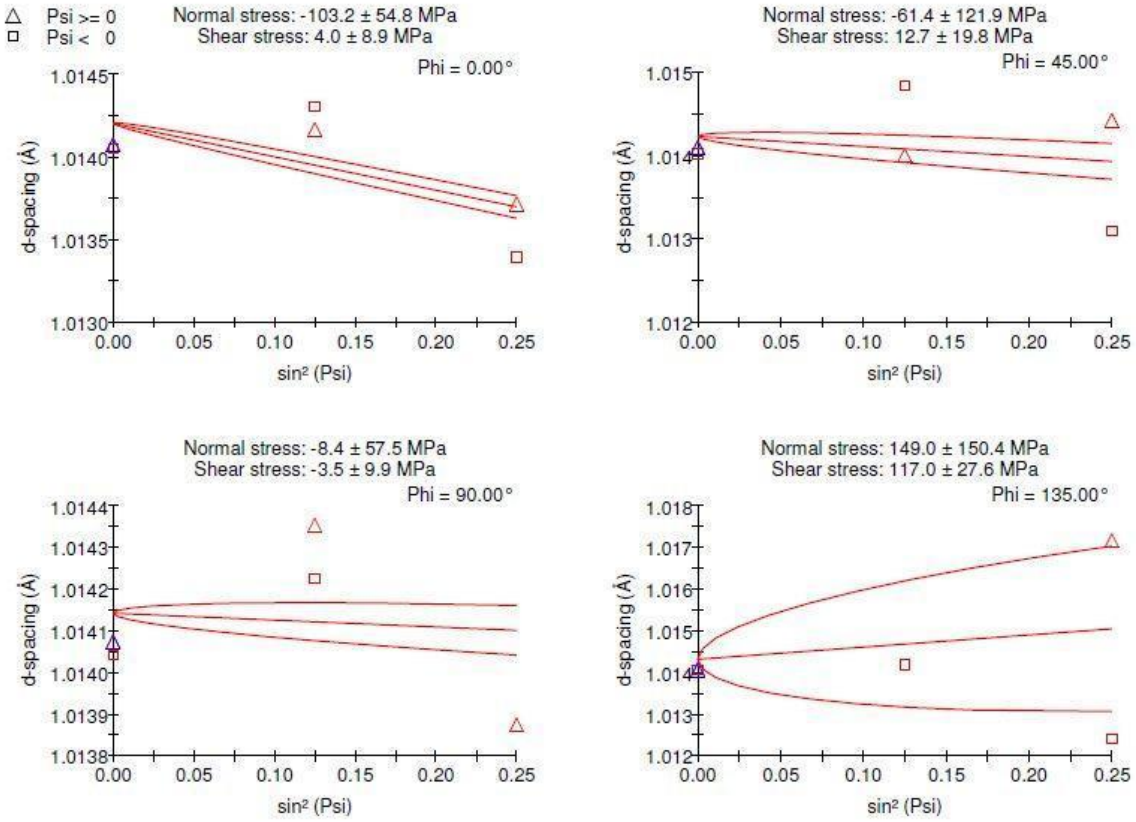

Figure 50: Stress plots of d-spacing versus $\sin^2\psi$ for aluminum 6061-T6 with traditional cut surface.

Stress plots for the fine MTP process of aluminum 6061-T6 did not provide the same consistent trends observed in the stress plots for the traditional turning. Stress plots from the fine MTP process of aluminum 6061-T6 resulted in more random stress values and types as shown in Figure 51 and Figure 53.

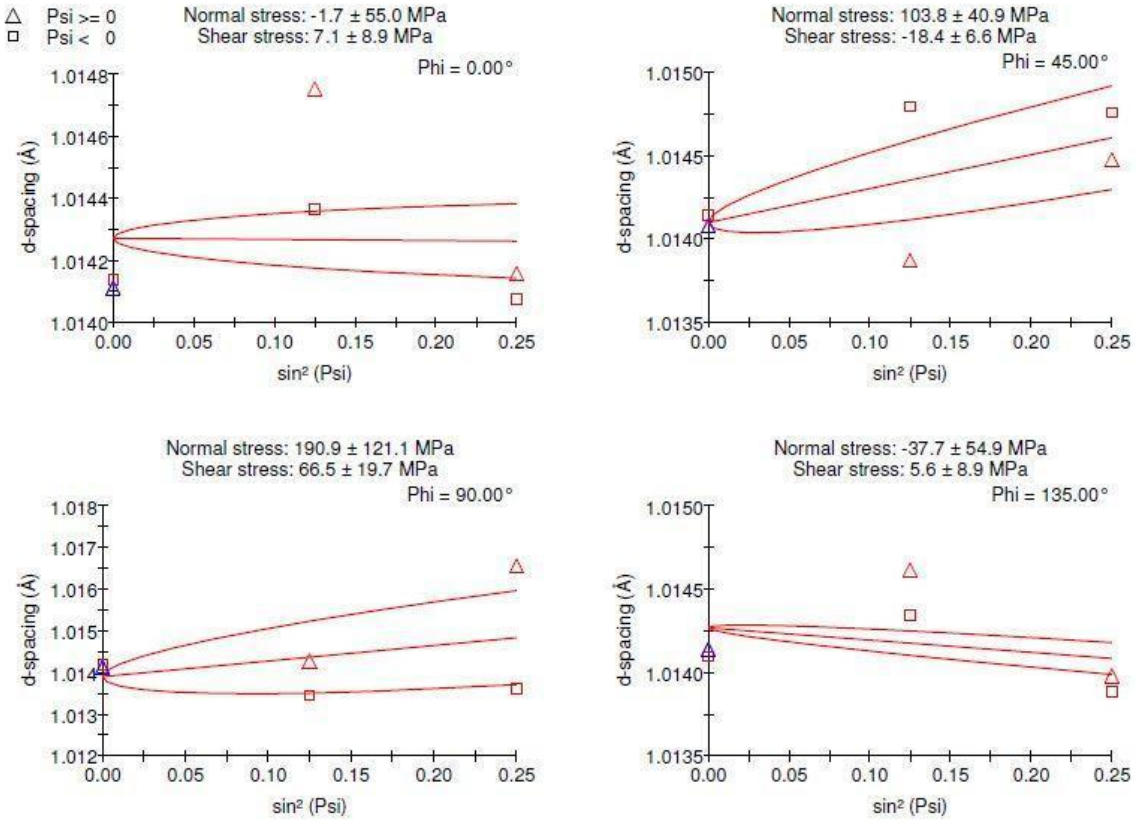

Figure 51: Stress plots of d-spacing versus $\sin^2\psi$ for aluminum 6061-T6 with fine MTP cut surface.

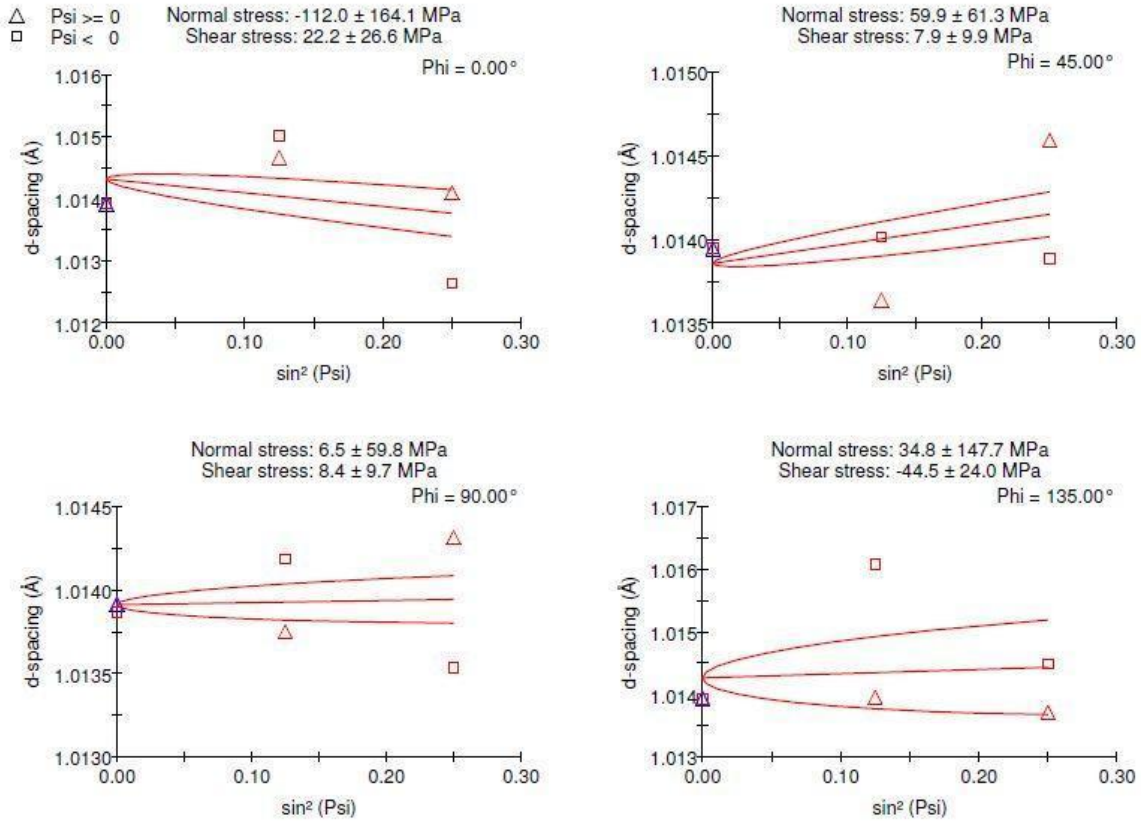

Figure 52: Stress plots of d-spacing versus $\sin^2\psi$ for aluminum 6061-T6 with traditional cut surface.

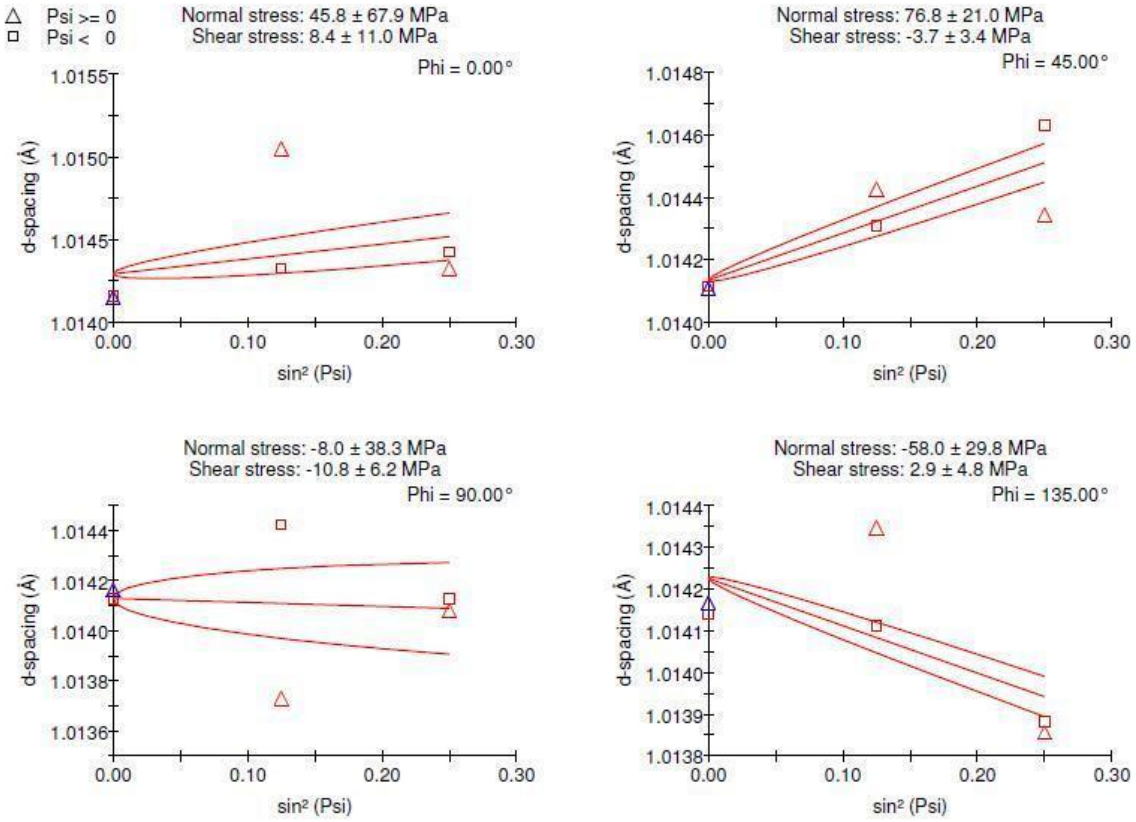

Figure 53: Stress plots of d-spacing versus $\sin^2\psi$ for aluminum 6061-T6 with fine MTP cut surface.

State of stress was equally random for the Inconel® 718 after being saw cut (Figure 54) in much the same fashion as it was for the aluminum 6061-T6. Narrow and broad ψ-splitting was observed for all Inconel® 718 stress plots from Figure 54 to Figure 58. Magnitudes of stress were significantly higher for Inconel® 718 than for the previous aluminum 6061-T6 as well as for the following tantalum 97Ta3W stress values.

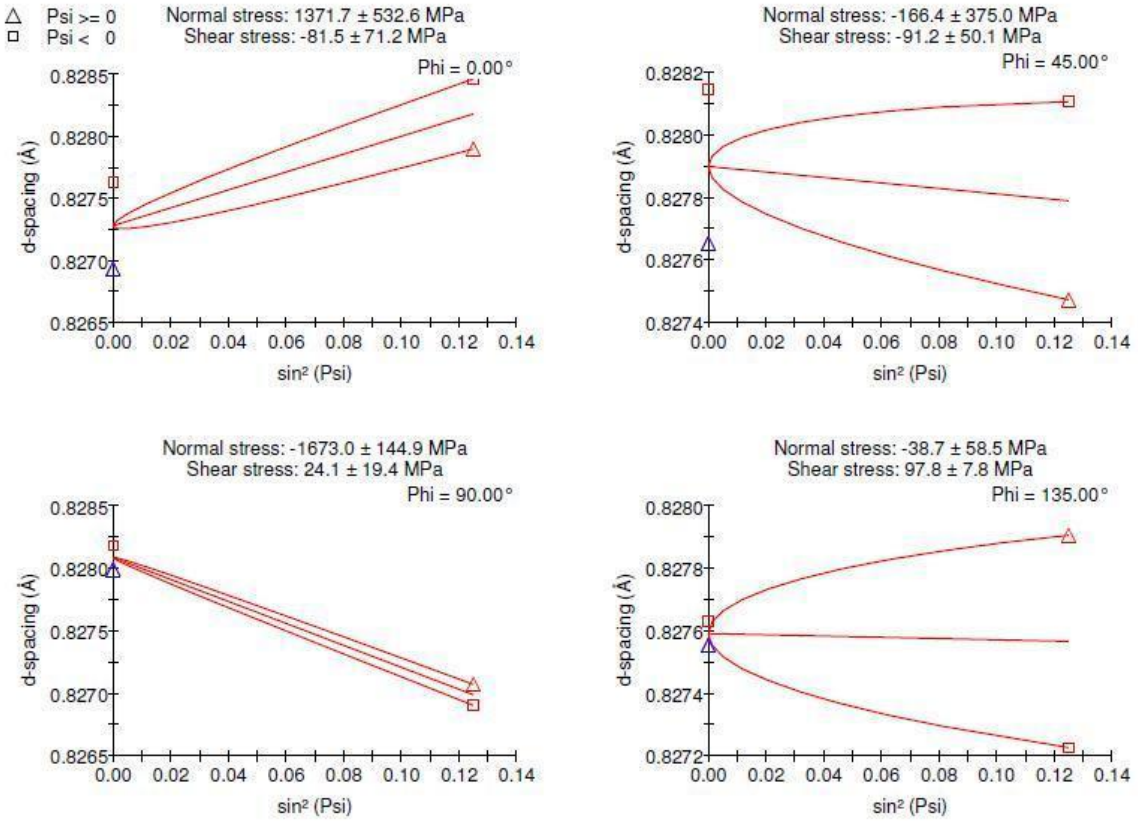

Figure 54: Stress plots of d-spacing versus $\sin^2\psi$ for Inconel® 718 with saw cut surface.

Normal stress for the Inconel® 718 sample after the saw cut operation (see Figure 54) did show compressive stress for three of the four phi orientations. Conversely, normal stress for traditional turning and fine MTP processes resulted in tensile stress for three of the four phi orientations. A specific trend was not determined for predicting the phi orientation of the compressive stress due to the irregular pattern seen in this data set. Traditional turning operations did not provide consistent magnitudes of stress (Figure 55 and Figure 57).

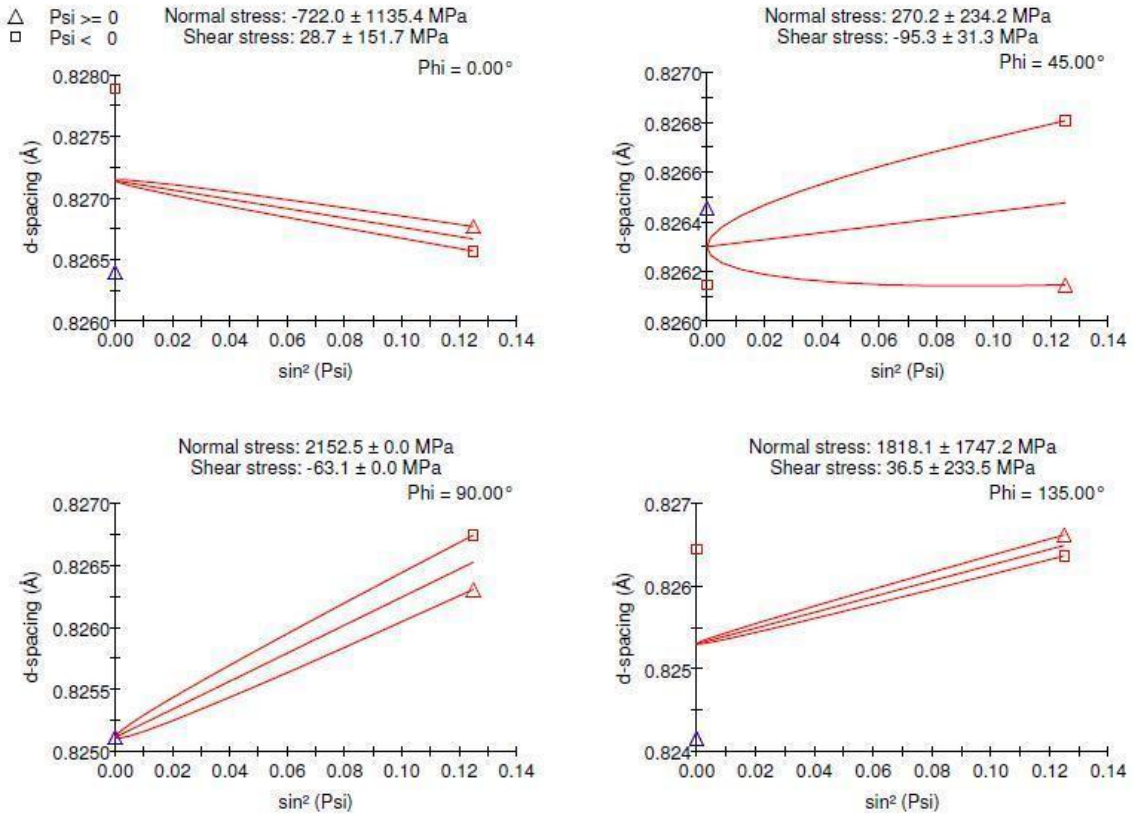

Figure 55: Stress plots of d-spacing versus $\sin^2\psi$ for Inconel® 718 with traditional cut surface.

While the fine MTP process also did not provide consistent magnitudes for the Inconel® 718 sample, the range of stress magnitudes for the fine MTP process had a smaller range of stress magnitude (Figure 56 and Figure 58).

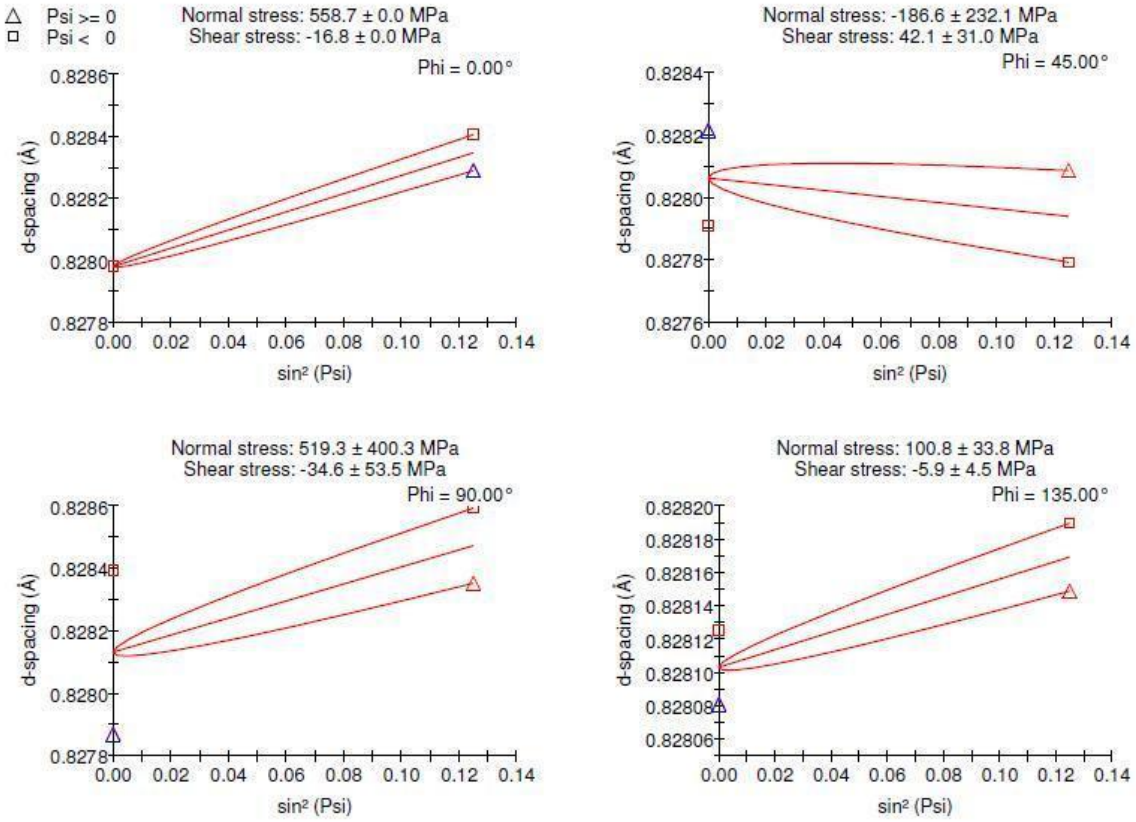

Figure 56: Stress plots of d-spacing versus $\sin^2\psi$ for Inconel® 718 with fine MTP cut surface.

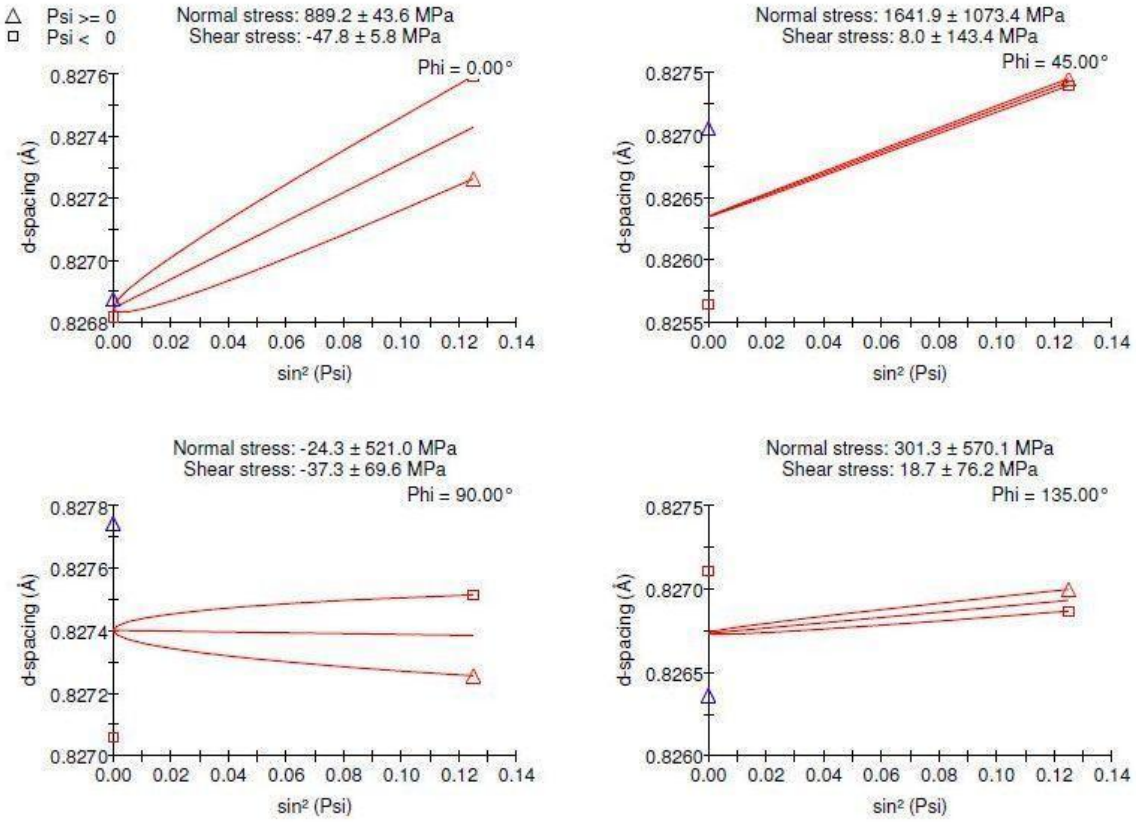

Figure 57: Stress plots of d-spacing versus $\sin^2\psi$ for Inconel® 718 with traditional cut surface.

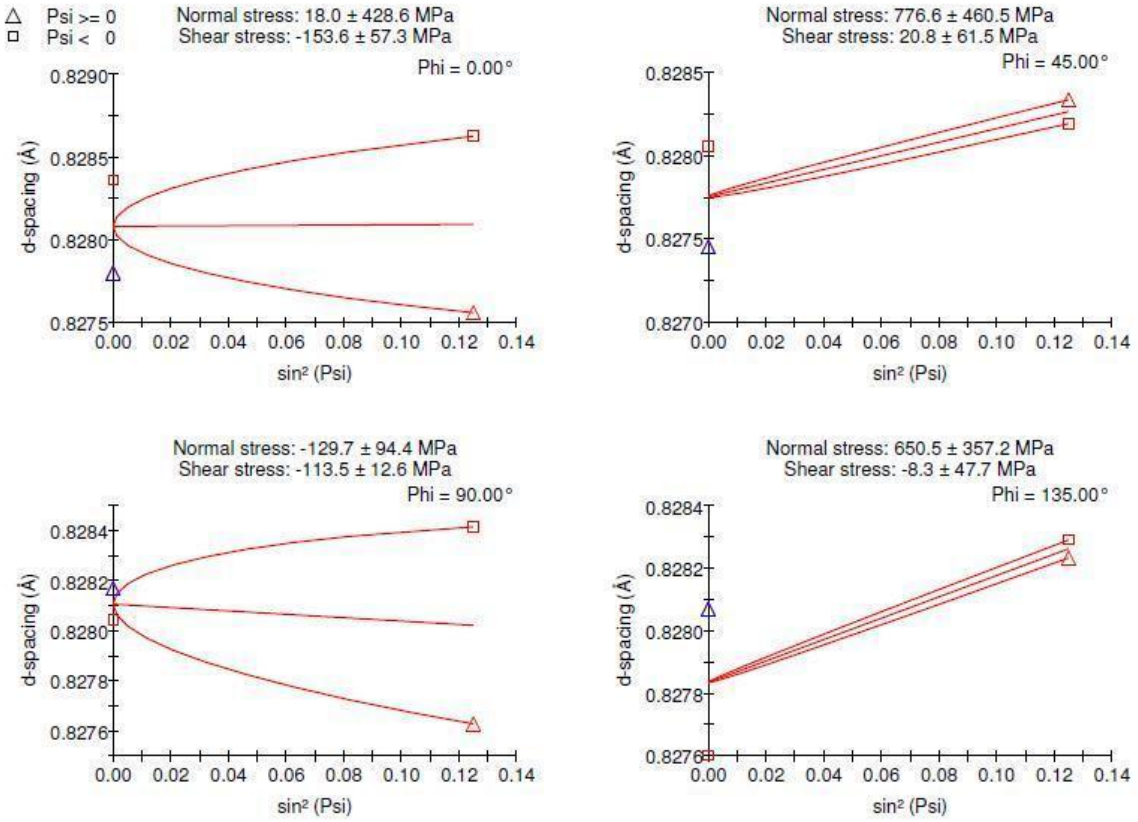

Figure 58: Stress plots of d-spacing versus $\sin^2\psi$ for Inconel® 718 with fine MTP cut surface.

Tantalum 97Ta3W was the only material to yield the same normal stress type for all four phi orientations scanned. Both samples (T-1 and T-2) had compressive stresses for stress scans after the saw cut operations (Figure 59 and Figure 60). This information was critical in verifying that a specific type of stress can be ingrained based upon the type of machining process as observed and evaluated from multiple phi orientations.

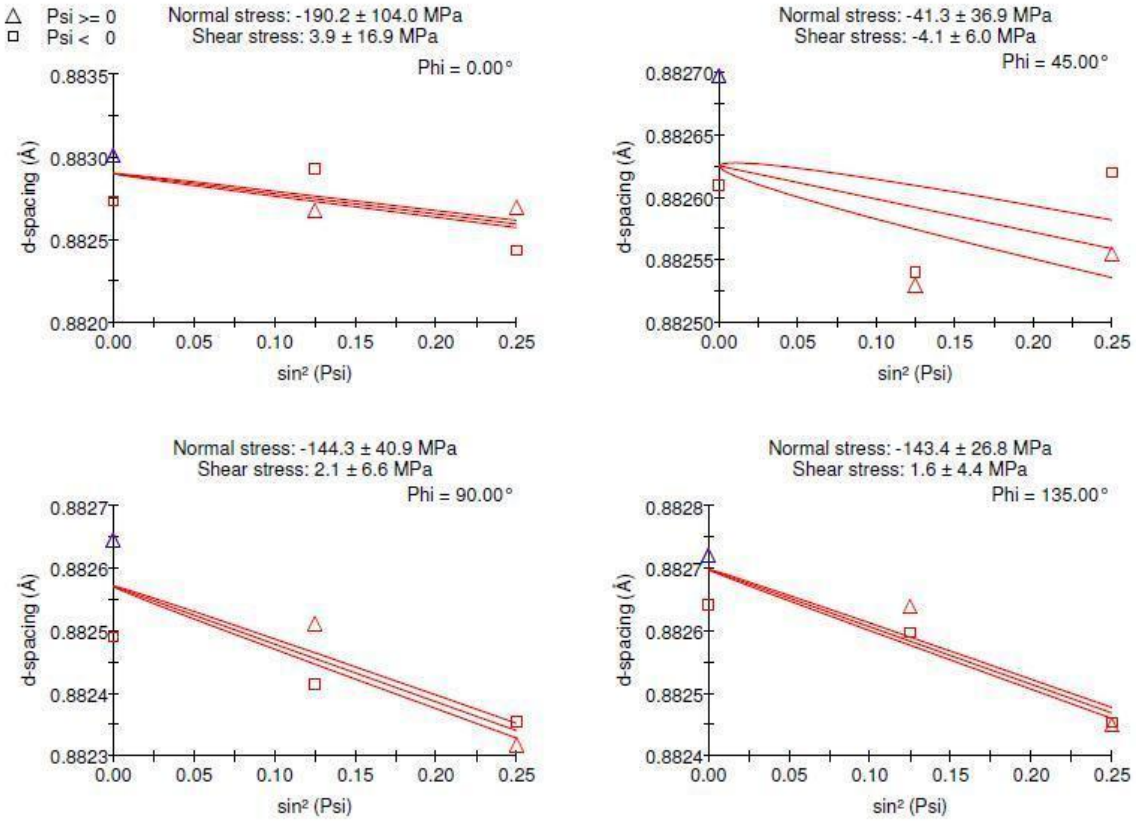

Figure 59: Stress plots of d-spacing versus $\sin^2\psi$ for tantalum 97Ta3W (sample T-1) with saw cut surface.

As mentioned previously, the first tantalum 97Ta3W sample used (T-1) was not useable for turning processes because the sample was initially cut too thin at the band saw for use with the soft jaws cut for holding samples in the lathe chuck. Since a boring tool insert was not available with a radius less than 1/16 inch, the soft jaws could not be cut to provide enough holding area on sample T-1 to guarantee repeatable alignment. Therefore, a thicker sample of tantalum 97Ta3W (sample T-2) was subsequently used for further analysis of turning operations.

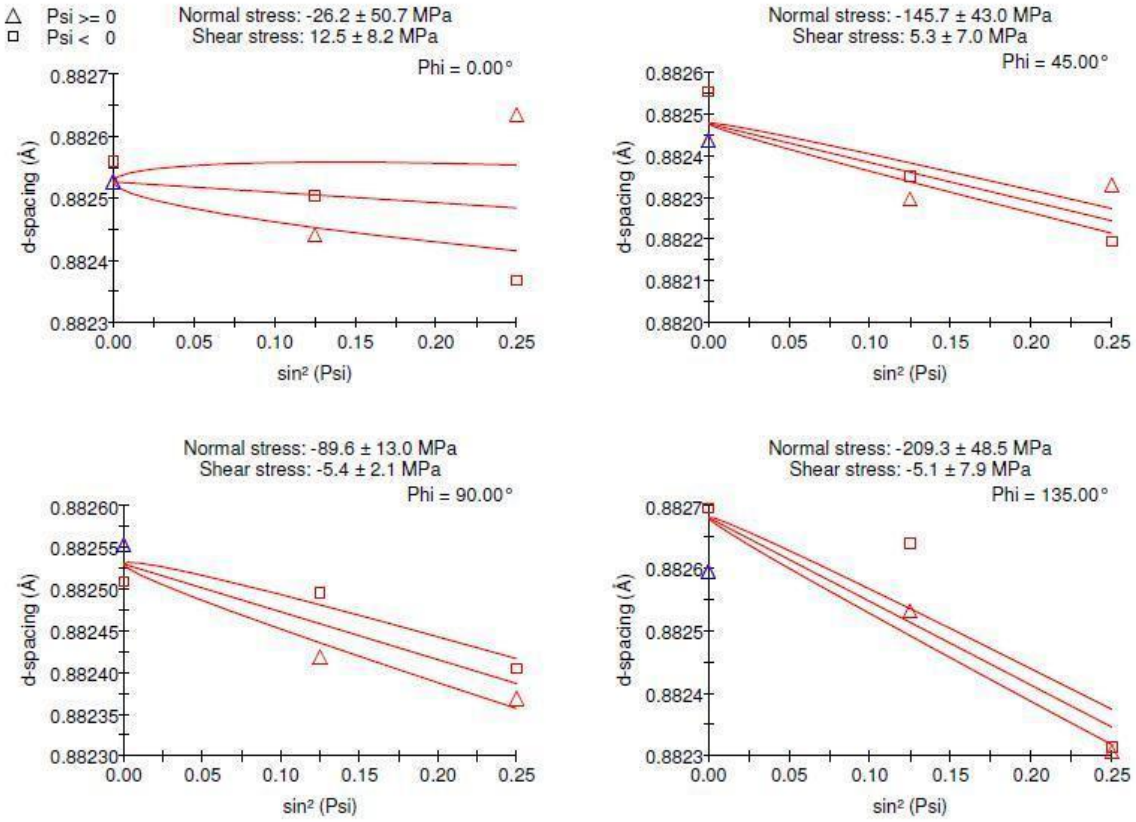

Figure 60: Stress plots of d-spacing versus $\sin^2\psi$ for tantalum 97Ta3W (sample T-2) with saw cut surface.

The traditional turning operation for tantalum 97Ta3W yielded tensile stress for three out of the four phi orientations (Figure 61).

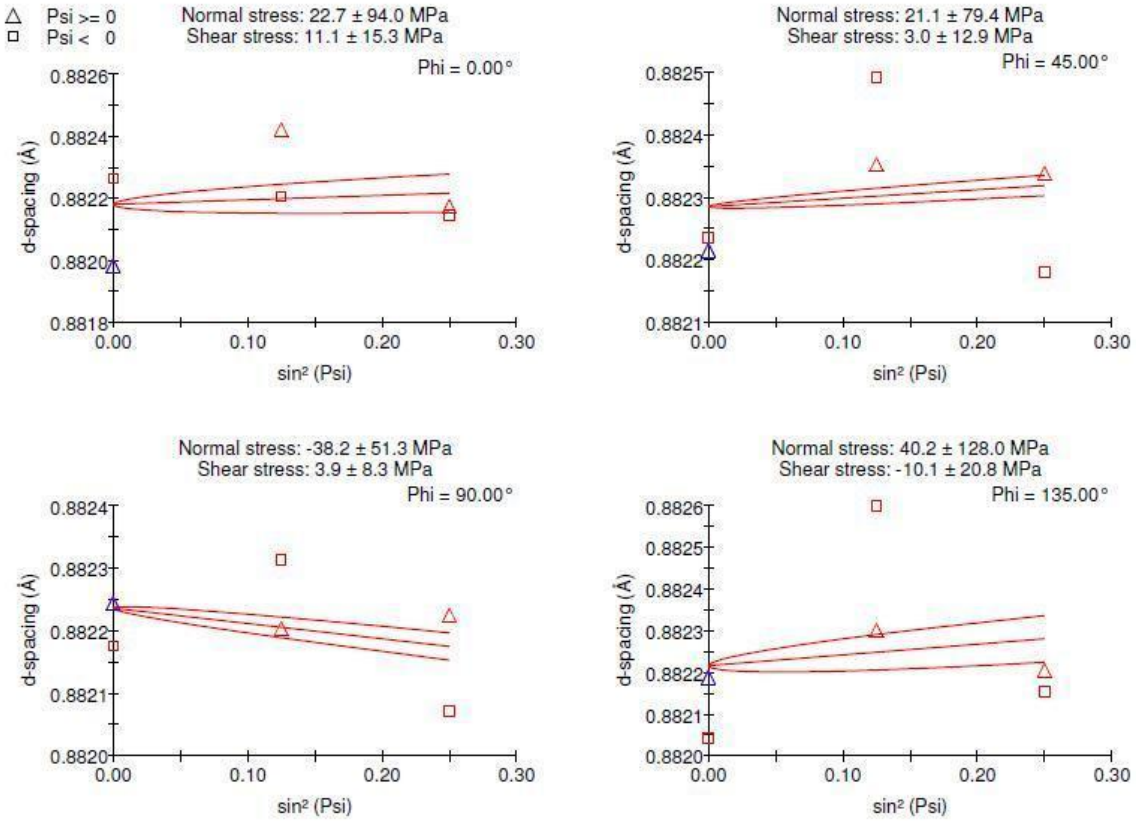

Figure 61: Stress plots of d-spacing versus $\sin^2\psi$ for tantalum 97Ta3W (sample T-2) with traditional cut surface.

Contrary to the traditional turning, the fine MTP process yielded compressive stress for three out of four of the phi orientations (Figure 62). The phi orientation with a tensile stress was only 7.0 MPa with estimated error of +/- 23.4 MPa. Therefore, the fine MTP process could be considered as a process to obtain predictable compressive residual stresses for tantalum 97Ta3W.

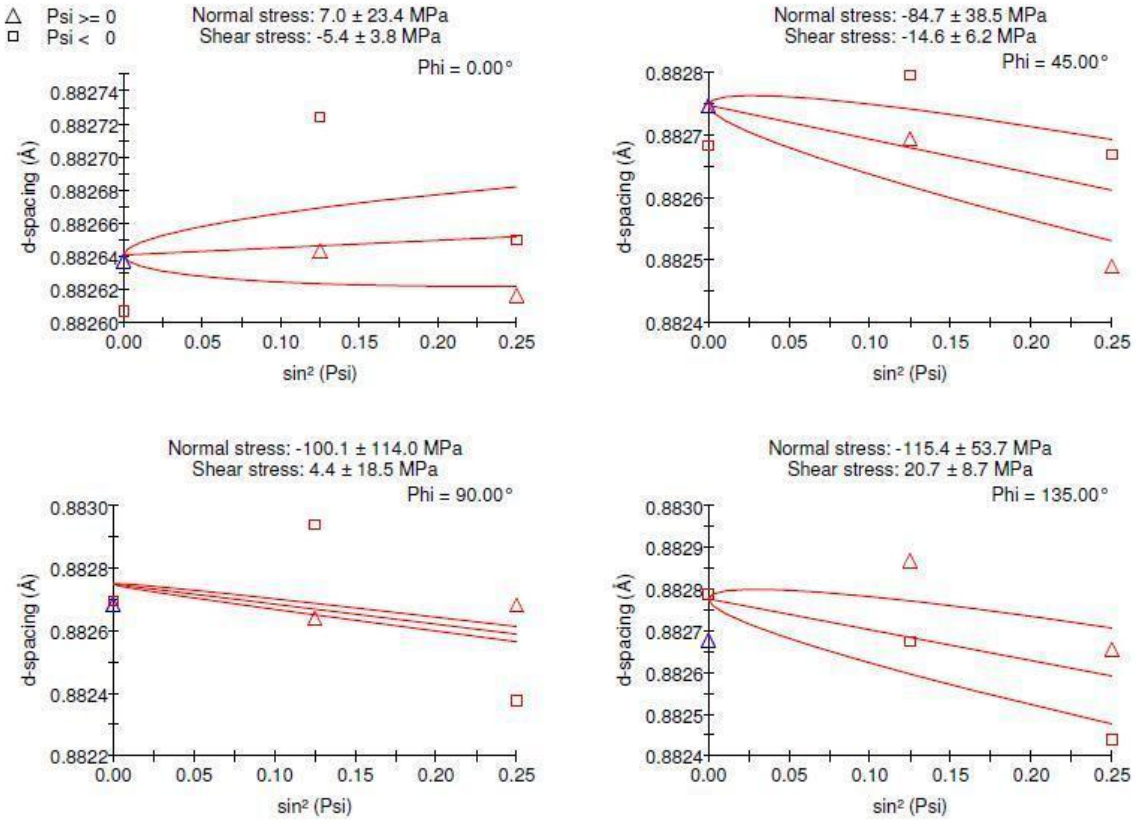

Figure 62: Stress plots of d-spacing versus $\sin^2\psi$ for tantalum 97Ta3W (sample T-2) with fine MTP cut surface.

Final interpretations of the results listed within this section and in Appendixes C & D are provided in the next section. Additionally, ideas for future research into this area are also recommended in the following (and concluding) section of this thesis.

CONCLUSIONS

Progress was made in preparing a proper research protocol for comparing an experimental modulated tool path (MTP) machining process with that of traditional machining techniques. Trial and test runs were made on several test materials with equipment determined and designation for use (e.g., saw, lathe, and XRD) during the design, development, and testing of the project experimental procedure. MATLAB™ programs CNC codes created for the modulated tool path process are provided in Appendix E for further review and refinement. From a short cylinder of Aluminum T6-6061, a few samples of traditional and modulated tool path turning processes were machined to verify the plausibility of the project.

The first attempts to machine samples resulted in visually good comparisons; however, the initial XRD scans had to be reassessed to meet time constraints and analytical equipment usage costs. After communicating with the XRD manufacturer, other appropriate materials were selected. Through experimental and documentation review, the copper tube on the XRD showed fluorescence at high 2Theta angles with alloys high in iron content. A stainless steel alloy with over 50% iron content had a fluorescent background that made stress analysis at high angles impractical (see Figure 63 and Figure 64). The peak at approximately 90° in Figure 63 and Figure 64 was only 60 counts higher than the fluorescent background. Since the XRD hardware configuration was limited, iron alloys were not used for this research. In addition to the aluminum alloy, Inconel® 718 (a nickel alloy) and 97Ta3W (a tantalum alloy) were selected for further stress analysis. Material phase identification diffractogram scans are provided in Appendix B of this thesis.

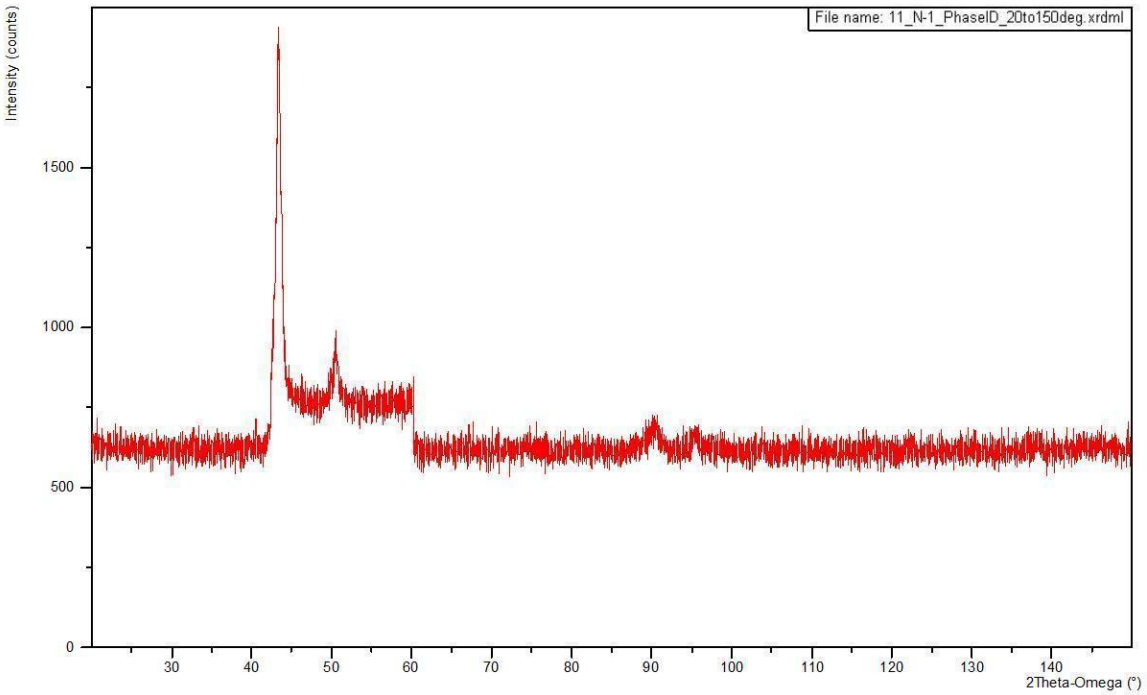

Figure 63: X-ray diffractogram for phase identification of stainless steel alloy.

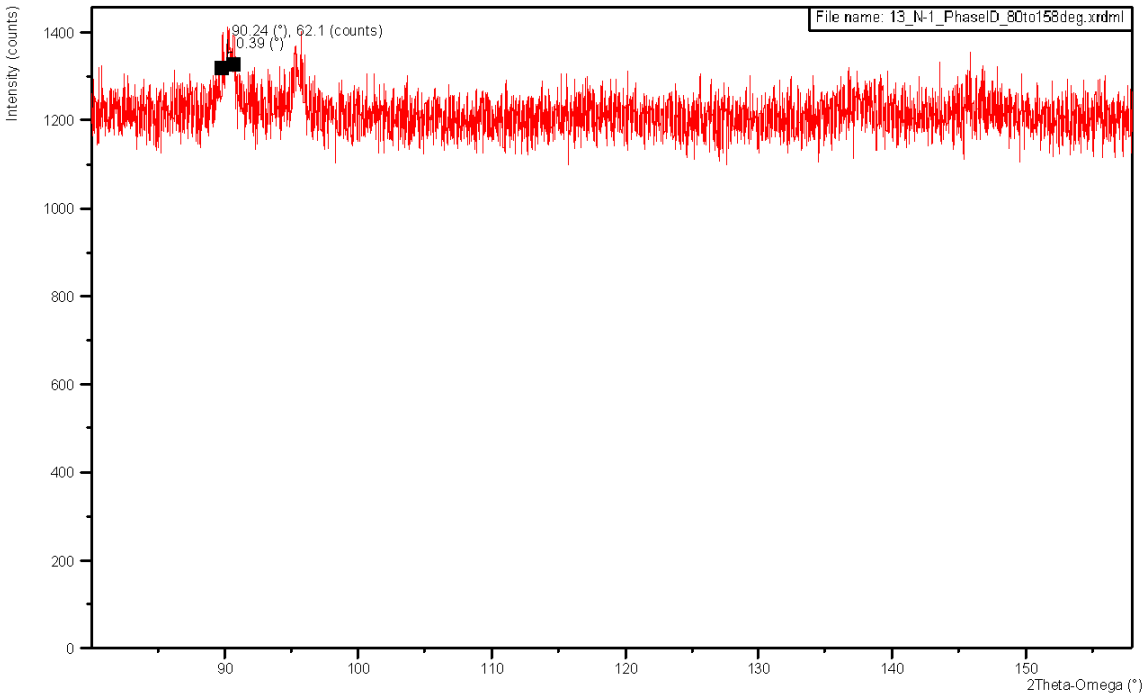

Figure 64: X-ray diffractogram for high angle peak identification of stainless steel alloy.

Peaks identified for stress measurement were scanned using a positive-only stress measurement scan. Material properties of yield strength and Poisson's ratio were used to perform the stress analysis of scanned peaks through Stress™ software. After each machining process, samples were oriented in a repeatable manner by use of the alignment mark on the sample. Then, the offsets were adjusted to locate the peak selected for stress analysis. Stress data was then compared to stress in the previous state. See Appendix C for stress comparison data and Appendix D for comparison plots.

As mentioned in the previous section, the plots for normal and shear stresses determined for each phi rotation did not provide a clear pattern. However, the strain-free d-spacing (referred to as d-spacing) offered another more viable comparison method. The raw data determined for each test material and its d-spacing characteristics is included in Appendix C of this thesis while associated plots are shown in Appendix D. Of all the material samples tested in this study, the aluminum sample showed the most promise for providing a potential dependable regimen for relating d-spacing to machining process type. The relative change in d-spacing between each turning process for aluminum was about +/- 0.10%. Comparing each process type to its first and second iteration for aluminum had a relative change of less than 0.05%.

Readings from the Inconel® 718 sample were not as repetitive per turning process type. Therefore, the idea that residual stress can be determined from the type of turning process could be more specific to the material properties than first realized. Furthermore, d-spacing for tantalum did show that the two saw cut operations were more similar than d-spacing for either traditional turning or fine modulated tool path. However, the relative

change in d-spacing from the traditional turning operation to the fine modulated tool path operation was about 0.05%.

Since the aluminum sample did show a possible trend, further development of this technique could prove that determining residual stress based on material properties and machining process may be a plausible way to modify machining methods to produce a part with residual stresses in a specified range. Additionally, the modulated tool path process did produce a clear advantage in chip length reduction. Materials or cutting processes that tend to form long strands of coiled chips could benefit by implementing a modulated tool path process. Maximum chip length could even be determined through further development of this aspect of the project quantitatively and proven experimentally.

Resulting stress state for normal stress based on turning process was not clearly identified for the aluminum 6061-T6 and the Inconel® 718; however, the tantalum 97Ta3W did provide different stress types based on turning process. With more time and effort, as well as the integration of the appropriate material analysis software for machining methods, a range of turning processes could be identified to provide a specific stress type with a given stress range. Further, to prevent creep fracture in the material, the compressive stresses would be preferred.

Given that the methods of stress analysis use the determined lattice structure to determine stress, the d-spacing is an important factor in measuring stress. Aluminum 6061-T6 and tantalum 97Ta3W offered a pattern in determining d-spacing. Both had identifiable differences of strain-free d-spacing from traditional turning to the fine modulated tool path process. Data did support that a gap existed between the d-spacing

range for traditional turning and fine modulated tool path process types—0.0008Å for aluminum 6061-T6 and 0.0004Å for tantalum 97Ta3W. More data would have to be gathered to verify the possible trend due to the relatively small changes in strain-free d-spacing.

A possible theory that was developed as part of this experiment relates residual stress for each material type and turning method. Each specific combination of turning process method and material type should result in a state where residual stress falls within a range for each combination group. With further development of this project, stress ranges could be defined for each process and material combination. Materials, such as the Inconel® 718, may have large stress ranges that overlap for various turning processes.

One limiting aspect of this project was related to use of the XRD. Access to the XRD was shared with other users in the Optics department of the institution. The shared use of the XRD, resulting in usage time constraints, meant that lengthy scans with more detail could not be performed. In addition, because other users were not known, setups could not be left to run for hours unattended without the risk of another user possibly interrupting a scan or removing and possibly discarding the samples. Further, due to time constraints, the opportunity to include the cobalt tube in the investigation was not realized. In future studies, it is recommended that that cobalt tube set-up be used to evaluate both the tool steel m-42 and the stainless steel nitronic 33 and provide for a more comprehensive material testing regimen, with subsequent data and results in the area of machining residual stress characterization.

Residual stress determination could provide benefits for high production volumes where a specific material could be analyzed with a sample of data. Also, several repeated

tests of a single surrogate material could be used to better evaluate modifications to the modulated tool path process in terms of achieving a desired level of residual stress.

REFERENCES

[1] Berglind, L., & Ziegert, J. (2013). “Chip Breaking Parameter Selection for Constant Surface Speed Machining.” ASME 2013 International Mechanical Engineering Congress and Exposition (pp. V02BT02A039-V02BT02A039). American Society of Mechanical Engineers.

[2] Skelton, R. C. (1968). "Turning with an oscillating tool." International Journal of Machine Tool Design and Research, 8(4), 239-259.

[3] Overcash, Jerald L. and Cuttino, James F. (2009). “In-Process Modeling of Dynamic Tool-Tip Temperatures of a Tunable Vibration Turning Device Operating at Ultrasonic Frequencies.” Journal of the International Societies for Precision Engineering and Nanotechnology, Volume 33, 505-515. University of North Carolina at Charlotte, 2008.

[4] Skelton, R. C. (1969). "Effect of ultrasonic vibration on the turning process." International Journal of Machine Tool Design and Research, 9(4), 363-374.

[5] Yemel’Yanov, V.S., Yevstyukhin, A.I.; Foster, Anne. (1969). The Metallurgy of Nuclear Fuel: Properties and Principles of the Technology of Uranium, Thorium, and Plutonium. Oxford: Pergamon Press.

[6] Vytautas et. al., O., Gaidys Rimvydas Dauksevicius Rolanas Mikuckyte Sandra (2013). "Study of Vibration Milling for Improving Surface Finish of Difficult-to-Cut Materials." Strojniski Vestnik / Journal of Mechanical Engineering, 59(6), 351-357.

[7] Liu, M., Takagi J. Tsukuda A. (2004). "Effect of tool nose radius and tool wear on residual stress distribution in hard turning of bearing steel." Journal of materials processing technology, 150(3), 234-241.

[8] Prevéy, P. (n.d.). X-Ray Diffraction Residual Stress Techniques. Lambda Technologies. Retrieved February 26, 2015, from http://www.lambdatechs.com/documents/200.pdf

[9] Bin and Helmi, S. B. a. A. H. (2010). "CURRENT STATUS AND FUTURE DIRECTION IN THE NUMERICAL MODELING AND SIMULATION OF MACHINING PROCESSES: A CRITICAL LITERATURE REVIEW." Machining Science and Technology, 14(2), 149-188.

[10] Maurotto, A., Muhammad, R., Roy, A., and Silberschmidt, V. V. (2013). "Enhanced ultrasonically assisted turning of a β-titanium alloy." Ultrasonics, 53(7), 1242-1250.

[11] X-Ray Diffraction. (2015). Bristol, United Kingdom: VEQTER Ltd. http://www.veqter.co.uk/residual-stress-measurement/x-ray-diffraction1

[12] Bragg's Law [Diagram]. (2015). http://www.veqter.co.uk/residual-stress-measurement/x-ray-diffraction1

[13] Voort, George Vander. (2015). "Metallography and Microstructure of Aluminum and Alloys." VACAERO International, Inc. http://vacaero.com/information-resources/metallography-with-george-vander-voort/1217-metallography-and-microstructure-of-aluminum-and-alloys.html

[14] "Aluminum 6061-T6; 6061-T651." (2015). Aerospace Specification Metals, Inc. and MatWeb, LLC. http://asm.matweb.com/search/SpecificMaterial.asp?bassnum=MA6061t6

[15] Inconel® alloy 718. (2012). Special Metals Corp. http://www.specialmetals.com/documents/Inconel%20alloy%20718.pdf

[16] Smithells, C.J. and Brandes, E.A. (1976.) Metals Reference Book: 5th ed. London: Buterworths. 86, 975-980.

[17] "Austenitic Stainless Steel." (2013). Steel Holdings Corporation, Ltd. http://www.shclimited.com/austenitic-stainless-steel.php

[18] "Armco Nitronic 33 Stainless Steel." (1986). Armco Inc. (Electralloy). http://www.electralloy.com/pdf/Nit_33.pdf

[19] "Tantalum Data." (2014). Eagle Alloys Corporation.

[20] Glazof, Michael V. (2013). "Physical Properties of Zirconium Alloys for Nuclear Applications in Support of UFD Campaign." Idaho National Laboratory: U.S. Dept. of Energy National Laboratory. http://www.miroslavgregoric.com/wp-content/uploads/2013/10/Modeling-of-Some-Physical-Properties-of-Zirconium-Alloys-for-Nuclear-Applications-in-Support-of-UFD-Campaign-Michael-V.-Glazoff-2013-5806474.pdf

[21] Wah, Chang. (2015). "Zirconium Alloy Zircaloy-4." ATI & MatWeb, LLC. http://www.matweb.com/search/datasheet.aspx?matguid=a265da2e4ff94c968a8ae344870a32e3&ckck=1

[22] Writer, Mark. (2015). "Uranium: Physical Properties." The University of Sheffield and WebElements, Ltd, UK. http://www.webelements.com/uranium/physics.html

[23] Ermrich, Martin and Detlef, Opper. (2013.) "XRD for the Analyst: Getting Acquainted with the Principles." Almelo, The Netherlands. PANalytical B.V.

[24] Hutchings, M.T., P.J. Withers, T.M. Holden, Torben Lorentzen. (2005). "Introduction to the Characterization of Residual Stress by Neutron Diffraction." CRC Press, Technology & Engineering.

[25] Zhang et. al., X., Arif, Muhammad, Liu, Kui, Kumar, A. Senthil, Rahman, Mustafizur (2013). "A model to predict the critical undeformed chip thickness in vibration-assisted machining of brittle materials." International Journal of Machine Tools and Manufacture, 69(0), 57-66.

[26] Chandra, N., Rahman Mustafizur Neo Ken Soon (2009). "Enhancing the performance of polycrystalline diamond tools for machining WC by ultrasonic elliptical vibration cutting method." Journal of Vacuum Science and Technology B: Microelectronics and Nanometer Structures, 27(3), 1241-1246.

[27] Peng et. al., Y. P., Liang Z. Wu Y. Guo Y. Wang C. (2011). "Effect of vibration on surface and tool wear in ultrasonic vibration-assisted scratching of brittle materials." International journal of advanced manufacturing technology, 59(1-4), 67-72.

[28] Taghi and Mohsen (2012). "Improving machinability of Inconel 718 with a new hybrid machining technique." International journal of advanced manufacturing technology, 66(5-8), 1025-1030.

[29] Nelson, Jameson K., “Acoustic Emission Detection of Metals and Alloys During Machining Operations.” (2012). College of Technology Masters Theses and Directed Projects. Paper 60. http://docs.lib.purdue.edu/techmasters/60

[30] Innovations Catalog (A-13-03143EN_in ed.). (2013). Latrobe, PA, USA: Kennametal Inc.

[31] “Latrobe Dynamax™ ASTM M42, DIN 1.3247 Super High Speed Steel.” (2006). Timken Latrobe Steel (now: Latrobe Specialty Steels Co.). http://www.matweb.com/search/datasheet.aspx?matguid=5d3aa050170c4b40874e7e94a4004439&ckck=1

[32] “M-42 High Speed Tool Steel.” (2015). Diehl Steel Company, Cincinnati, OH. http://www.diehlsteel.com/products/high-speed-steel/m-42

[33] “General Information: Heat Treatment of Tool Steels.” (2015). Crucible Industries. http://crucible.com/eselector/general/generalpart2.html

[34] Fitzpatrick, M.E., Fry, A.T., Holdway, P., Kandil, F.A., Shackleton, J., & Suominen, L. (2005). “Determination of Residual Stresses by X-Ray Diffraction—Issue 2.” National Physical Laboratory. Teddington, Middlesex, United Kingdom. http://www.npl.co.uk/upload/pdf/Determination_of_Residual_Stresses_by_X-ray_Diffraction_-_Issue_2.pdf

[35] Anderoglu, Osman. (2004). “Residual Stress Measurement Using X-Ray Diffraction.” Texas A&M University.

APPENDIX A: XRD FIXTURES

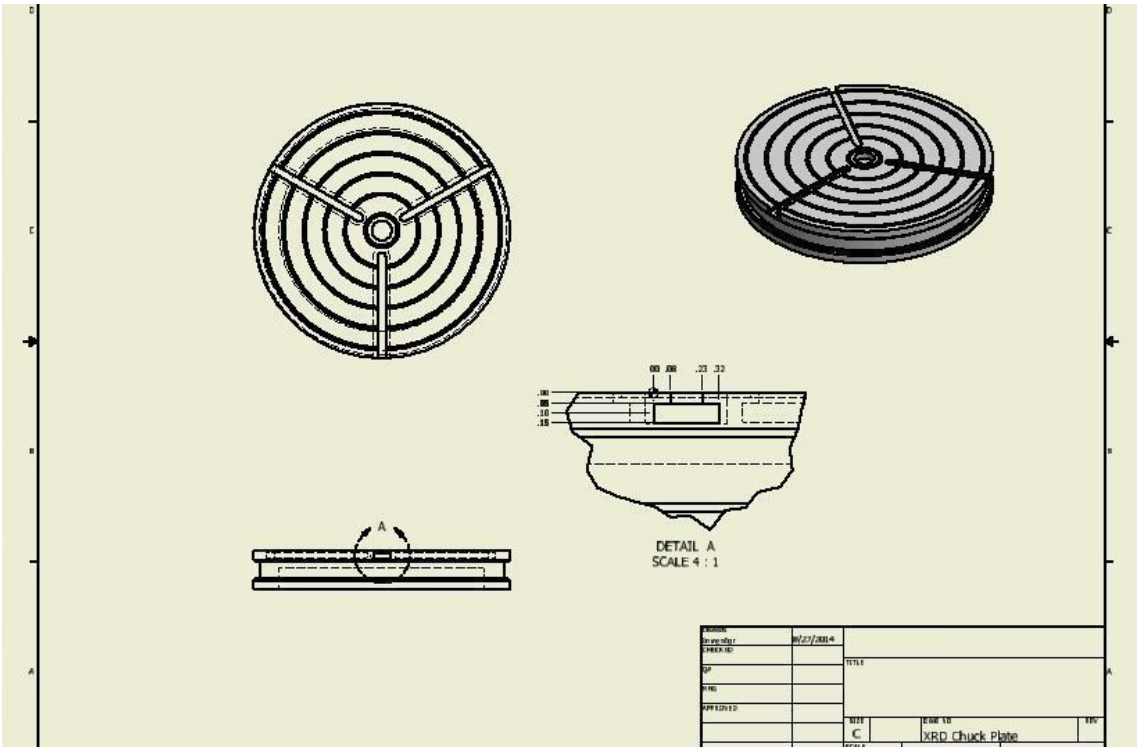

Figure 65: XRD mounting surface plate was measured and modeled to determine a suitable fixture.

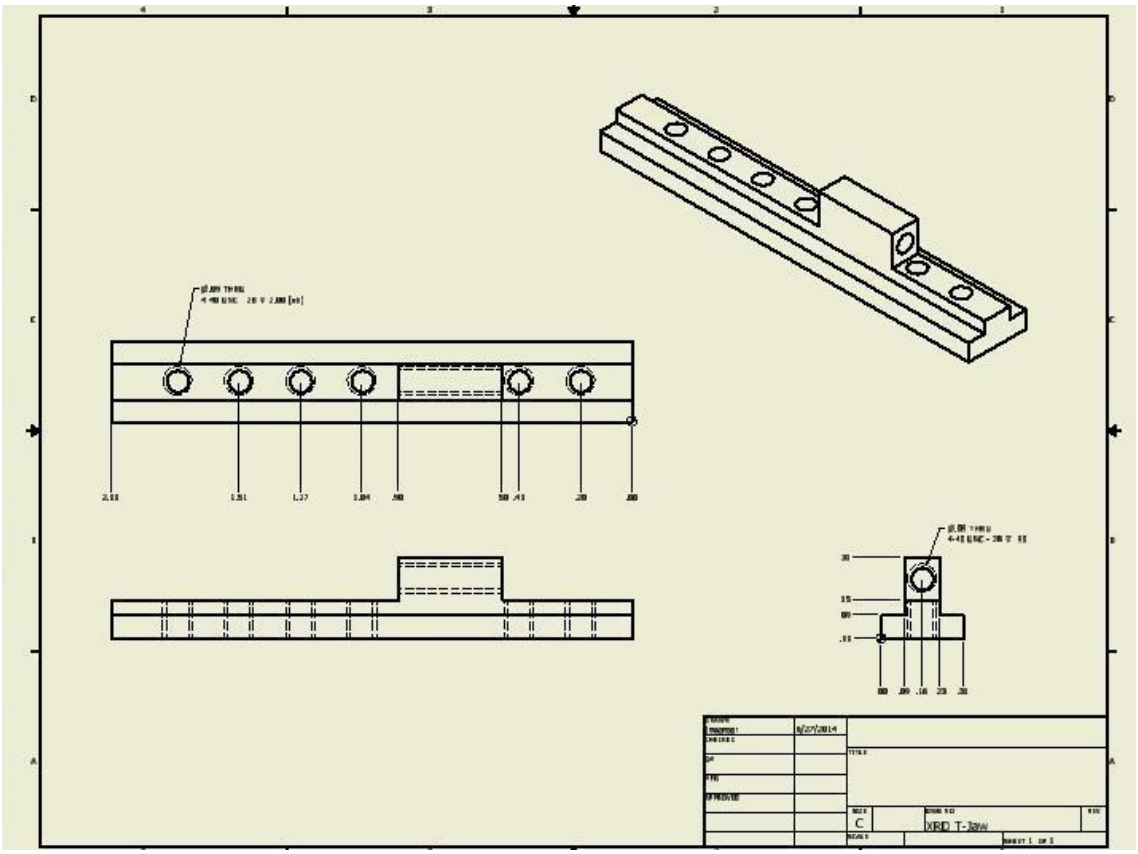

Figure 66: Blueprint for designed fixture to hold samples on mounting surface.

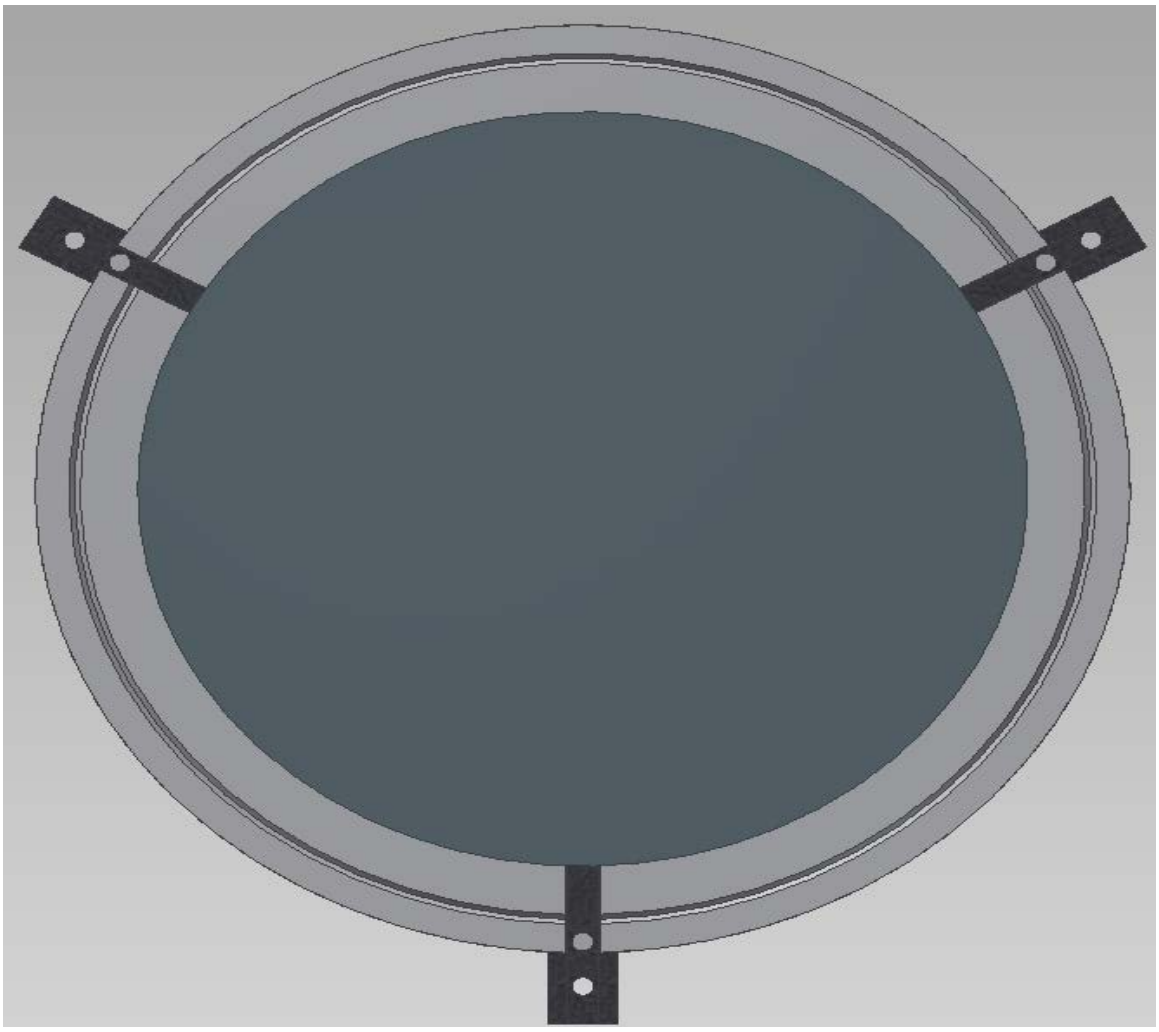

Figure 67: Top View of sample on XRD mounting face plate with T-jaw fixtures.

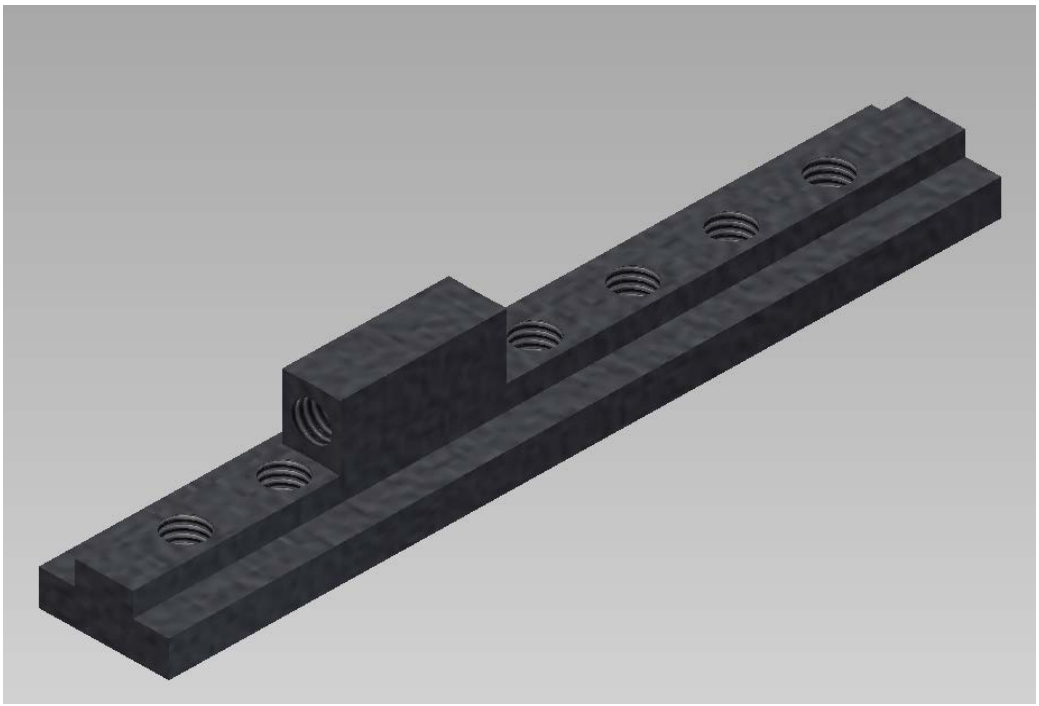

Figure 68: Isometric view of T-jaw fixture.

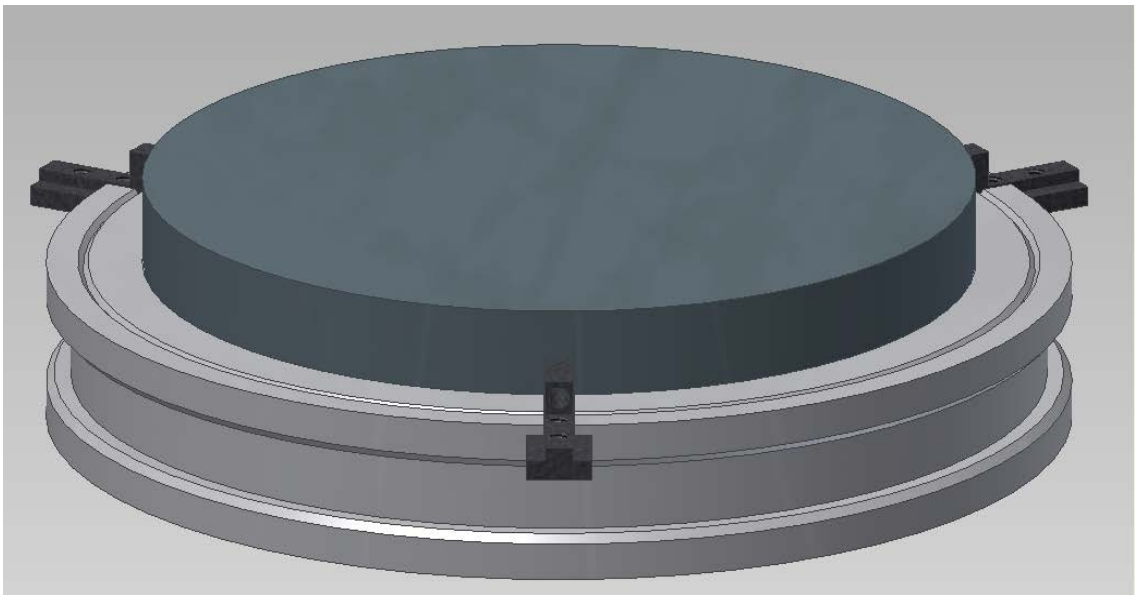

Figure 69: Low angle view of mounted sample.

APPENDIX B: PHASE IDENTIFICATION SCANS

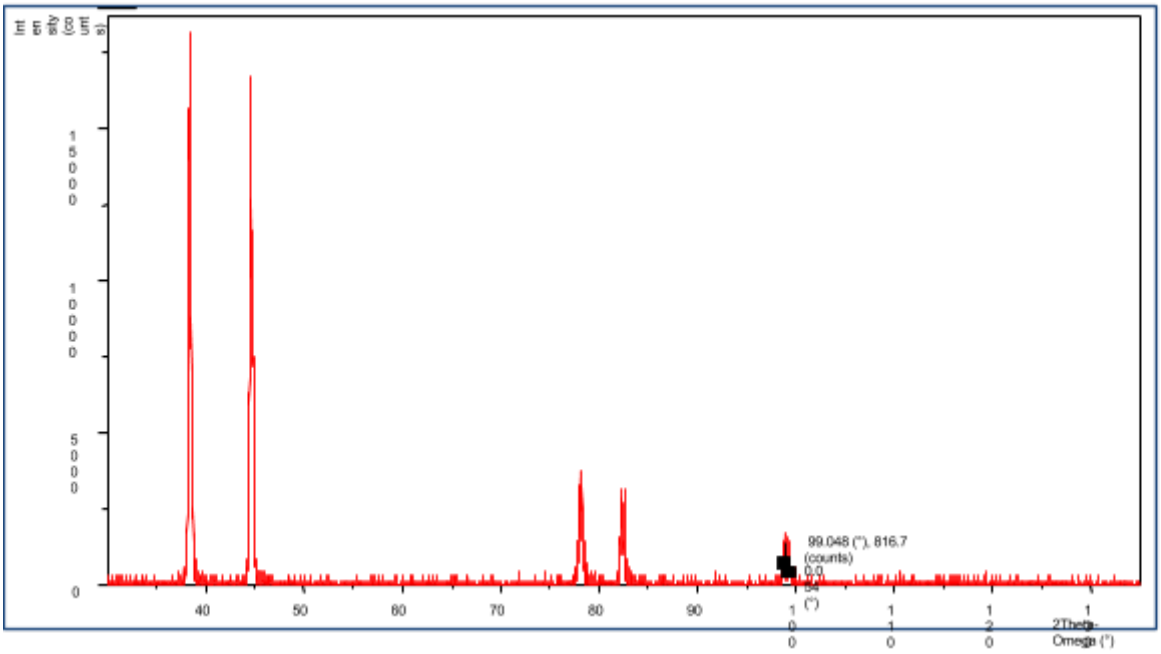

Figure 70: Aluminum phase ID from 20° to 135° 2Theta with peak at 99.048° identified for stress analysis.

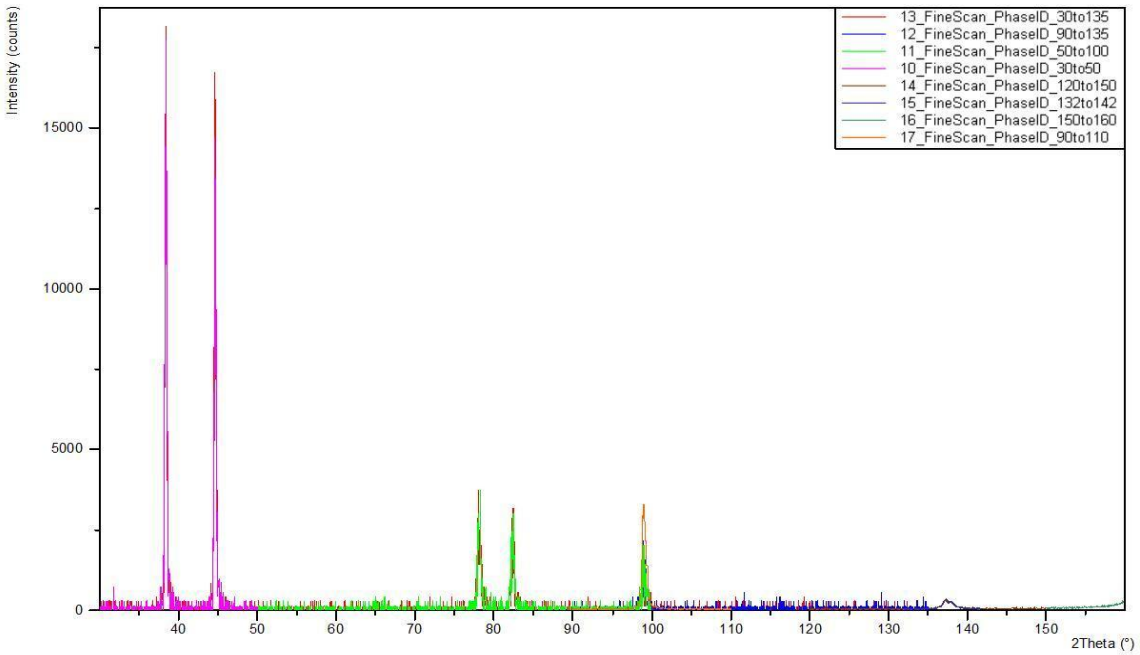

Figure 71: Supplemented phase ID scans from 20° to 150° 2Theta.

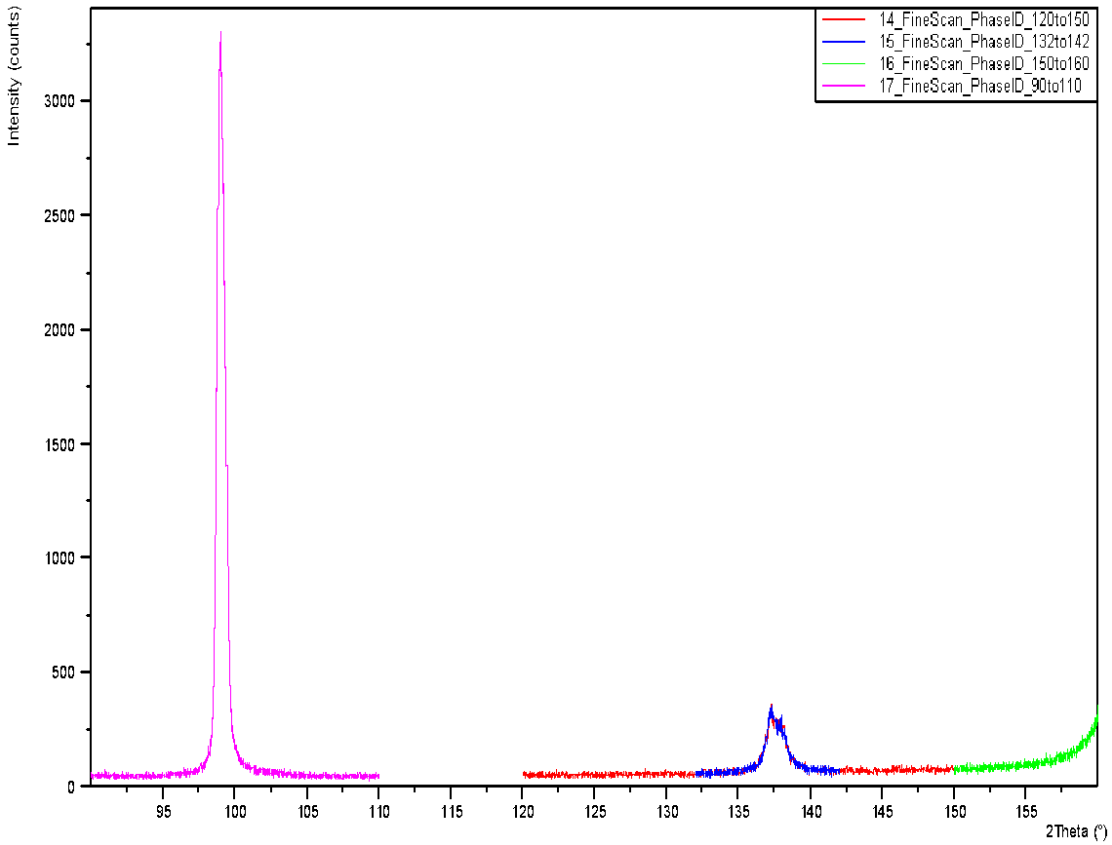

Figure 72: Aluminum high angle peaks identified for stress analysis from multiple 2Theta scans.

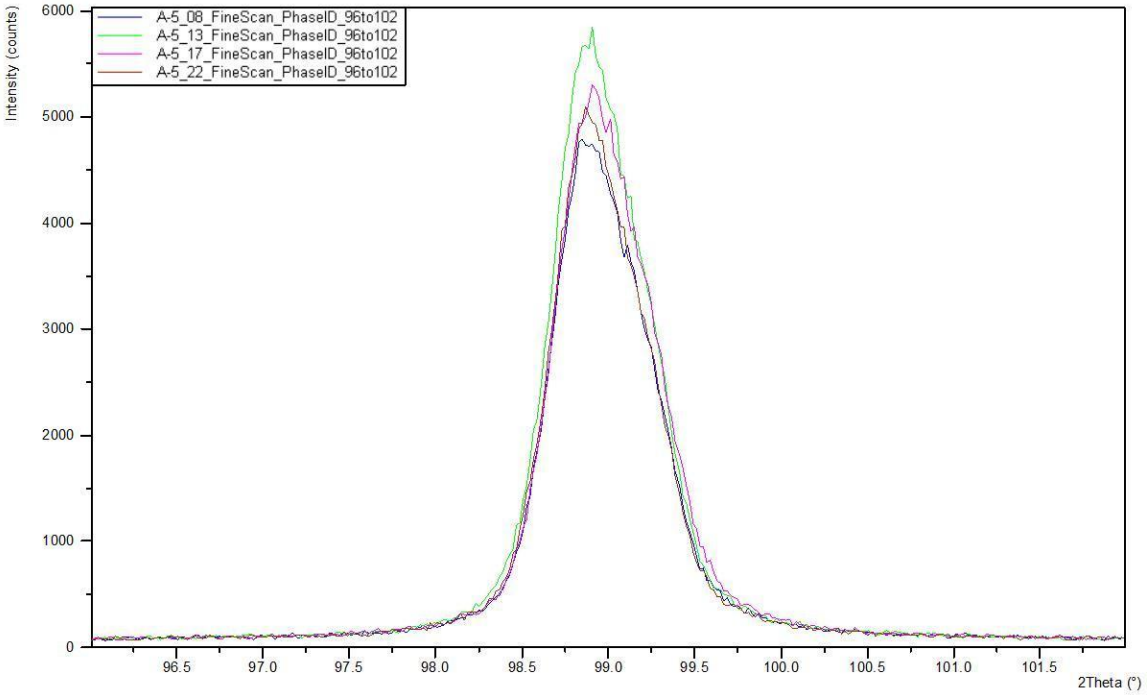

Figure 73: Multiple post process scans of sample A-5.

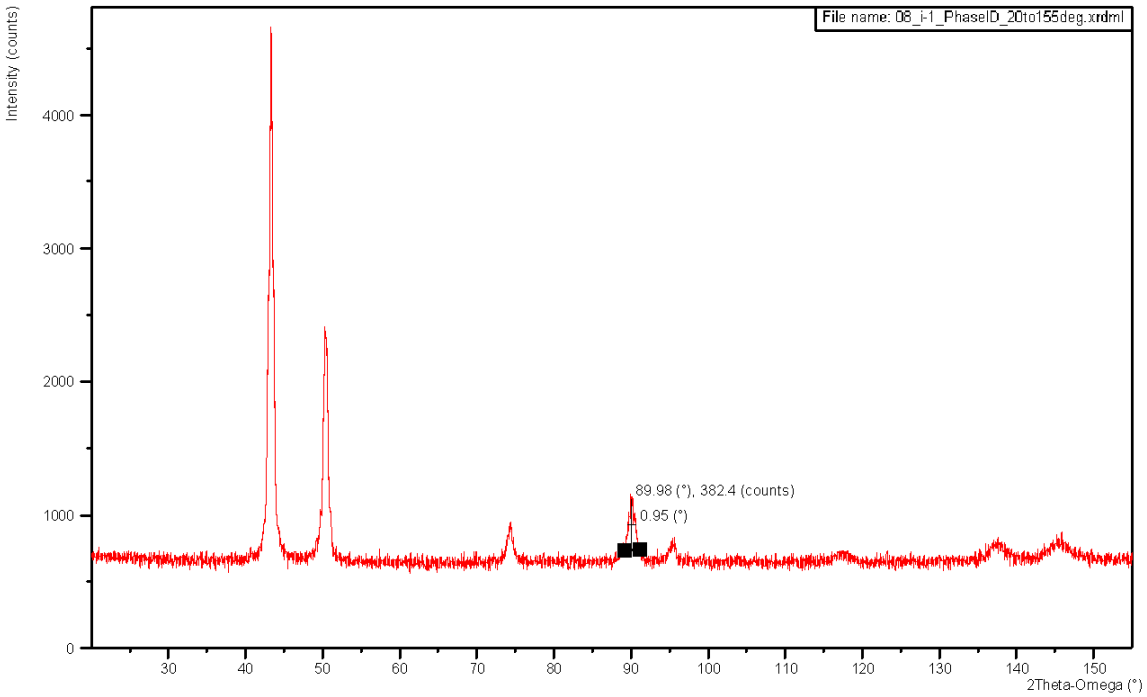

Figure 74: Inconel® 718 phase ID scan from 20° to 155° 2Theta with peak at 89.98° identified.

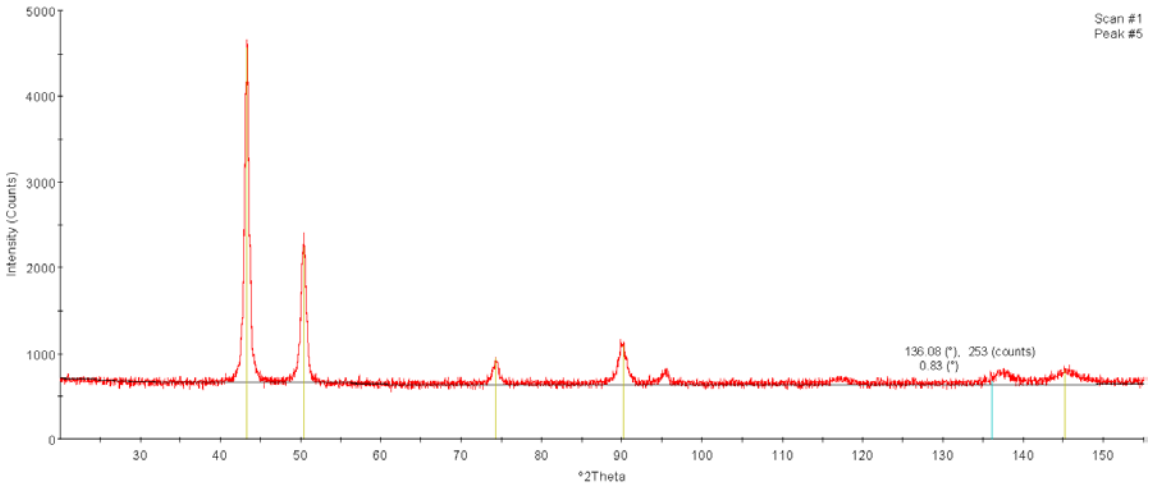

Figure 75: Inconel® 718 phase ID scan from 20° to 155° 2Theta with peak at 136.08° identified.

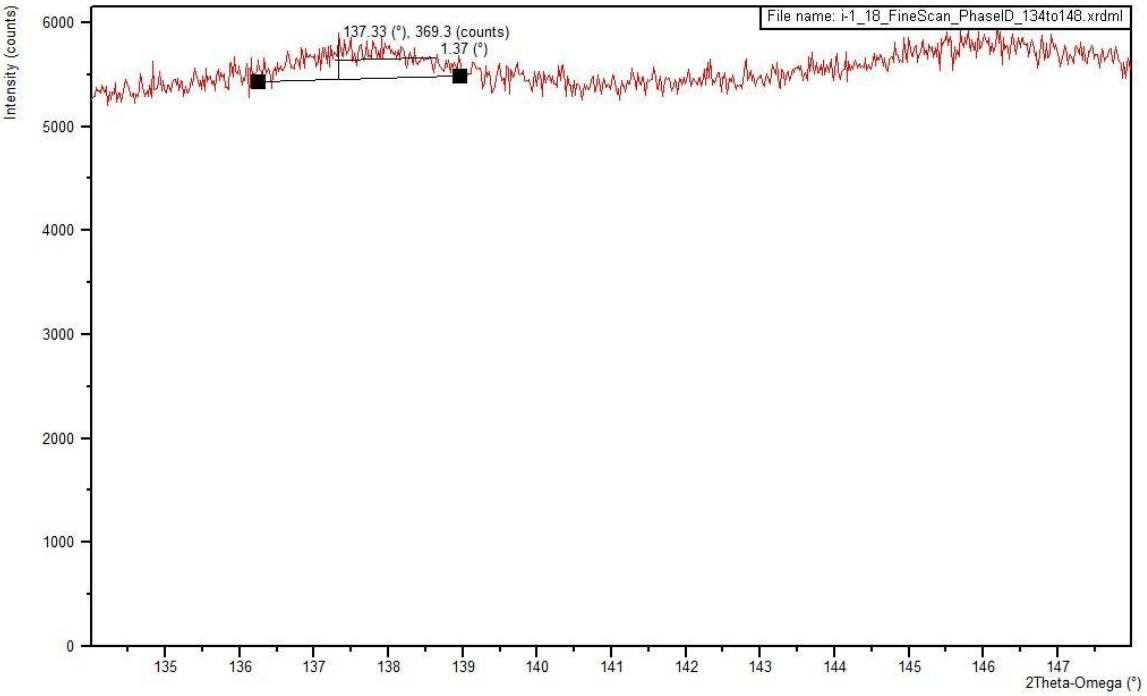

Figure 76: Inconel® 718 phase ID scan with peak at 137.33° 2Theta identified showing net height of 369.3 counts (post traditional turning process).

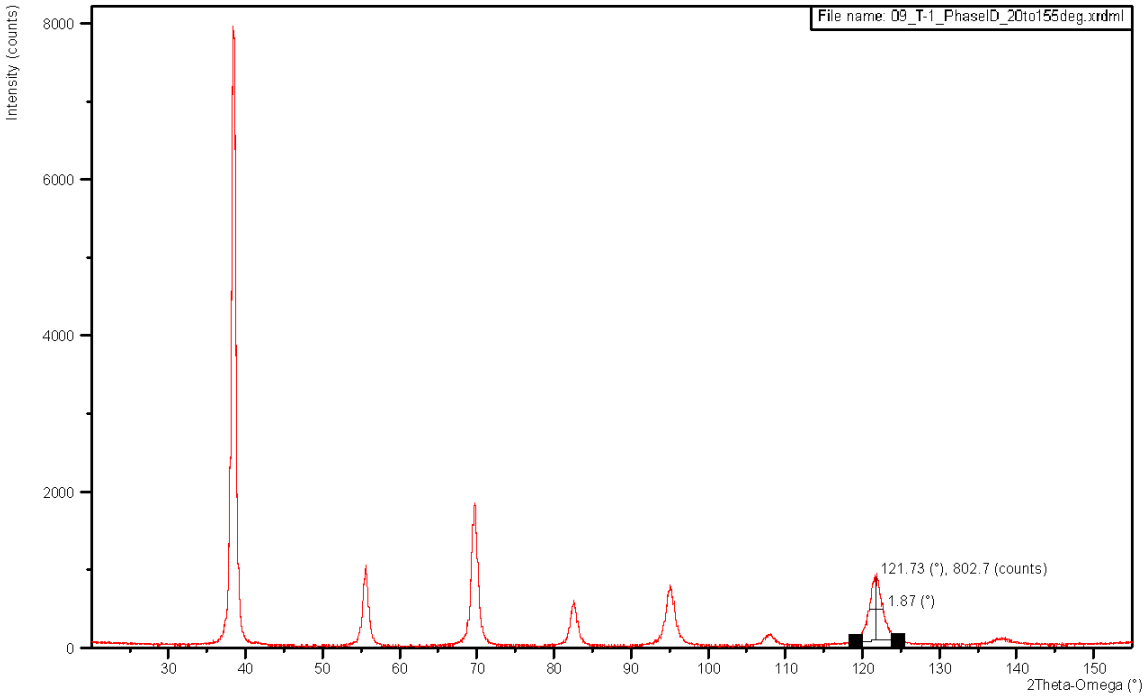

Figure 77: 97Ta3W phase ID scan from 20° to 155° 2Theta with peak at 121.73° identified.

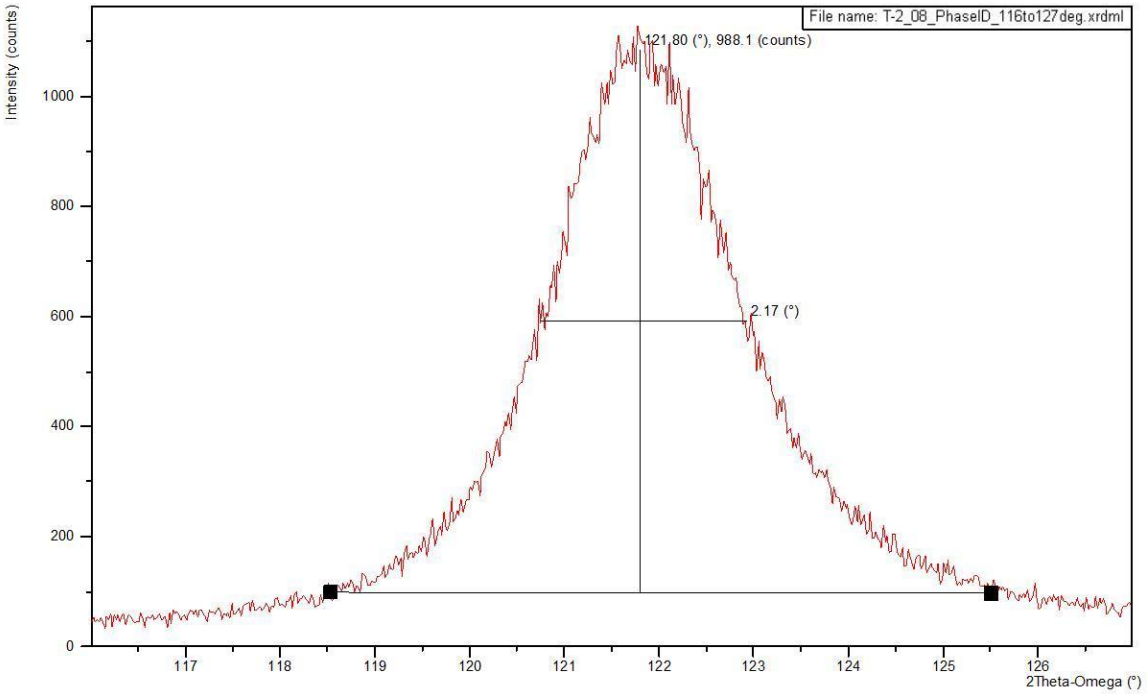

Figure 78: 97Ta3W phase ID scan with peak at 121.80° 2Theta identified showing net height of 988.1 counts (post traditional turning process).

APPENDIX C: STRESS DATA

(Tables are saved as images to fit pages.)

Table 5: Table indicating change in surface stress of sample materials after being machined.

Stresses in the specimen reference frame										
Material	Sample ID	Cut Operation	File Name	Phi (°)	SigmaPhi (MPa)	StdDev (MPa)	TauPhi (MPa)	StdDev (MPa)	Sig11+Sig22 (MPa)	StdDev (MPa)
Alum	A-5	Saw Cut	A-5_05_Stress_Rough_FaceCut	0	(124.0)	139.1	37.8	22.6	(62.5)	90.5
Alum	A-5	Saw Cut	A-5_05_Stress_Rough_FaceCut	45	373.7	99.7	3.2	16.2	188.3	64.9
Alum	A-5	Saw Cut	A-5_05_Stress_Rough_FaceCut	90	(83.9)	334.2	(191.9)	54.2	(42.3)	217.3
Alum	A-5	Saw Cut	A-5_05_Stress_Rough_FaceCut	135	(50.0)	23.1	16.4	3.7	(25.2)	15.0
Alum	A-5	Traditional	A-5_09_Stress_TraditionalCut	0	(103.3)	283.0	(47.7)	45.9	(52.0)	184.1
Alum	A-5	Traditional	A-5_09_Stress_TraditionalCut	45	(61.4)	159.9	69.1	25.9	(30.9)	104.0
Alum	A-5	Traditional	A-5_09_Stress_TraditionalCut	90	434.7	341.8	4.1	58.9	178.1	164.7
Alum	A-5	Traditional	A-5_09_Stress_TraditionalCut	135	149.0	56.2	131.5	10.3	5.0	38.4
Alum	A-5	Fine MTP	A-5_14_Stress_FineMTP	0	1192.5	434.2	(121.1)	70.4	600.8	282.4
Alum	A-5	Fine MTP	A-5_14_Stress_FineMTP	45	219.2	38.6	(39.4)	6.3	110.4	25.1
Alum	A-5	Fine MTP	A-5_14_Stress_FineMTP	90	190.9	125.8	65.7	20.4	96.2	81.8
Alum	A-5	Fine MTP	A-5_14_Stress_FineMTP	135	(37.7)	64.5	18.8	10.5	(19.0)	41.9
Alum	A-5	Traditional	A-5_18_Stress_TraditionalCut	0	(269.4)	187.3	(6.5)	30.4	(135.7)	121.8
Alum	A-5	Traditional	A-5_18_Stress_TraditionalCut	45	243.0	63.8	(30.4)	10.4	122.4	41.5
Alum	A-5	Traditional	A-5_18_Stress_TraditionalCut	90	296.5	173.6	(67.4)	28.2	149.4	112.9
Alum	A-5	Traditional	A-5_18_Stress_TraditionalCut	135	392.4	108.5	(50.3)	17.6	197.7	70.6
Alum	A-5	Fine MTP	A-5_23_Stress_FineMTP	0	45.8	223.1	45.5	36.2	23.1	145.1
Alum	A-5	Fine MTP	A-5_23_Stress_FineMTP	45	394.2	224.4	108.0	36.4	198.6	146.0
Alum	A-5	Fine MTP	A-5_23_Stress_FineMTP	90	(8.0)	322.3	5.0	52.3	(4.0)	209.7
Alum	A-5	Fine MTP	A-5_23_Stress_FineMTP	135	(58.0)	160.2	5.2	26.0	(29.2)	104.2
Inconel	I-1	Saw Cut	i-1_06_Stress_sawcut	0	957.0	532.7	(3.0)	71.2	259.2	204.0
Inconel	I-1	Saw Cut	i-1_06_Stress_sawcut	45	450.4	991.9	(91.3)	132.6	122.0	379.9
Inconel	I-1	Saw Cut	i-1_06_Stress_sawcut	90	(1514.5)	1164.1	24.1	155.6	(410.2)	445.9
Inconel	I-1	Saw Cut	i-1_06_Stress_sawcut	135	(479.7)	502.2	98.3	67.1	(129.9)	192.4
Inconel	I-1	Traditional	i-1_11_Stress_TraditionalCut	0	(722.0)	1135.4	28.7	151.7	(195.5)	434.9
Inconel	I-1	Traditional	i-1_11_Stress_TraditionalCut	45	13.9	802.8	60.5	107.3	3.8	307.5
Inconel	I-1	Traditional	i-1_11_Stress_TraditionalCut	90	1037.1	0.0	(231.9)	0.0	374.5	0.0
Inconel	I-1	Traditional	i-1_11_Stress_TraditionalCut	135	(3162.2)	2553.6	(92.0)	341.2	(856.5)	978.1
Inconel	I-1	Fine MTP	i-1_15_Stress_FineMTP	0	558.7	0.0	(16.8)	0.0	201.8	0.0
Inconel	I-1	Fine MTP	i-1_15_Stress_FineMTP	45	(186.6)	232.1	42.1	31.0	(50.6)	88.9
Inconel	I-1	Fine MTP	i-1_15_Stress_FineMTP	90	475.7	356.3	(34.5)	47.6	128.8	136.5
Inconel	I-1	Fine MTP	i-1_15_Stress_FineMTP	135	83.9	709.4	(103.6)	94.8	22.7	271.7
Inconel	I-1	Traditional	i-1_19_Stress_TraditionalCut	0	889.2	43.6	(47.8)	5.8	240.8	16.7
Inconel	I-1	Traditional	i-1_19_Stress_TraditionalCut	45	1641.9	1073.4	8.0	143.4	444.7	411.1
Inconel	I-1	Traditional	i-1_19_Stress_TraditionalCut	90	(24.3)	521.0	(37.3)	69.6	(6.6)	199.6
Inconel	I-1	Traditional	i-1_19_Stress_TraditionalCut	135	301.3	570.1	18.7	76.2	81.6	218.4
Inconel	I-1	Fine MTP	i-1_23_Stress_FineMTP	0	18.0	428.6	(153.6)	57.3	4.9	164.2
Inconel	I-1	Fine MTP	i-1_23_Stress_FineMTP	45	496.0	568.6	53.4	76.0	134.3	217.8
Inconel	I-1	Fine MTP	i-1_23_Stress_FineMTP	90	(988.0)	94.4	(131.8)	12.6	(267.6)	36.2
Inconel	I-1	Fine MTP	i-1_23_Stress_FineMTP	135	983.0	516.5	134.2	69.0	266.2	197.8
Tantalum	T-1	Saw Cut	T-1_05_Stress_sawcut	0	(190.2)	104.0	3.9	16.9	(91.7)	64.7
Tantalum	T-1	Saw Cut	T-1_05_Stress_sawcut	45	(41.3)	36.9	(4.1)	6.0	(19.9)	23.0
Tantalum	T-1	Saw Cut	T-1_05_Stress_sawcut	90	(144.3)	40.9	2.1	6.6	(69.6)	25.5
Tantalum	T-1	Saw Cut	T-1_05_Stress_sawcut	135	(143.4)	26.8	1.6	4.4	(69.1)	16.7
Tantalum	T-2	Saw Cut	T-2_05_Stress_sawcut	0	(26.2)	50.7	12.5	8.2	(12.6)	31.5
Tantalum	T-2	Saw Cut	T-2_05_Stress_sawcut	45	(145.7)	43.0	5.3	7.0	(70.2)	26.7
Tantalum	T-2	Saw Cut	T-2_05_Stress_sawcut	90	(89.6)	13.0	(5.4)	2.1	(43.2)	8.1
Tantalum	T-2	Saw Cut	T-2_05_Stress_sawcut	135	(209.3)	48.5	(5.1)	7.9	(100.9)	30.2
Tantalum	T-2	Traditional	T-2_10_Stress_TradTurn	0	22.7	94.0	11.1	15.3	10.9	58.5
Tantalum	T-2	Traditional	T-2_10_Stress_TradTurn	45	21.1	79.4	3.0	12.9	10.2	49.5
Tantalum	T-2	Traditional	T-2_10_Stress_TradTurn	90	(38.2)	51.3	3.9	8.3	(18.4)	31.9
Tantalum	T-2	Traditional	T-2_10_Stress_TradTurn	135	40.2	128.0	(10.1)	20.8	19.4	79.6
Tantalum	T-2	Fine MTP	T-2_14_Stress_FineMTP	0	7.0	23.4	(5.4)	3.8	3.4	14.6
Tantalum	T-2	Fine MTP	T-2_14_Stress_FineMTP	45	(84.7)	38.5	(14.6)	6.2	(40.8)	24.0
Tantalum	T-2	Fine MTP	T-2_14_Stress_FineMTP	90	(100.1)	114.0	4.4	18.5	(48.3)	71.0
Tantalum	T-2	Fine MTP	T-2_14_Stress_FineMTP	135	(115.4)	53.7	20.7	8.7	(55.6)	33.4

Table 6: Table indicating d-spacing and change in d-spacing per alloy.

Cut Operation	File Name	d-spacing	Δ d-spacing from previous	% Δ d-spacing from previous	% Δ d-spacing per process type
Saw Cut	A-5_05_Stress_Rough_FaceCut	1.01318			
Traditional	A-5_09_Stress_TraditionalCut	1.01339	-0.00021	-0.02%	0.00%
Fine MTP	A-5_14_Stress_FineMTP	1.01426	-0.00087	-0.09%	-0.04%
Traditional	A-5_18_Stress_TraditionalCut	1.01344	0.00082	0.08%	
Fine MTP	A-5_23_Stress_FineMTP	1.01465	-0.00121	-0.12%	
Saw Cut	i-1_06_Stress_sawcut	0.83016			
Traditional	i-1_11_Stress_TraditionalCut	0.82563	0.00453	0.55%	-0.37%
Fine MTP	i-1_15_Stress_FineMTP	0.82915	-0.00352	-0.42%	0.12%
Traditional	i-1_19_Stress_TraditionalCut	0.82871	0.00044	0.05%	
Fine MTP	i-1_23_Stress_FineMTP	0.82812	0.00059	0.07%	
Saw Cut	T-1_05_Stress_sawcut	0.88241			-0.01%
Saw Cut	T-2_05_Stress_sawcut	0.88246	-0.00005	-0.01%	
Traditional	T-2_10_Stress_TradTurn	0.88224	0.00022	0.02%	
Fine MTP	T-2_14_Stress_FineMTP	0.88266	-0.00042	-0.05%	

Table 7: Peak search results of stress scan series for Aluminum 6061-T6 sample A-5 after saw cut.

Scan Name	Scan No.	Peak No.	Peak pos. (°2Theta)	d-spacing (Å)	sin²Psi
A-5_05_Stress_Rough_FaceCut	1	1	98.8782	1.01393	0
A-5_05_Stress_Rough_FaceCut	2	2	98.7021	1.01527	0.125
A-5_05_Stress_Rough_FaceCut	3	3	98.87	1.01399	0.25
A-5_05_Stress_Rough_FaceCut	4	4	98.8728	1.01397	0
A-5_05_Stress_Rough_FaceCut	5	5	98.8831	1.01389	0.125
A-5_05_Stress_Rough_FaceCut	6	6	98.6027	1.01602	0.25
A-5_05_Stress_Rough_FaceCut	7	7	98.874	1.01396	0
A-5_05_Stress_Rough_FaceCut	8	8	99.1193	1.01211	0.125
A-5_05_Stress_Rough_FaceCut	9	9	99.5402	1.00896	0.25
A-5_05_Stress_Rough_FaceCut	10	10	98.8752	1.01395	0
A-5_05_Stress_Rough_FaceCut	11	11	98.8355	1.01425	0.125
A-5_05_Stress_Rough_FaceCut	12	12	98.8789	1.01393	0.25
A-5_05_Stress_Rough_FaceCut	13	13	98.8769	1.01394	0
A-5_05_Stress_Rough_FaceCut	14	14	98.8225	1.01435	0.125
A-5_05_Stress_Rough_FaceCut	15	15	99.0458	1.01266	0.25
A-5_05_Stress_Rough_FaceCut	16	16	98.881	1.01391	0
A-5_05_Stress_Rough_FaceCut	17	17	98.8253	1.01433	0.125
A-5_05_Stress_Rough_FaceCut	18	18	98.6694	1.01552	0.25
A-5_05_Stress_Rough_FaceCut	19	19	98.877	1.01394	0
A-5_05_Stress_Rough_FaceCut	20	20	98.923	1.01359	0.125
A-5_05_Stress_Rough_FaceCut	21	21	98.3284	1.01812	0.25
A-5_05_Stress_Rough_FaceCut	22	22	98.8801	1.01392	0
A-5_05_Stress_Rough_FaceCut	23	23	98.9059	1.01372	0.125
A-5_05_Stress_Rough_FaceCut	24	24	98.9411	1.01346	0.25

APPENDIX D: STRESS PLOTS

Charts illustrating change in surface stress of sample material after being machined.

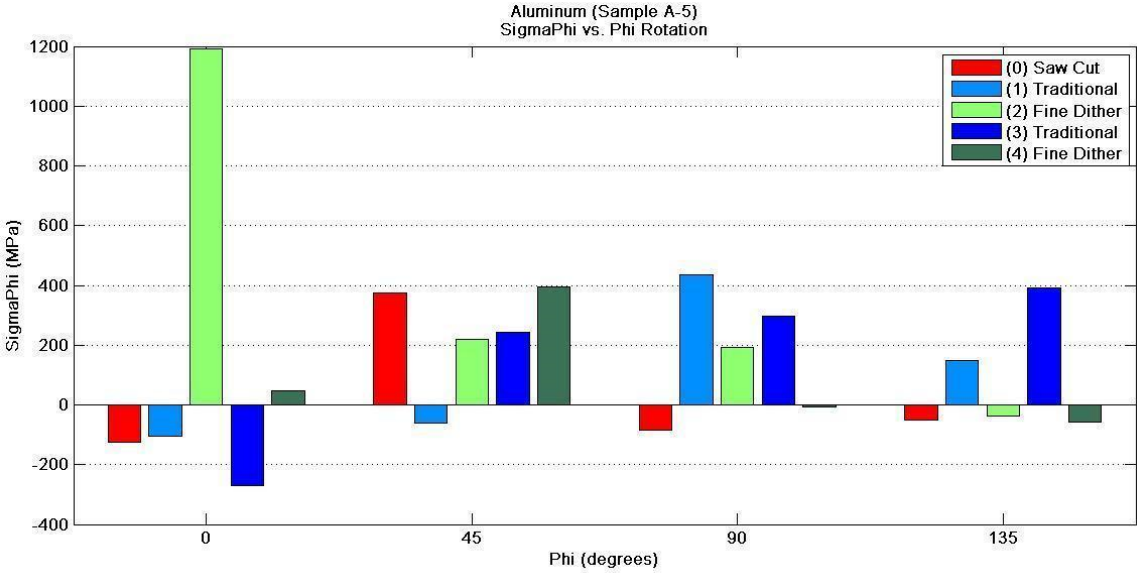

Figure 79: Normal stress (SigmaPhi) grouped by Phi rotation.

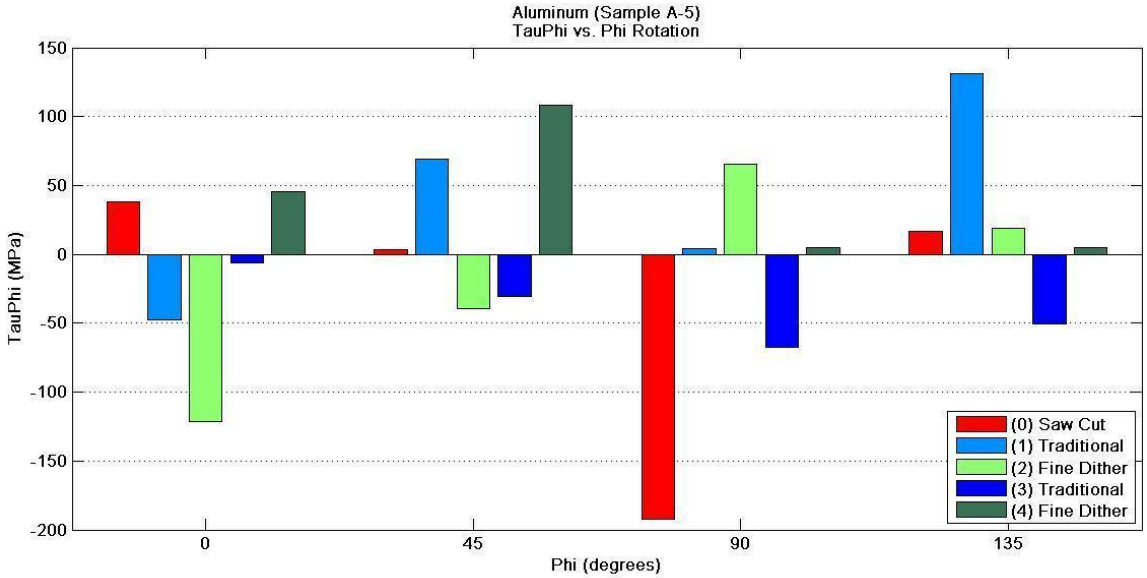

Figure 80: Shear stress (TauPhi) grouped by Phi rotation.

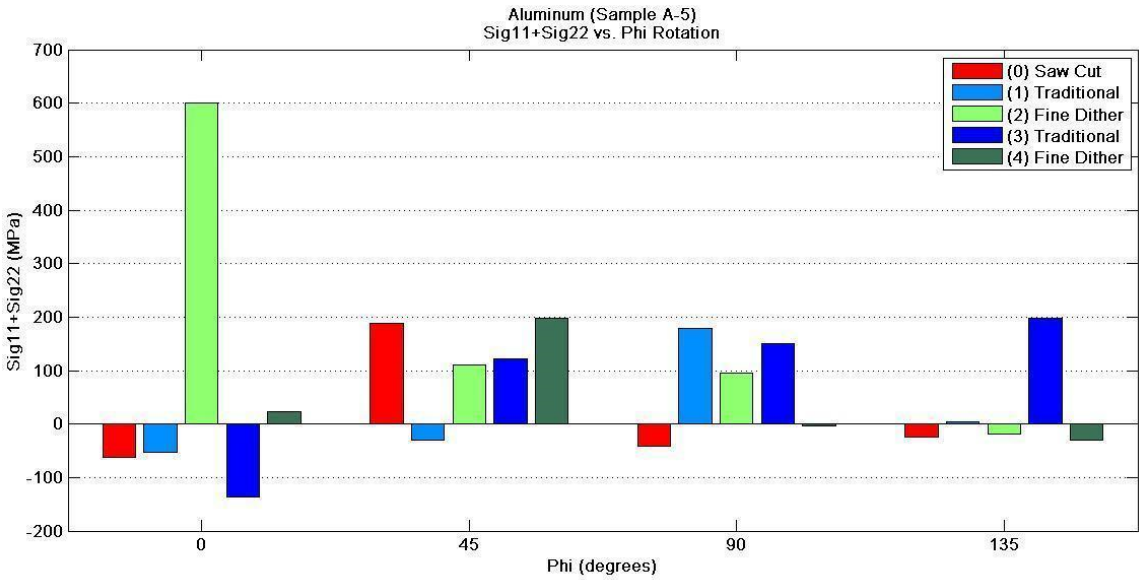

Figure 81: Normal stress (Sig11+Sig22) grouped by Phi rotation.

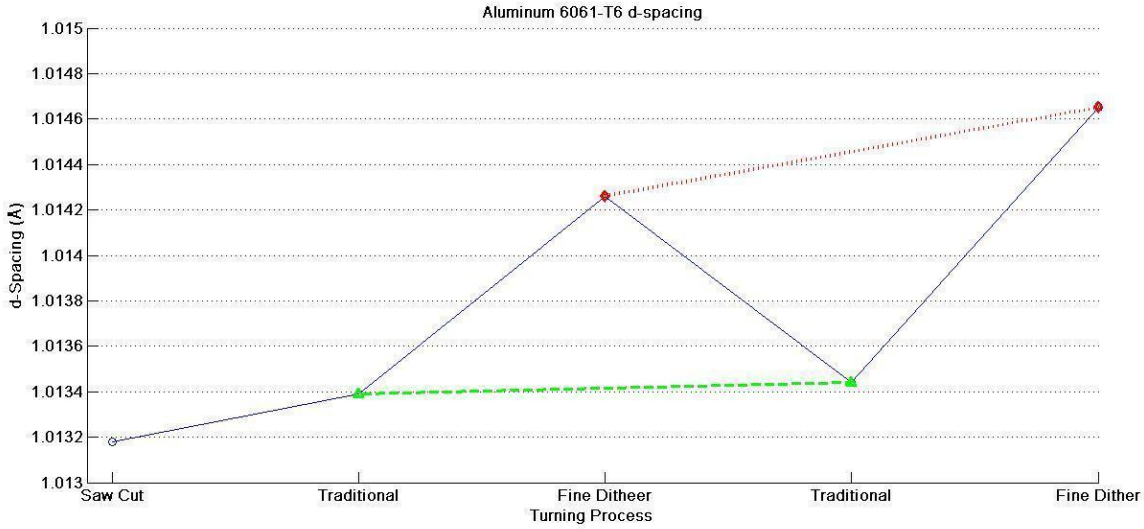

Figure 82: Strain-free d-spacing plotted linearly with progression of sample operations.

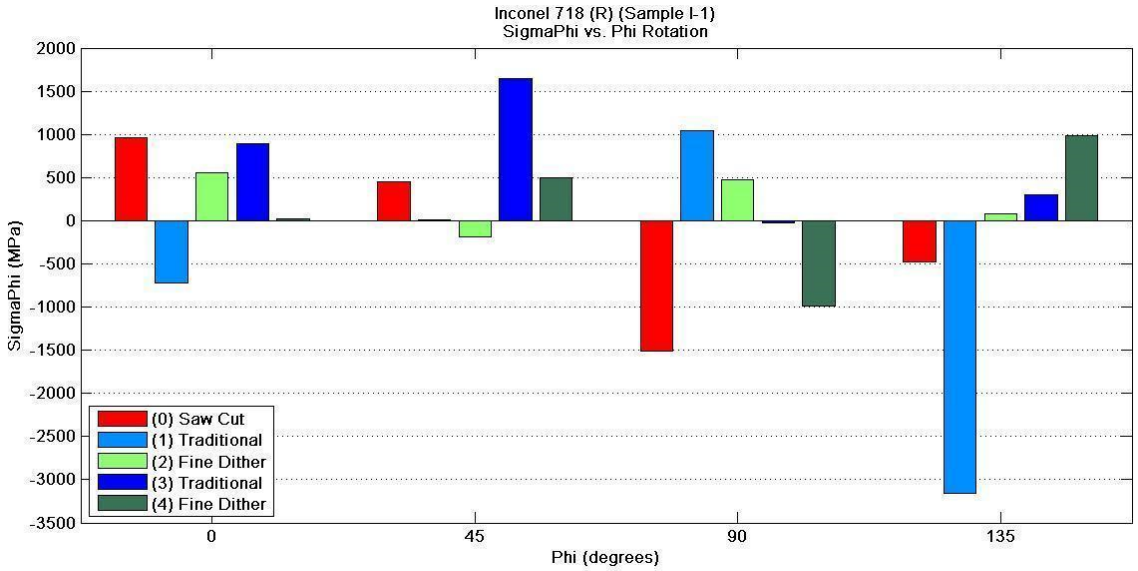

Figure 83: Normal stress (SigmaPhi) grouped by Phi rotation.

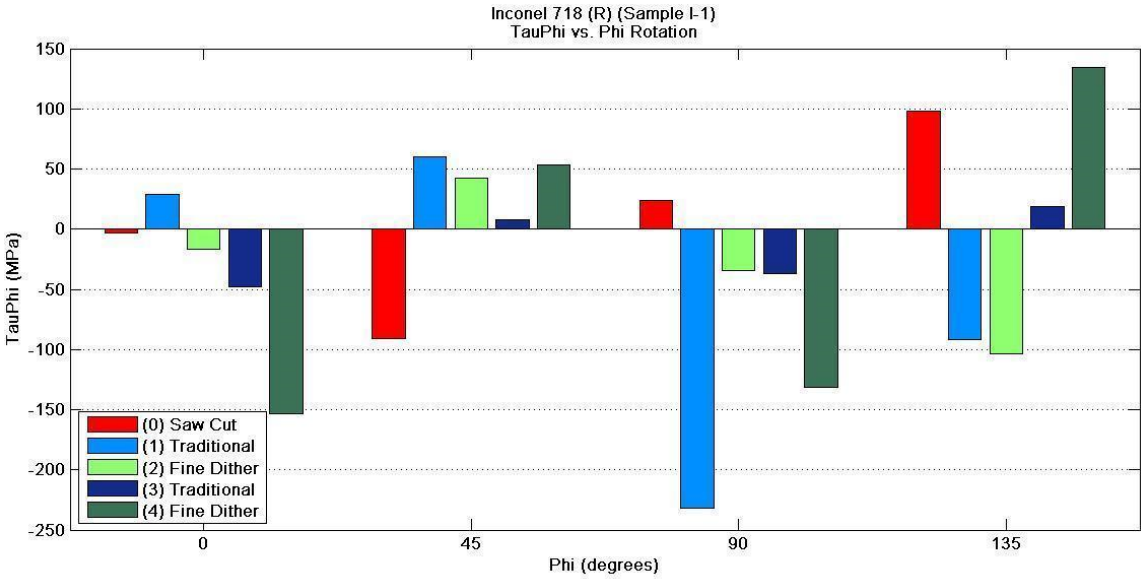

Figure 84: Shear stress (TauPhi) grouped by Phi rotation.

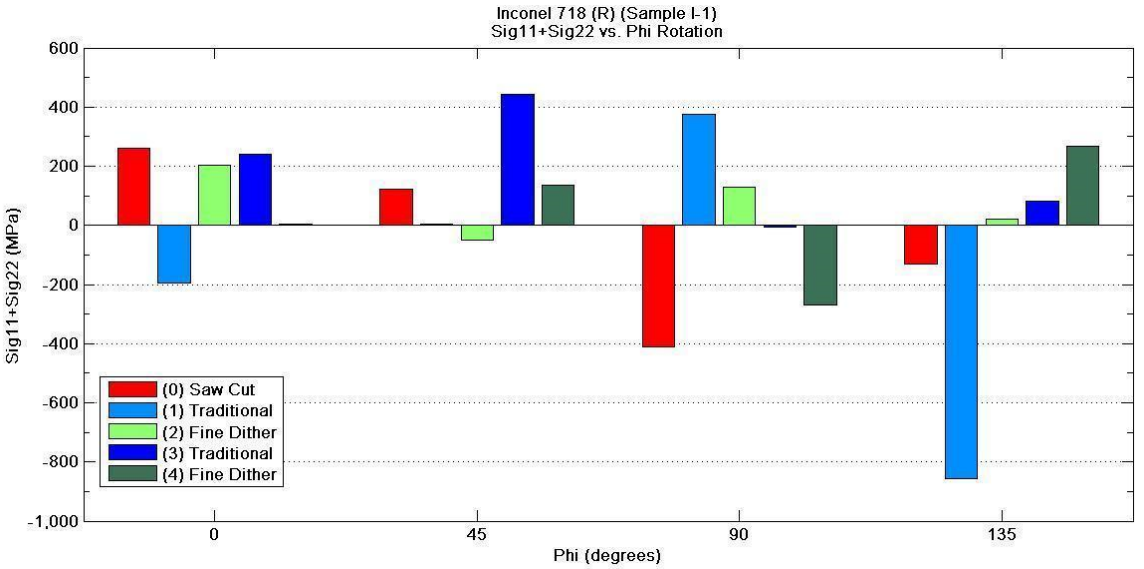

Figure 85: Normal stress (Sig11+Sig22) grouped by Phi rotation.

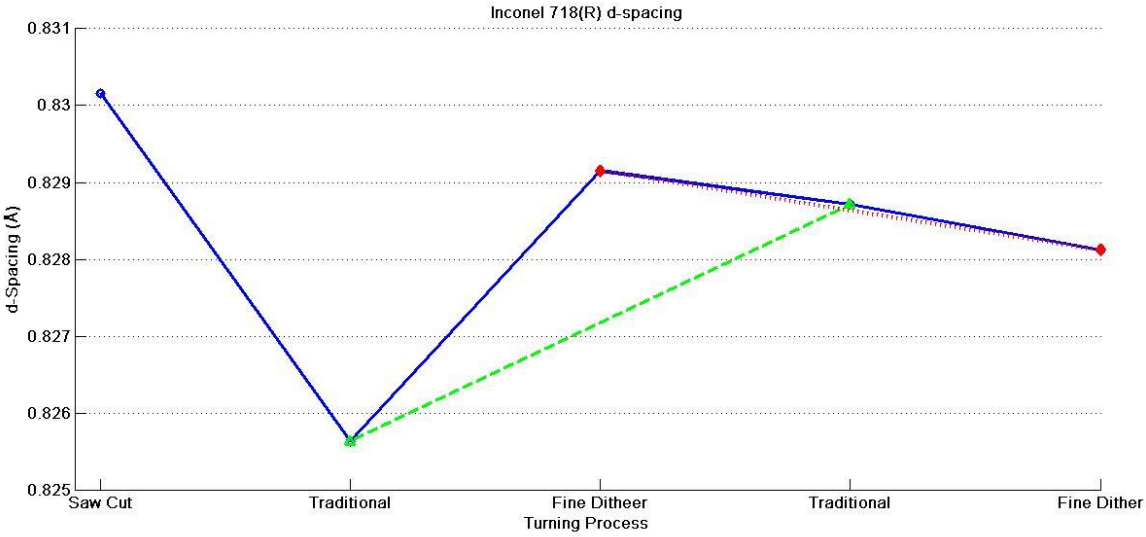

Figure 86: Strain-free d-spacing plotted linearly with progression of sample operations.

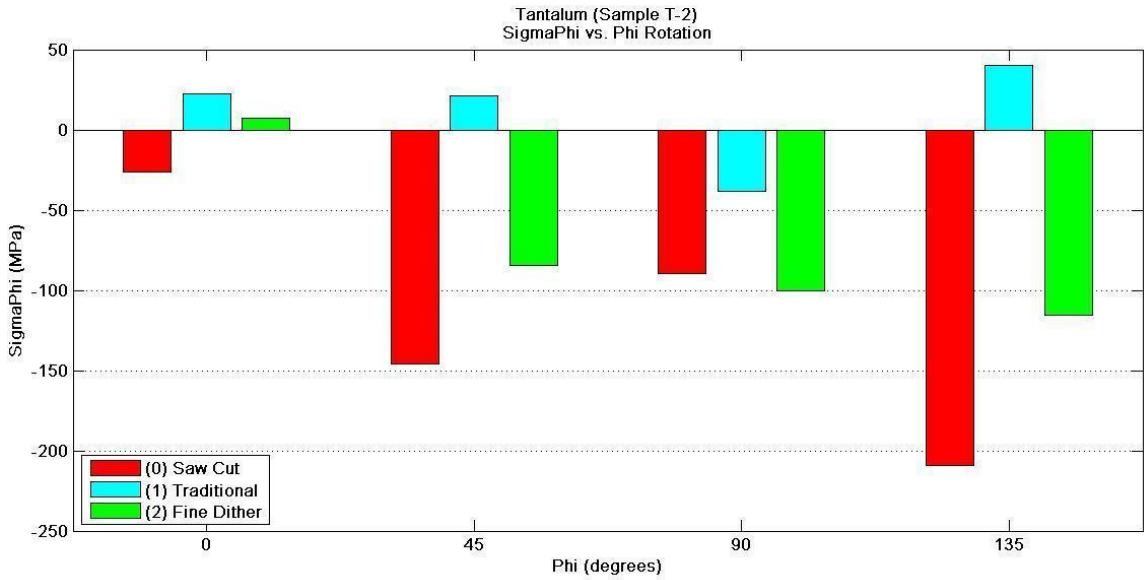

Figure 87: Normal stress (SigmaPhi) grouped by Phi rotation.

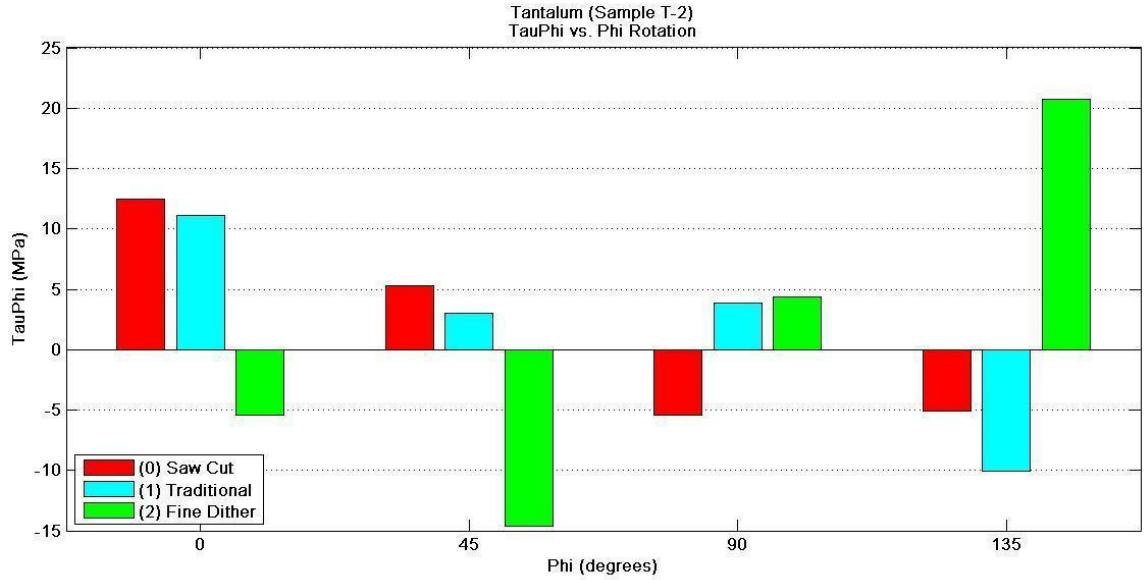

Figure 88: Shear stress (TauPhi) grouped by Phi rotation.

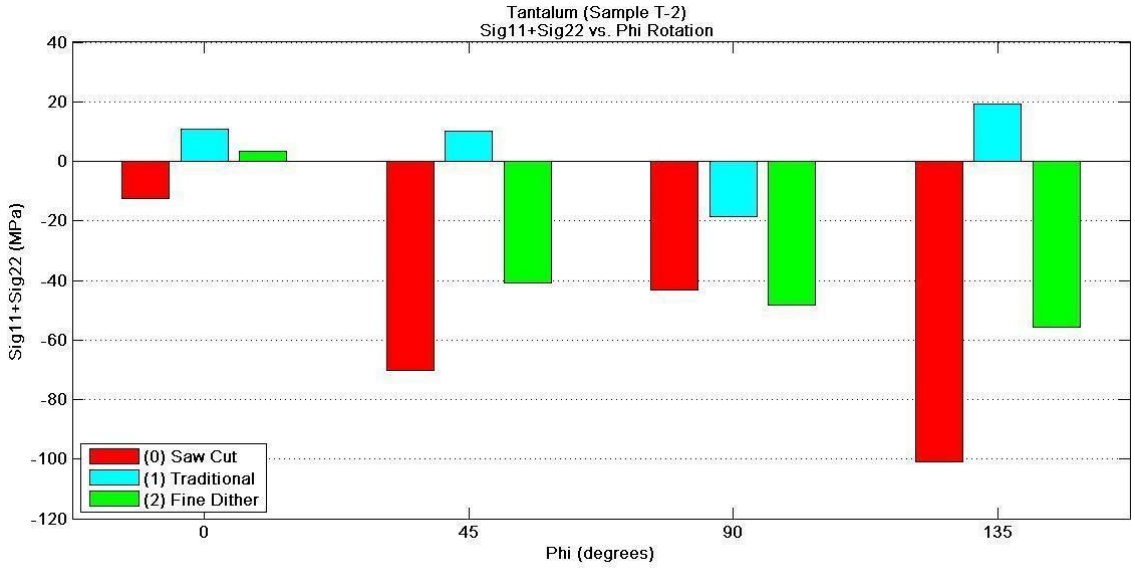

Figure 89: Normal stress (Sig11+Sig22) grouped by Phi rotation.

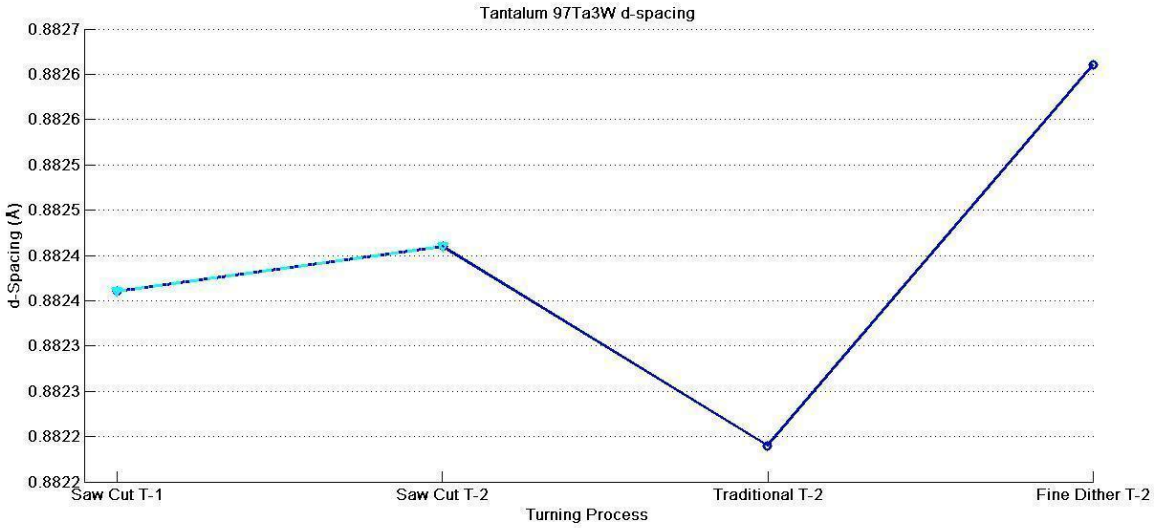

Figure 90: Strain-free d-spacing plotted linearly with progression of sample operations.

APPENDIX E: MATLAB™ and CNC code

Table 8: Brief summation of codes listed in Appendix E.

Summary of Code Development		
Program Name	**Code Purpose**	**Code Output**
ZSineCode	Create single sine wave in Z-axis for face cutting on lathe.	X & Z coordinates (1000 points--CNC code over 1000 lines.)
ZSineCode_Rev_07	Multiple sine wave version of ZSineCode to increase surface flatness.	X & Z coordinates (4000 points--CNC code over 4000 lines.)
FineMTP	Reduction of CNC file size by using subroutine to create a modulated tool path process with higher frequency of cuts in X direction.	CNC style code (Can be compressed to less than 20 lines of CNC code.)

```
%   ZSineCode.m
% Single sine wave modulated tool path process

clear all
close all
clc

D=4.0 ;  %Stock Diameter
DoC=.010;    %Depth of Cut
omega=1;      %Frequency
DoS=.002;   %Depth of Step
theta=0;    %Phase Shift
E=0;        %Offset-Engagement into material (Shift from -DoC to +DoC)
step=[0:1:(D/2/DoS)]; %Number of Steps
X=D-2*step*DoS;
Z=DoC*sin(omega*step+theta)+E;

figure
plot(X,Z,'+-')
```

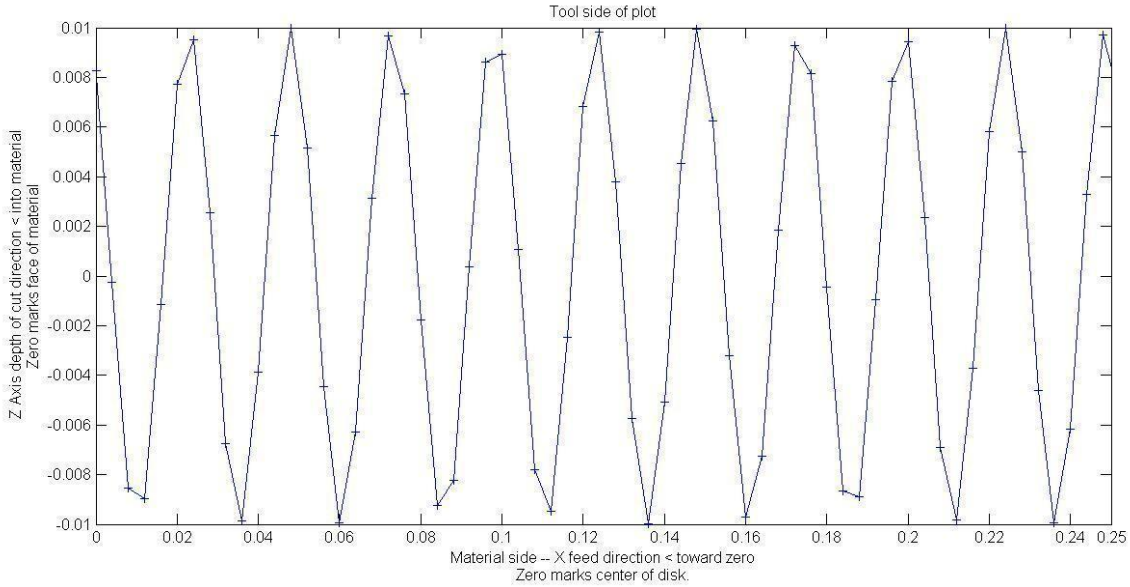

Figure 91: ZSineCode plotted output of data points at last 0.25 inches of diametrical travel.

```
%   ZSineCode_Rev_07.m
% Four sine waves for modulated tool path process

close all
clear all
clc

D=4.0 ;     %Stock Diameter
DoC=.010;   %Depth of Cut
omega=1;    %Frequency
DoS=.002;   %Depth of Step
theta=pi;    %Phase Shift
theta_2=pi/2;
E=-1*DoC*.8;        %Offset-Engagement into material (Shift from -DoC
to +DoC)
E_1=-1*DoC*.9;
step=[0:1:(D/2/DoS)]; %Number of Steps
X=D-2*step*DoS;
Z=DoC*sin(omega*step+0)+0;

figure
plot(X,Z,'+-')
hold on

DoC_1=DoC*.2;
X_1=X-DoS/2;
Z_1=DoC_1*sin((omega*step)+theta)+E;
plot(X_1,Z_1,'ro:')

DoC_2=DoC*.1;
X_2=X_1-DoS/2;
Z_2=DoC_2*sin((omega*step)+theta_2)+E_1;
plot(X_2,Z_2,'ks--')

DoC_3=DoC_2;
X_3=X_1+DoS/2;
Z_3=DoC_3*sin((omega*step)-theta_2)+E_1;
plot(X_3,Z_3,'gd-.')

phase_1=[X.' Z.'];
phase_2=[X_1.' Z_1.'];
phase_3=[X_2.' Z_2.'];
phase_4=[X_3.' Z_3.'];

dlmwrite('phase_1.xls',phase_1,'\t',0,0)
dlmwrite('phase_2.xls',phase_2,'\t',0,0)
dlmwrite('phase_3.xls',phase_3,'\t',0,0)
dlmwrite('phase_4.xls',phase_4,'\t',0,0)
```

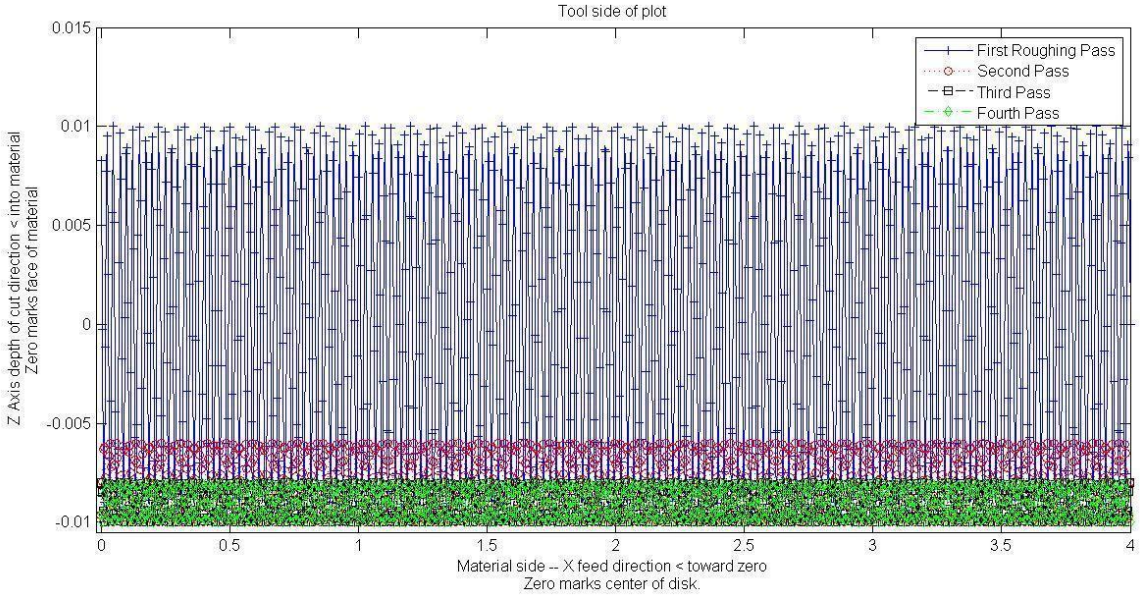

Figure 92: ZSineCode_Rev_07 points plotted from 4.0 inch diameter to 0 (center of sample part).

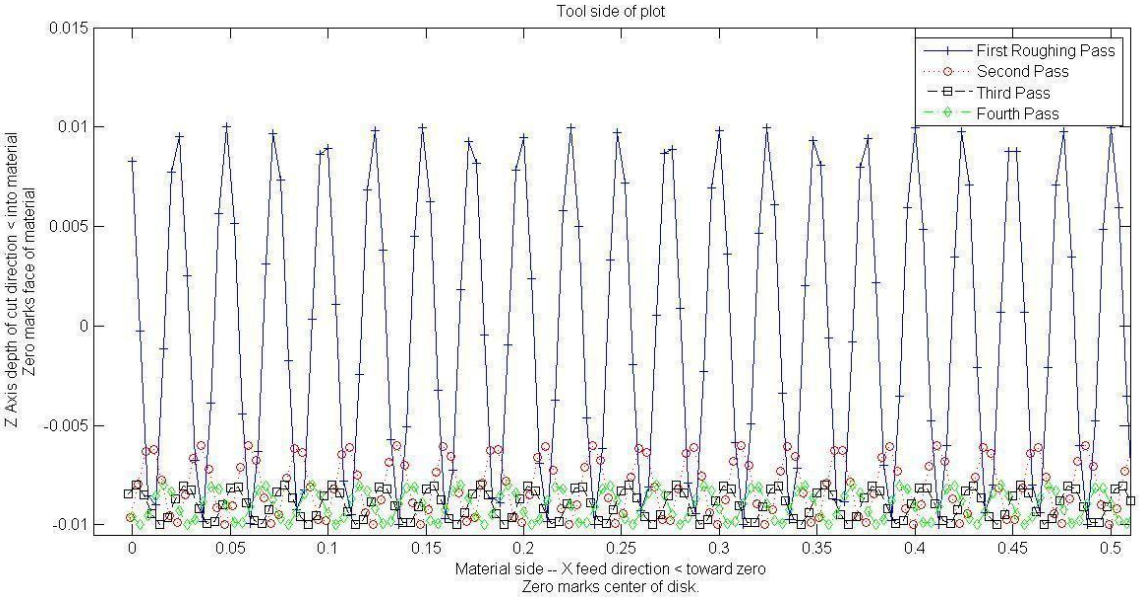

Figure 93: Final 0.5 inch diametrical travel from ZSineCode_Rev_07.

```
%   FineMTPStart.m
% Fine Modulated Tool Path Cycle Start

a=cell(100,10);     % Creates empty cell of 100 rows by 10 columns
a{1,1}='O51040';    % Program name
a{2,1}='T4';        % Selected Tool
a{3,1}='G50';       %
a{3,2}='S1500';     % Maximum Spindle Speed [RPM]
a{4,1}='G97';       % Cancel CSS
a{4,2}='S1500';
a{4,3}='M03';       % Starts the Spindle Forward
a{5,1}='G96';       % CSS
a{5,2}='S1500';
a{5,3}='M03';       % Starts the Spindle Forward

%   FineMTP_Alum.m
% Program creates code for Fine Modulated Tool Path Cycle
% Aluminum

% R1/64"
clear all
close all
clc
D=4.000;            % Diameter [inch]
Ap=0.001;           % Depth of Cut [inch]
L=D/Ap;             % Number of loops

a=cell(100,10);     % Creates empty cell of 100 rows by 10 columns
a{1,1}='%';
a{2,1}='O10101';    % Program name "o1245" "1" matl (A=1, N=2,T=3)"2"
coat(0=un, 1=coat) "3"(Radius)"45" (DOC in thou.)
a{3,1}='T4';        % Selected Tool
a{4,1}='G50';       %
a{4,2}='S1500';     % Maximum Spindle Speed [RPM]
a{5,1}='G97';       % Cancel CSS
a{5,2}='S1500';
a{5,3}='M03';       % Starts the Spindle Forward
a{6,1}='G96';       % CSS
a{6,2}='S600';      % VNMS331 K313
a{6,3}='M08';       % Coolant On
% Starting Position
a{7,1}='G00';       % Rapid Move
a{7,2}='X4.5';      % Move outward
a{8,1}='G00';       % Move toward part
a{8,2}='X4.1';
a{8,3}='Z0.02';

a{9,1}='M03';
a{9,2}='F0.009';    % Feed Rate for -MS .006-.015 [inch]

a{10,1}='N1000';    % Start Line 0
a{10,2}='G01';      % Linear move
a{10,3}='X';

a{10,4}=D;          % Diameter
```

```
a{10,5}='Z';
a{10,6}='0.000';

a{11,1}='M97';      % To Execute a local sub-routine
a{11,2}='P1001';    % Jumps to line N1001 after the M30
a{11,3}='L';        % Repeat
a{11,4}=L;
a{12,1}='G01';
a{12,2}='X';
a{12,3}='4.05';
a{12,4}='Z';
a{12,5}='0.100';

%a{19,1}='G28';        % Home

a{20,1}='M30';      % End of main Program

a{21,1}='N1001';    % Start Line 1
a{21,2}='G01';
a{21,3}='U';        % Incremental X
a{21,4}='0.000';    % Hold
a{21,5}='W';        % Incremental Z
a{21,6}='-.010';    % Cut

a{22,1}='N1002';    % Start Line 2
a{22,2}='G01';
a{22,3}='U';        % Incremental X
a{22,4}='0.000';    % Hold
a{22,5}='W';        % Incremental Z
a{22,6}='0.005';    % Clear

a{23,1}='N1003';    % Start Line 3
a{23,2}='G01';
a{23,3}='U';        % Incremental X
a{23,4}=-1*Ap;        % Move in
a{23,5}='W';        % Incremental Z
a{23,6}='0.005';    % Clear

a{30,1}='M99';      % Jumps back to the line after the local sub-
routine call in main program
```

- - - - - - - - - - - -

```
'%'    []     []     []     []     []     []     []     []     []
'O10101'      []     []     []     []     []     []     []     []     []
'T4'   []     []     []     []     []     []     []     []     []
'G50'  'S1500'[]     []     []     []     []     []     []     []
'G97'  'S1500''M03'  []     []     []     []     []     []     []
'G96'  'S600'  'M08'  []     []     []     []     []     []     []
```

'G00'	'X4.5'	[]	[]	[]	[]	[]	[]	[]	[]	
'G00'	'X4.1'	'Z0.02'	[]	[]	[]	[]	[]	[]	[]	
'M03'	'F0.009'		[]	[]	[]	[]	[]	[]	[]	[]
'N1000'		'G01'	'X'	4.	'Z'	'0.000'	[]	[]	[]	[]
'M97'	'P1001'	'L'	4000	[]	[]	[]	[]	[]	[]	
'G01'	'X'	'4.05'	'Z'	'0.100'	[]	[]	[]	[]	[]	
[]	[]	[]	[]	[]	[]	[]	[]	[]	[]	
[]	[]	[]	[]	[]	[]	[]	[]	[]	[]	
[]	[]	[]	[]	[]	[]	[]	[]	[]	[]	
[]	[]	[]	[]	[]	[]	[]	[]	[]	[]	
[]	[]	[]	[]	[]	[]	[]	[]	[]	[]	
[]	[]	[]	[]	[]	[]	[]	[]	[]	[]	
[]	[]	[]	[]	[]	[]	[]	[]	[]	[]	
'M30'	[]	[]	[]	[]	[]	[]	[]	[]	[]	
'N1001'		'G01'	'U'	'0.000'	'W'	'-.010'	[]	[]	[]	[]
'N1002'		'G01'	'U'	'0.000'	'W'	'0.005'	[]	[]	[]	[]
'N1003'		'G01'	'U'	-0.0010	'W'	'0.005'	[]	[]	[]	[]
[]	[]	[]	[]	[]	[]	[]	[]	[]	[]	
[]	[]	[]	[]	[]	[]	[]	[]	[]	[]	
[]	[]	[]	[]	[]	[]	[]	[]	[]	[]	
[]	[]	[]	[]	[]	[]	[]	[]	[]	[]	
[]	[]	[]	[]	[]	[]	[]	[]	[]	[]	
[]	[]	[]	[]	[]	[]	[]	[]	[]	[]	
'M99'	[]	[]	[]	[]	[]	[]	[]	[]	[]	

APPENDIX F: GENERAL PROCEDURE

General Procedure

1. Use “General Conditions” form to track material treatments and note any relevant observances of material condition or process parameters.
2. Start with less expensive materials to perfect a repeatable procedure.
3. Less expensive material procedure:
    a. Use a milling machine to score a straight line along the length of round bar material for repeatability—especially with XRD.
    b. Use Wellsaw 613 horizontal band saw to saw materials to .375 inch (maximum thickness)

i. Sawing oversize and skim cutting in the lathe will provide a flatter surface.

ii. Saw can be used at low feed rate to obtain straight cuts to provide parallel cut faces within $1/64^{th}$ of an inch.

    c. Use Haas TL-1 to provide flat faces perpendicular to circumference

i. Material should be set with scored mark directly opposite of the center of jaw #1 (between jaws # 2 and # 3).

ii. Material should be set with rear face flush against seat of jaws.

iii. Machine without coolant.

iv. Turn surfaces to provide repeatable results.

    d. Mark sample on opposite surface of analysis with sample designation.

i. Samples shall be marked as “X-#” where X is the letter designation for the material type and # is the sample number per material type.

1. Material type designations for this project shall be:

    a. A: Aluminum 6061-T6

    b. I: Inconel® 718

    c. M: Tool Steel M-42

    d. N: Stainless Steel Nitronic 33

    e. T: Tantalum 97Ta3W

    f. Z: Zircaloy-4

2. Sample numbers shall be whole numbers starting at “1” and increasing by one per sample.

    e. Use PANalytical X’Pert XRD to analyze residual stresses in material.

i. Sample should be held so that in the vertical (upright) position the score mark on the sample is at the bottom (against fixture jaw or setscrew tip).

ii. Set XRD hardware and software parameters to analyze the sample. (Further details were listed in step 5.)

1. “Z” scan is used to set correct Z-axis offset.
2. “2-Theta” scan should be used to set XRD parameters.
3. “2Theta-Omega” scan should be used for determining peaks.
4. “Stress measurement” scan should be used to analyze a single peak—between 100° and 140°.

iii. Save results in appropriate digital forms.

1. XRD files (.xrdml) should be saved for stress analysis.
2. Comma separated file (.csv) of data collected should be created since .csv can be opened in spreadsheet programs.

3. Microsoft image file (.emf) should be created to note major peaks.

f. Use Haas TL-1 to turn sample as specified.

i. Material should be set with scored mark directly opposite of the center of jaw #1 (between jaws # 2 and # 3).

ii. Material should be set with rear face flush against seat of jaws.

iii. Machine without coolant when possible

iv. Select a Z-axis depth (3.f.iv.1.) and a cut pattern (3.f.iv.3.) to perform on sample.

1. Sample turnings should vary in depth of cut as stated below:

a. .010 in. (This depth was used in Z-axis.)

b. .015 in.

c. .030 in.

2. Use constant surface speed specific to each material and insert as determined from Kennametal® *Innovations Catalog*.

3. Sample turnings should use differing cut patterns.

a. “Traditional” direct and continuous feed into material.

b. “Rough MTP” rough cutting prior to cleanup of surface of modulated tool path.

c. “Multiple MTP” finish cutting modulated tool path in overlapping passes.

d. “Fine MTP” finish cutting modulated tool path in small increments.

g. Note insert type and condition.

h. Deburr outer edge of sample to prevent any burrs on the circumference from interfering with the XRD fixtures.

i. Skip to step 5. to collect and analyze stress data.

4. More expensive material procedure:

    a. Follow steps outlined in step 3. with the exception of using a cold cut saw in place of the horizontal band saw in step 3. b.

    b. Repeat steps 3.e. through 3.f. at least three times for each configuration from 3.f.iv. per sample.

5. Collect and analyze stress data for samples.

    a. X-Ray Safety

        i. Read and be familiar with X-Ray safety practices.

        ii. Obtain safety certification to use X-Ray equipment.

        iii. Wear proper personal protection equipment (PPE) if required.

        iv. Wear X-Ray dosimeters during time around X-Ray equipment.

        v. Use Geiger counter to determine background radiation levels and radiation levels around machine and tube enclosure.

        vi. Record radiation readings from Geiger counter.

        vii. (After completing XRD analysis, record exposure time.)

        viii. With radiation levels in safe range, proceed with XRD operation in step 5.b.

        ix. Identify angles of XRD motion to prevent accidental collisions using figure below as reference.

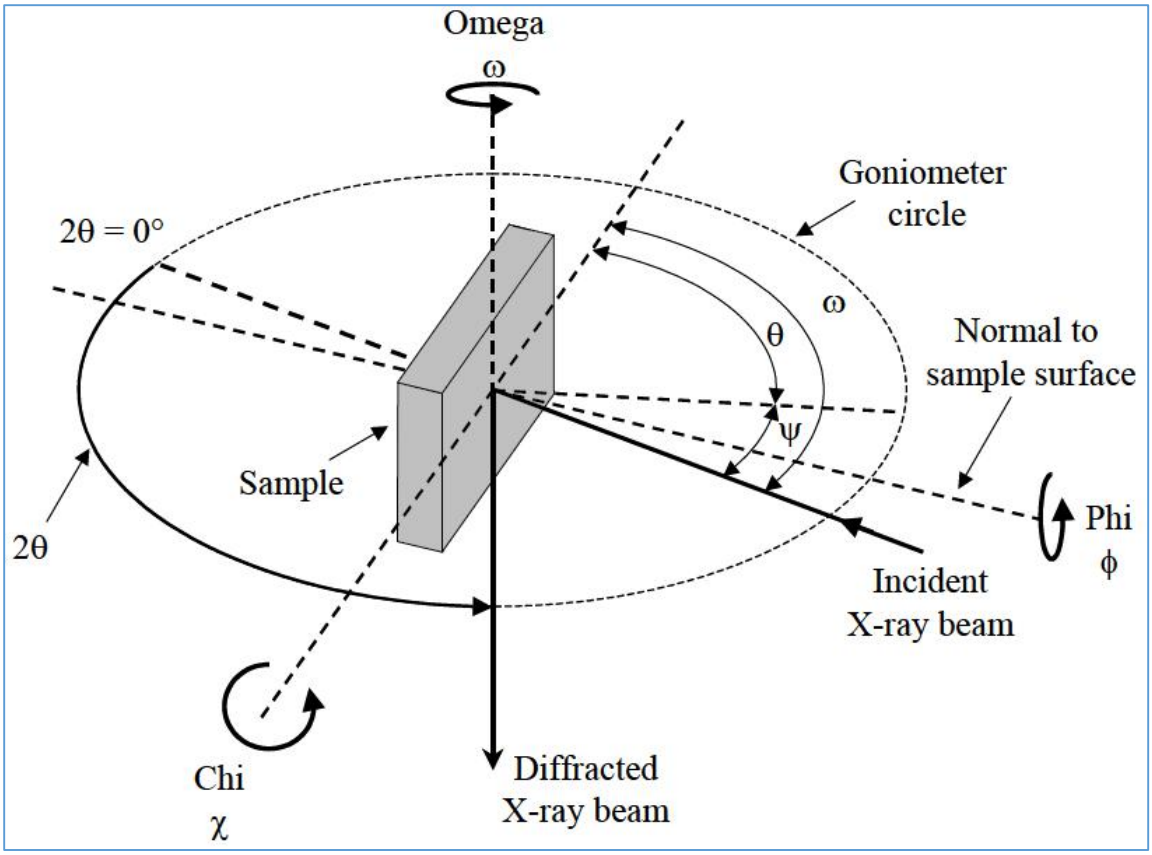

Figure 94: XRD axes of motion. (Image courtesy of National Physical Laboratory [34]).

b. Setup and operation PANalytical® X'Pert Pro MRD™ X-Ray Diffraction machine and XRD Data Collect ® software.

   i. Verify coolant temperature is within an acceptable range by observing the digital thermometer—monitor this throughout the use of the XRD to maintain safety awareness.

   ii. Setup optics and hardware for beam alignment and sample orientation.

      1. Select anode tube for tube housing model PW3373/10

         a. Copper (type that was installed and aligned)

b. Cobalt (purchased but, not able to install and would require alignment)

c. Chrome (typical of ASTM standard)

2. Correctly position tube housing.

a. Set at standard scan position.

b. Use set screw to secure tube housing in place.

3. Place mirror next to tube housing.

a. Mirror should be close enough to activate safety switch on tube housing.

b. Use set screw to secure tube housing in place.

4. Insert incident side hardware (rectangular bars).

a. 1/32° slit

b. Cu 0.2, Ni 0.02, 18269 attenuation plate.

5. Insert divergent side hardware

a. 0.27° slit

b. 0.04 RAD soller slit

c. Receiver (PW3011/20)

iii. Verify that nothing inhibits the movement of the XRD platform and receiving apparatus.

iv. Close shielding doors of XRD.

v. Access X'Pert Data Collector™

vi. Select Triple-Axis operation method.

vii. Set voltage and amperage levels.

1. Voltage at 45 kilovolts (kV)
2. Amperage at 40 milliamps (mA)

viii. Set all offsets to zero positions (direct beam setting).

ix. Visually verify that no object (sample stage) is blocking receiver.

x. Use manual 2Theta scan to align beam and receiver.

1. Default scan settings were used for 2Theta scan.
2. Resulting peak was used to determine 2Theta offset which was used for “Fine Calibration” setting.

xi. Close shutter.

xii. Open shielding doors.

xiii. Mount Sample

1. Rotate sample stage to flat position to allow easy mounting of sample without having to prevent sample from falling from vertical orientation.
2. Use XRD fixtures to hold sample on mounting stage.
    a. Align sample by locating the alignment mark on circumference with XRD fixture closest to operator at “zero” position(s) of orientation.
    b. Center sample on stage by using calipers or other measuring instrument to verify that sample position can be repeated.

xiv. Close shielding doors.

xv. Rotate sample to vertical position for scans.

xvi. Use manual Z scan to set sample stage offset.

1. Based on sample thickness (10 millimeter (mm) maximum), set range to scan four mm range evenly split around expected Z offset.
2. Record maximum intensity (plateau shaped plot).
3. Use “move mode” to adjust Z offset in an attempt to split the beam in half.

xvii. Use manual Omega scan to align sample surface parallel with beam (orientation correction).

1. Default scan settings were used for Omega scan.
2. Adjust Z offset so that peak is approximately half of Z (plateau) maximum intensity.
3. Repeat process 5.b.xvii.1. and 5.b.xvii.2. as necessary to achieve a peak that is half of the maximum plateau intensity of the Z scan.

xviii. Close shutter.

xix. Set sample offsets.

1. Z and Omega scans from steps 5.b.xvi. and 5.b.xvii. provide sample offsets for Z position and Omega rotation.
2. Click “Set New as Zero” to set sample offsets.

xx. Change optics hardware for “Automatic” scans (5.b.xxi. & 5.b.xxii.)

1. Use 5.b.ii. as a reference

2. Incident side hardware
    a. Remove 5.b.ii.4.a. 1/32° slit
    b. Remove 5.b.ii.4.b. Cu0.2, Ni 0.02, 18269 attenuation plate
    c. 1/2° slit (replaces 5.b.ii.4.a. 1/32° slit)
    d. Ni 0.02, 2.42 attenuation plate (replaces 5.b.ii.4.b. Cu 0.2, Ni 0.02, 18269 attenuation plate)
3. Divergent side hardware
    a. Remove 5.b.ii.5.a. 0.27° slit
    b. Keep 5.b.ii.5.b. 0.04 RAD soller slit
    c. Keep 5.b.ii.5.c. Receiver (PW3011/20)

xxi. Run “Absolute” scan in 2Theta-Omega range
1. Scan across 2Theta range to determine identifiable peaks.
2. Staying within machine constraints, scan from 20° to 150° 2Theta if possible
3. Reduce scan range to isolate peak and local background for reduced scan times.

xxii. Run “Stress Measurement” scan
1. To show option “Stress Measurement”
    a. Go to “User Settings”
    b. Open “Measurement Types and Data Folders”
    c. Go to tab “Multiple Scan”
    d. Select “Stress Measurement”

e. Click “OK”

f. Stress measurement should now be an option in automatic scans.

2. Stress Measurement settings

   a. Choose tilt axis

      i. Omega (scans are shifted)-(this option was selected for time constraints).

      ii. Chi (a better but more time consuming alternative)

   b. Tilt Range

      i. Positive only (minimum for stress measurements—later replaced with 5.xxii.2.b.ii.)

      ii. Positive + pseudo negative (measurements in both directions required for shear stress)

   c. Set Scan Axis to 2Theta-Omega

   d. Set Scan Mode to Continuous

   e. Set Scan Position (Identified Peak Position)

      i. 99° 2Theta for Aluminum

      ii. 137.5° 2Theta for Inconel® 718

      iii. 121.7° 2Theta for Tantalum

   f. Select $\sin^2$Psi options

      i. Appropriate range is from 0.8 to 0.1

ii. A desired number of shifts would be about seven.

g. 2Theta axis options

i. Range of scan in 2Theta axis should include base of peak (6.0000° was the standard used for this report)

ii. Set step size was set to 0.0400

iii. Time per step(s):

1. 0.50 for Aluminum
2. 1.00 for Inconel® 718
3. 0.50 for Tantalum

h. Select Phi steps

i. Minimum of two Phi-steps for range of 0° to 90° Phi rotation.

ii. Use four Phi-steps for range from 0° to 135° Phi rotation (this option was used)

iii. More time consuming option of six Phi-steps would have provided a range from 0° to 150° Phi rotation.

3. Run stress measurement scan
4. Save file to be analyzed by Stress™ software

c. Use Panalytical's Stress program to analyze material stress from scans.

i. Open Stress™ software

ii. Create a new stress analysis from stress scan.

iii. Select material data from database (specific alloy data was entered into database)

1. Aluminum 6061-T6
    a. Cell Symmetry: Cubic
    b. Young's Modulus: 68.9 GPA
    c. Poisson's Ratio: 0.33
2. Inconel® 718 (*Inconel*, 2012)
    a. Cell Symmetry: Cubic
    b. Young's Modulus: 205 GPA
    c. Poisson's Ratio: 0.30
3. Tantalum 97Ta3W ("Tantalum", 2014)
    a. Cell Symmetry: Cubic
    b. Young's Modulus: 186 GPA
    c. Poisson's Ratio: 0.35

iv. Save stress analysis for comparisons

6. Repeat process as needed.
    a. Repeat exact process for determining limitation of accuracy.
    b. Repeat with one variation in machining process to observe how changing that variable compares to the control process.
7. Determine material hardness with Wilson® Rockwell hardness tester.
    a. Refer to table below for setup.

Table 9: Probe, preload, and load settings for hardness scales.

Rockwell Hardness Test Scales Used			
Scale Symbol	**Indenter Type**	**Preliminary Force (kg)**	**Total Force (kg)**
B	Ball (1/16 in.)	10.0	100.0
C	Spheroconical Diamond	10.0	150.0

b. Start with Rockwell® "C" scale.
    i. Set to "C" scale on digital read out (DRO) screen.
    ii. Use spheroconical diamond indenter labeled for "C" scale.
    iii. Calibrate machine using marked samples.
    iv. Test material(s) on "C" scale to identify hardness and determine which scale is needed.
        1. For numbers above 10 on "C" scale, take five more readings on "C" scale.
        2. For numbers below 30 on "C" scale, take five readings on "B" scale.
        3. For numbers below 10 on "C" scale, take five readings on "B" scale.
        4. (Materials used in this experiment were expected to be on the B or C Rockwell® hardness scale ranges.)
c. Test materials that scored below 30 on Rockwell® C scale on Rockwell® B scale.
    i. Set to "B" scale on digital read out (DRO) screen.
    ii. Use ball (1/16 in.) indenter labeled for "B" scale.
    iii. Calibrate machine using marked samples if available.

iv. Test material(s) on “B” scale to identify hardness.

v. (Material(s) tested previously and expected data should only include testing of materials not likely to damage indenter ball.

8. Create a report including all significant findings.
    a. Create a table of stress data.
    b. Create charts of stress data.